5-2012

Metallurgical Effects on Long-Term Creep-Rupture in a New Nickel-Based Alloy

John P Shingledecker
jshingle@utk.edu

To the Graduate Council:

I am submitting herewith a dissertation written by John P Shingledecker entitled "Metallurgical Effects on Long-Term Creep-Rupture in a New Nickel-Based Alloy." I have examined the final electronic copy of this dissertation for form and content and recommend that it be accepted in partial fulfillment of the requirements for the degree of Doctor of Philosophy, with a major in Materials Science and Engineering.

George M. Pharr, Major Professor

We have read this dissertation and recommend its acceptance:

Easo George, Michael L. Santella, John D. Landes

Accepted for the Council:
Dixie L. Thompson

Vice Provost and Dean of the Graduate School

(Original signatures are on file with official student records.)

Metallurgical Effects on Long-Term Creep-Rupture in a New Nickel-Based Alloy

A Dissertation Presented for
the Doctor of Philosophy
Degree
The University of Tennessee, Knoxville

John P. Shingledecker
May 2012

DEDICATION

To my wife Jennifer
who endured numerous sacrifices
so I could complete this work

ACKNOWLEDGEMENTS

LEGAL NOTICE/DISCLAIMER

otherwise, does not necessarily constitute or imply its endorsement, recommendation, or favoring by the Department of Energy and/or the State of Ohio; nor do the views and opinions of author expressed herein necessarily state or reflect those of said governmental entities."

ABSTRACT

A series of creep-rupture studies were conducted on a new nickel-based alloy, Inconel Alloy 740, for use in Advanced Ultrasupercritical (A-USC) Steam boiler applications. The research quantitatively showed, for the first time, that the formation of a small amount of eta phase during long-term creep testing at 750 degrees Celsius does not degrade the rupture strength or ductility of the alloy. A unique full-scale pressurized tubular creep test was conducted, and a new analysis methodology was developed to evaluate the effect of cold-straining on the creep performance of tube bends made from the alloy. The results showed that 15% cold-work was detrimental to creep strength and ductility in the alloy and lower strain limits should therefore be imposed for typical manufacturing processes. A comprehensive study on the influence of composition and grain size on the alloy was completed. The research focused on creep data analysis, microstructural studies, and computational thermodynamics and showed that grain size, not gamma prime volume fraction or eta phase formation, was the critical parameter influencing creep strength in the alloy. The research also showed that small changes in the aluminum to titanium ratio in the alloy dramatically change the eta phase thermal stability. Results suggests that a large amount of eta phase (above 7 volume %) may reduce creep-rupture ductility (but not strength); however, more research is needed to validate this finding. The accuracy of computational thermodynamics was established for volume fraction and thermal stability of eta phase formation, but deficiencies were noted in kinetic (eta phase precipitation) calculations. In summary, the research shows that provided cold-work and grain size are appropriately controlled, Inconel 740 has predictable creep strength and ductility despite the potential for variations in microstructure. This is most likely due to the formation of gamma prime denuded or precipitate free zones along grain boundaries where creep damage is concentrated.

TABLE OF CONTENTS

LIST OF TABLES

LIST OF FIGURES

1. INTRODUCTION

Motivation for the Research

Increased efficiency and decreased emissions of pulverized coal-fired boilers can be achieved by increasing steam temperatures and pressures [1]. An Advanced Ultrasupercritical (A-USC) steam boiler with steam parameters of 760°C and 35MPa could reach efficiencies of 48%, which would cause a decrease in CO_2 emissions of about 22% compared to standard subcritical boiler technology in the United States [2]. The critical barrier to reaching a steam temperature of 760°C is the limitation of current boiler materials that can be fabricated and put into service for long times in such an aggressive environment [3]. The creep-rupture strength of various steam boiler materials, grouped by alloy class, is shown in Figure 1-1. Using the basis of temperature for rupture in 100,000 hours at 100MPa (which is the approximate stress value at which pipe wall thickness can be kept low enough to minimize the potential for thermal fatigue cracking), the 9-12% chromium steels have a temperature limit of ~620°C (current state of the art USC boiler technology today), the austenitic alloys of ~690°C, and the solid solution strengthened nickel-based alloys of ~720°C (alloys 617 and Haynes 230 on the plot). Thus an age-hardenable nickel-based alloy (such as Inconel 740 or Haynes 282) will be the only material with the requisite strength for 760°C steam temperatures.
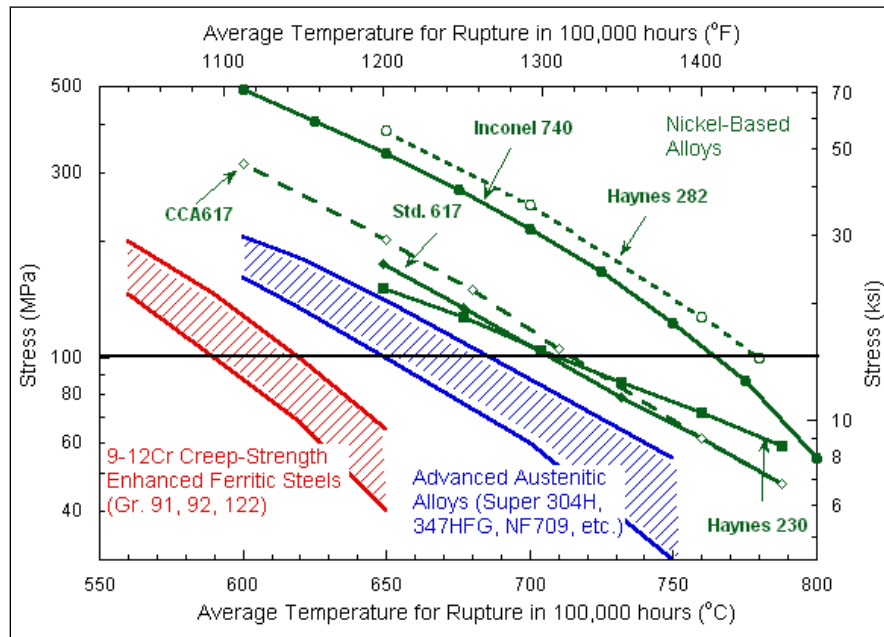
Figure 1-1 Average 100,000 hour rupture strength as a function of stress and temperature for candidate steam boiler materials

Inconel ® alloy 740 was developed to meet the rigorous demands of the A-USC boiler environment. The alloy 263 composition, shown in Table 1-1, was used as a basis for the development of Inconel 740 because it has very good weldability (for an age-hardenable alloy) and the available data showed it had the potential to meet the A-USC creep strength target.   The major alterations to the chemistry in Inconel 740 compared to 263 were the increase in Cr content and decrease in Mo to improve hot corrosion (fireside) resistance and the alteration of Al, Ti, and Nb levels for improved creep-rupture strength [4]. The amount of Al+Ti (the major elements which form the gamma prime strengthening precipitate) was kept nearly constant as higher Al+Ti content will increase the alloy creep strength but significantly decrease weldability. Laboratory corrosions tests on Inconel 740 met the targeted hot corrosion rates [4], and initial strength projections, based on short-term data, showed the alloy should meet a target of 100MPa 100,000 hour rupture strength at 760°C [3].

Table 1-1 Nominal Compositions (wt%) of Inconel Alloy 740 and Alloy 263 [5,6]

Alloy	C	Ni	Cr	Mo	Co	Al	Ti	Nb	Mn	Fe	Si
263	0.06	Bal	20.0	5.8	20	0.5	2.1		0.3	0.7	0.3
740	0.03	Bal	25.0	0.5	20.0	0.9	1.8	2.0	0.3	0.7	0.5

The design stress limits of boiler components subjected to loads and temperatures which could cause creep are typically set through extrapolation of shorter-term stress-rupture data by use of time-temperature parameters. However, recent findings showing inaccuracies in the projection of long-term creep-rupture performance based on short-term rupture data has raised significant issues related to these methods. In response to field failures and the availability of longer-term creep-rupture data which showed lower than predicted strength after long-term tests, the time dependent stress allowable values for a number of new steels have been reduced [7]. A lack of understanding of the microstructural changes in these materials and how they affected creep-rupture behavior were one reason for the optimistic strength projections (which were later lowered). Thus, it is imperative that microstructural evolution and its effect on long-term creep performance be understood for new materials if they are to be utilized by code bodies for high-energy pressure-retention components operating in the creep regime.

Background

Due to its potential for use in A-USC boiler components and the need to understand and ultimately control variables which influence long-term creep-rupture strength, the research in this study focused entirely on Inconel ® Alloy 740. Microstructural studies primarily based on isothermal aging experiments have been conducted on Inconel ® alloy 740, but no study has been conducted to clarify how these microstructural changes, or other microstructural parameters, may influence creep strength. Additionally, boiler fabrication processes involve cold-work which can be detrimental to creep strength and ductility in some nickel-based alloys. Therefore, performance of the alloy subjected to cold-worked and/or guidance on the need to reheat-treat cold-worked components is required. Since, boiler components are subject to complex multiaxial stress states, some influence on muliaxial creep damage is also needed. The following sections provide a review of: studies on microstructural development in Inconel ® alloy 740, the importance of gamma prime volume fraction and grain size on the creep of certain nickel-based alloys, effects of eta phase formation on creep behavior in nickel and iron based superalloys, cold-work effects in nickel-based alloys, and a brief discussion on multiaxial creep.

Microstructural Development in Inconel 740

Inconel 740 is an age-hardenable nickel-based superalloy which is typically furnished in the solution annealed condition. The recommended aging condition is 4 to 16 hours at 760 to 800°C [5] which produces an equiaxed grain structure with some twin boundaries, clean grain boundaries, and a fine distribution of gamma prime precipitates within the grains as shown in Figure 1-2 (a). Evans et al. [8] showed that after creep testing at 816°C for 2060 hours, the microstructure changes dramatically as shown in Figure 1-2 (b). A platelet phase, identified as eta phase extends from the grain and twin boundaries, and the grain boundaries show at least two distinct precipitates via BSE imaging contrast. These were identified as $M_{23}C_6$ carbides and a G-phase silicide. An occasional intragranular MC carbide was identified along with the gamma prime after creep testing.

Zhao et al studied the microstructural changes after aging Inconel 740 for various times at temperatures between 593 to 849°C. SEM evaluation of grain boundaries after 1,000 hours showed no change at 593°C, the precipitation of carbides and possible G-phase at 704°C, the same phases plus some eta platelets extending from the grain boundaries about 1μm in length at 750°C, and copious amounts of eta phase extending through the entire grains at 849°C in addition to the other grain boundary precipitates [9]. Vasudevan et al [10] studied the gauge (stressed) and shoulder (low-stress) regions of Inconel 740 after creep testing and found that after only ~300 hours at 800°C, eta phase platelets had precipitated and grown across the entire grains in the stressed region but no eta phase was observed in the low-stress region on the same

3

sample; thus indicating a stress component to the kinetics of eta phase formation and growth.

It has been shown experimentally [11] and through calculations [12] that changes in the Al:Ti ratio in Inconel 740 will change the eta phase stability. Thermodynamic calculation results from ref. [12] are shown in Figure 1-3 which show decreasing Ti (effectively increasing the Al:Ti ratio) decreases the phase stability temperature range and the amount (weight percent) of eta phase in Inconel 740. The eta phase composition is Ni_3Ti with minor substitution of Nb for Ti in some cases. Eta phase grows at the expense of the gamma prime precipitates thus lowering its volume fraction. Based on their thermodynamic calculations, the authors in ref. [12] conclude the Inconel 740 composition can be 'improved' by reducing or eliminating eta phase. The simple presumption is that eta phase is a detriment to creep strength because it (a) reduces the amount of gamma prime and (b) reduces ductility. However, these unquestioned assumptions may not be correct within the context of the alloy and the desired application. Other researchers have suggested alterations to the chemical composition of Inconel 740 for improved weldability (resistance to liquation cracking), but no mention of the effects these chemistry changes may have on creep strength were discussed [13].

(a)   (b)
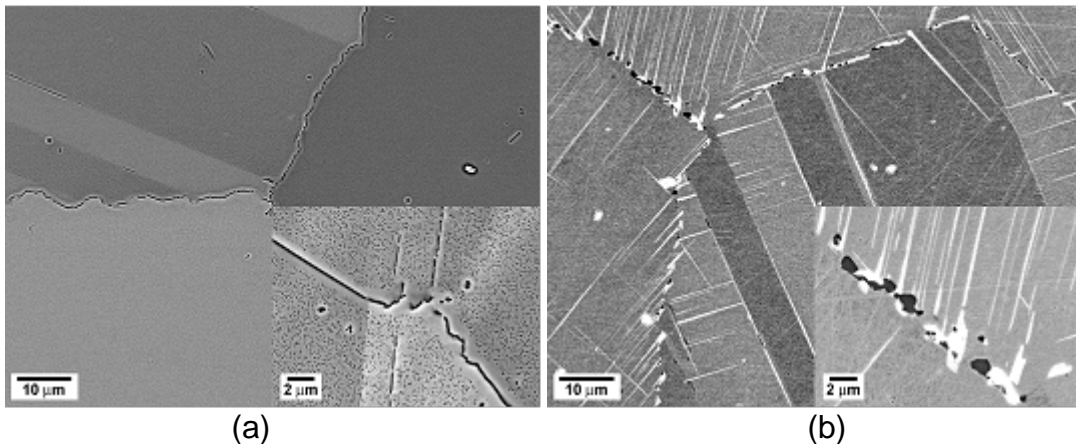
Figure 1-2 SEM images of Inconel Alloy 740 in the solution annealed and age-hardened conditions (a) and after creep testing at 816°C and 138MPa for 2060 hours (b) [8]
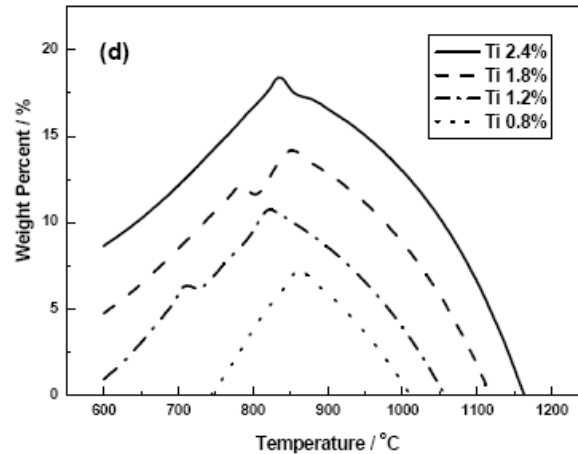
Figure 1-3 Calculated effect of Ti content on eta phase stability in Inconel 740 [10]

Gamma Prime Volume Fraction and Grain Size

The assumption that an increase in gamma prime volume fraction should, for the same alloy, improve creep resistance and thus creep-rupture strength has supporting experimental evidence. Gibbons and Hopkins clearly showed a decrease in creep rate and increase in rupture life for two sets (coarse and fine-grained) of modified IN597 alloys with varying amounts of gamma prime. However, after overaging for 10,000 hours at 850°C, the minimum creep rates of the fine-grained materials were nearly identical regardless of gamma prime volume fraction. This was attributed to a change in the creep mechanism which was postulated to switch from a dislocation cutting mechanism for the unaged material with fine gamma prime precipitates to a bowing mechanism for the overaged material with coarse gamma prime. Thus, the effectiveness of increasing gamma prime volume fraction on creep strength may depend on the operative *creep mechanism.* Manonukul et al. showed a similar effect of overaging in Nimonic 263 by creep testing after aging for 8, 30, 146, and 490 hours [15]. The creep-strain versus time behavior was similar for the short-term aged materials, but for the materials aged beyond 30 hours, the creep-rate increased and rupture time decreased.

Another consideration for microstructural effects in age-hardenable nickel-based superalloys is that gamma prime volume fraction may not be a constant. Generally, studies have shown constant gamma prime volume fraction, but there are exceptions when gamma prime is metastable [16] or when there are precipitation reactions [17]. In constructing a TTT diagram for Nimonic 263, Zhao et al showed the kinetics of the gamma prime to eta phase transformation were very sluggish and in some cases took 10,000 to 20,000 hours to complete [16].

5

Qin et al have reported increasing volume fractions of gamma prime with increasing aging time up to 10,000 hours in a nickel-based alloy casting [17]. While some of the changes may be due to the initial precipitation of gamma prime, the authors did not address non-uniform distributions of gamma prime. Stevens and Flewitt examined the changes in gamma prime with aging time in Inconel 738 and concluded that coarse cuboids grow at the expense of finer spheroids with the result being the total volume fraction of gamma prime remains approximately constant with time [18].

A third important consideration for creep-rupture behavior in these alloys is grain size effects. Gibbons and Hopkins studied a model Ni-20Cr-Ti-Al alloy system and systematically varied the gamma prime volume fraction from 0 to 31% by producing heats of material with differing Al and Ti contents, and processed the alloys to produce multiple grain sizes for each heat [19]. The results of this study are shown in Figure 1-4 (left) which shows the effect of varying gamma prime volume fraction on minimum creep rate. While increasing gamma prime results in reducing the creep-rate as expected, the effect of grain size is dependent on the amount of gamma prime. For the alloy with 5% gamma prime, little grain size effect is observed, but for the higher volume fraction alloys, the grain size effect can be the dominate effect, where a small change in grain size can essentially outweigh an ~10% change in volume percent of gamma prime. This effect has also been shown in commercial alloys where a study of Inconel 597 with two grain sizes showed the effect of gamma prime volume fraction on minimum creep rate was more pronounced for the coarse grained material (Figure 1-4 right) [14]. Gibbons and Hopkins combined all available creep data on gamma prime volume fraction and grain size and found that the effectiveness of increasing creep resistance with increasing gamma prime volume fraction was reduced by reducing the applied stress or volume fraction of gamma prime for a given creep rate [14].
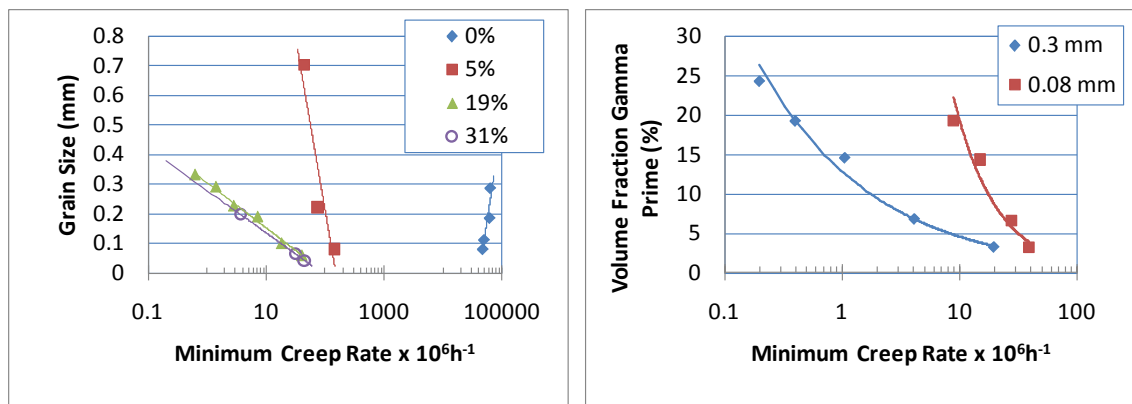
Figure 1-4 Effect of grain size and gamma prime volume fraction on minimum creep rate for model Ni-Cr-Al-Ti alloys, after [19,14]

Eta Phase and Creep-Rupture Behavior

As described previously, the FCC eta phase precipitates in Inconel 740. The role of eta phase in nickel-based superalloys is not well understood. In the engineering resource Superalloys – A Technical Guide [20] eta phase is described as 'sometimes' being a primary strengthening precipitate, it ambiguously states that the 'extent to which it (eta) contributes directly to strengthening depends on the alloy and its processing,' and in describing the 'potentially beneficial role of gamma prime envelops' it also states that there is a 'remote possibility that the areas are really eta…' No supporting data nor any references are provided on eta and its influence on strengthening in ref. [20].

Studies on eta phase give conflicting results. Sun et al. suggested P additions to GH761 (wrought nickel-based superalloy) 'lowered the stability of gamma prime and eta preferentially formed reducing stress-rupture life' [21]. However, this was a very limited study based on four creep tests which showed little change in post-test elongation and only very minor eta phase precipitation. Remy et al studied microstructure and creep-rupture properties of the Fe-Ni superalloy 706 with various heat-treatments [22]. The study found that the long-term creep-rupture properties were similar regardless of aging treatment provided a stabilizing heat-treatment was first performed to cause intergranular precipitation of eta phase. A simple heat-treatment which did not precipitate eta phase increased short-term creep rupture life but decreased long-term creep-rupture life with a similar effect on creep rate as shown in Figure 1-5. The authors concluded the 'results show that neither large intergranular platelets nor a fairly large gamma prime depleted zone…appear to be detrimental to creep properties."
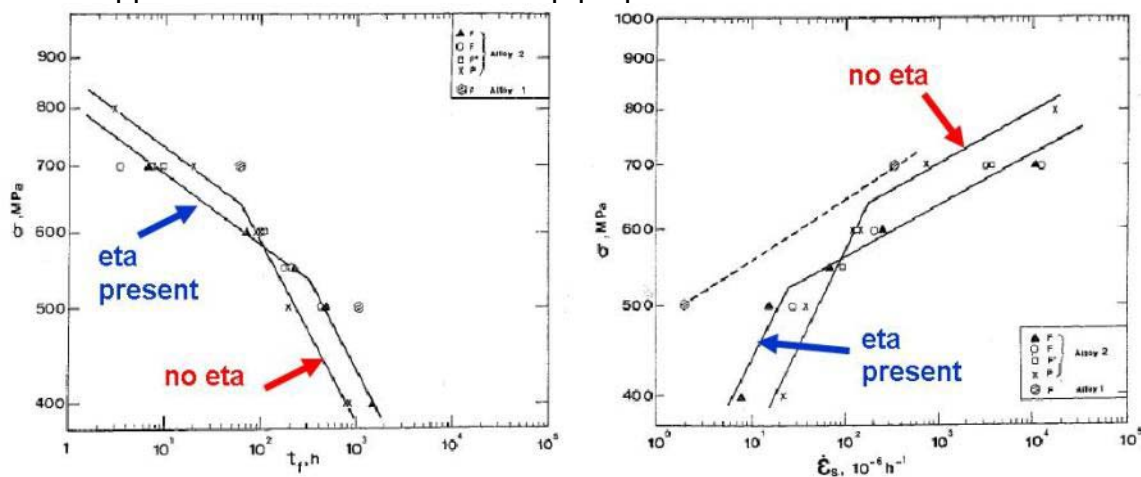
Figure 1-5 Plots of time to rupture (left) and creep rate (right) as a function of stress for alloy 706 with various heat-treatments to purposely produce or eliminate intergranular eta precipitation [22]

Muller and Rosler studied creep crack growth in alloy 706 and found that creep-crack growth resistance increased (growth rate decreased) with heat-treatments which caused precipitation of eta phase platelets extending into the grains, but when film-like eta phase formed the resistance decreased [23]. Gu et al. conducted alloy development creep screening tests on four alloys based on Udimet 720Li. Four alloys were tested with varying predicted levels of gamma prime [24]. The alloy which exhibited the lowest creep rate and longest rupture time contained eta phase, but the other alloys did not. One possible explanation of this behavior by the authors was that the 'eta phase supplies extra creep resistance to the matrix.' Eta phase observed in creep studies on Nimonic 263 [25] and superalloy castings [17] was concluded to have no effect on creep behavior. Other research has shown for Fe-Ni superalloy A286 [26] and for Inconel 706 [20] eta phase is detrimental to low-cycle fatigue, but no discussion on creep was provided.

Cold-work and creep

The fabrication of power-boiler equipment requires cold-working of materials including bending, swaging, and straightening. Cold-formed steel and stainless steel components have failed during high-temperature service in boilers due to various mechanisms including dynamic recrystallization and ductility impairment (also known as strain induced precipitation hardening – SIPH). Age-hardenable nickel-based alloys are subject to additional mechanisms for loss of creep strength due to cold-straining.

Research by Dyson and Rogers [27], Loveday and Dyson [28], and Zhang and Knowles [25] all showed prestrain in aged nickel-based alloys causes a reduction in creep strength and creep ductility. Dyson and Rogers prestrained Nimonic 80A creep specimens from 0 to 15% after standard heat-treatment and aging [27]. Creep tests on these specimens showed a progressive loss of creep resistance, time to rupture, and rupture ductility with increasing pre-strain. Quantitative optical metallography showed increasing grain-boundary cavitation with increasing prestrain suggesting the loss of ductility was related to enhanced cavity density while the decrease in creep resistance was postulated to be due to an increase in mobile dislocation density. Zhang and Knowles conducted a similar study by prestraining Nimonic 263 after aging [25]. Similar to the previous study they found increased cavity density resulting in decreased rupture life and ductility with increasing prestrain, but minimum creep rate did not show as pronounced an effect as Dyson and Rogers. The authors suggest a "slip band induced cavitation mechanism" is responsible for the observed behavior. Loveday and Dyson conducted a 9% prestrain creep experiment on IN597 and found microcracks in carbides after prestraining which were studied in detail and found to be related to the sites for subsequent creep cavitation during testing suggesting a particle microcracking mechanism [28].

All studies on cold-deformed age-hardenable nickel-based alloys show a decrease in creep-rupture strength due to a combination of mechanisms including: increased mobile dislocation density, enhanced cavitation due to slip bands, and particle microcracking. In all these cases, cold-work was applied after the aging heat-treatment (i.e. gamma prime was already precipitated). For construction of boiler components with nickel-based alloys, it may be advantageous to cold deform the material in the solution annealed condition and then age the material. Mechanisms of increased dislocation density or slip-band enhanced cavitation may be reduced or eliminated if the aging treatment is sufficient to stress-relieve the material prior to precipitation of gamma prime causing hardening of the matrix. Experimental studies on solid-solution strengthened nickel-based alloys suggest these alloys are not susceptible to these mechanisms [29]. Thus, for Inconel 740 it will be necessary to determine the effect of cold-strain on solution annealed material prior to aging to develop proper rules for cold-straining of components.

Multiaxial stress states

Boiler components are routinely subjected to complex multiaxial stress states during high-temperature service in the creep regime. A material's ability or inability to redistribute stress during multiaxial creep is critical to the performance of components. Materials with high rupture ductility are generally able to 'shed load' or allow for redistribution of stress, but materials with low rupture ductility may begin to cavitate or crack due to high principle stresses resulting in failure under multiaxial stress. Many nickel-based super-alloys have very low creep-rupture ductility, and therefore it is a concern for Inconel 740. One economical method for testing a material's behavior in multiaxial stress states is notched bar creep-rupture testing [30-32]. Creep testing with various notch geometries allows for a range of triaxial stresses to be generated in a standard uniaxial creep frame. Prior to this work, no long-term notched bar creep-rupture experiments on Inconel 740 were available.

Summary of Issues and Structure of This Dissertation

Inconel ® alloy 740 is a prime candidate alloy for construction of an A-USC steam boiler designed to operate at temperatures up to 760°C. To utilize the alloy for this application and have confidence in long-term creep-rupture predictions, extensive data and a detailed knowledge of the alloy's creep behavior are required.

A review of literature on the alloy and similar alloys was conducted which shows the following. Inconel ® alloy 740 is a wrought age-hardenable nickel-based alloy which is strengthened by gamma prime precipitates and forms eta phase during high-temperature thermal exposure. Both the amount of gamma prime and eta phase are dependent on alloy chemistry. There is no consensus on the role of eta phase on creep strength or ductility in nickel-based alloys, and thus there is a need to clarify the role of eta phase in the alloy. Furthermore, while the volume fraction of gamma prime is important for creep strength, the grain size of the alloy should also be considered. Since the alloy will be subjected to typical boiler fabrication processes, improved knowledge of the effect of cold-work (pre-strain) in the alloy is required. Finally, the use of this alloy in boiler components subjected to various loading requires additional understanding of creep strength and ductility under muliaxial stress.

To address these separate but related challenges in understanding the creep-rupture behavior in Inconel ® alloy 740, this dissertation is divided into three main chapters which are 'stand-alone' papers. Chapter 2 is a focused study on the role of eta phase formation on creep strength and ductility. Notched bar tests (including a unique Bridgeman notch test) were included in this test program to illuminate effects of multiaxial stress state. This chapter is the first research, to the author's knowledge, that quantitatively shows the formation of a small amount of eta phase does not adversely affect creep strength or ductility.

Chapter 3 addresses the effect of cold-work on creep-rupture strength and ductility. The novel approach taken was to test full-size boiler components (tube bends) which make the results directly related to field components. The chapter presents a new analysis methodology for separating the material (cold-work) and geometric (multi-axial) creep effects. Utilizing this method, the data show Inconel ® alloy 740 has similar reductions in creep strength and ductility when compared to other nickel-based alloys. The notched bar research in Chapter 2 was utilized for the ductility analysis in Chapter 3.

Chapter 4 contains an analysis of a large database of creep-rupture tests covering a range of temperatures and times up to 24,000 hours. The work focuses on validating the use and limitations of computational thermodynamics

for prediction of phase stability, an evaluation of grain size effects independent of chemistry, and an evaluation of microstructure (gamma prime and eta phase) independent of grain size. Six different chemistries (heats) and multiple grain sizes in the same heat were examined as part of this comprehensive study. The work shows eta phase does not affect the creep strength of Inconel ® alloy 740, but may reduce creep ductility at greater than 7wt%. The results showed good correlation between computational and experimental results for eta phase thermal stability but not for the kinetics of its formation. Finally, the results showed a clear effect of grain size on creep strength in the alloy with no discernable difference with changing gamma prime volume fraction. Detailed conclusions based on these three chapters are provided in the final chapter of this report.

Chapter 1 References

1. R. Viswanathan, R. Purgert, U. Rao. "Materials for Ultra-Supercritical Coal-Fired Power Plant Boilers." *Materials for Advanced Power Engineering 2002, Proceedings Part II*. Forschungszentrum Julich GmbH, 2002. 1109-1129

2. R. Viswananthan, J.F. Henry, J. Tanzosh, G. Stanko, J. Shingledecker, B. Vitalis, R. Purgert. "U.S. Program on Materials Technology for Ultra-Supercritical Coal Power Plants." *Journal of Materials Engineering and Performance.* Vol. 14 (3) June 2005. 281-292

3. J.P. Shingledecker, I.G. Wright. "Evaluation of the Materials Technology Required for a 760°C Power Steam Boiler." *Proceedings to the 8th Liege Conference on Materials for Advanced Power Engineering 2006.* Forschungszentrum Jülich GmbH (2006) pp. 107-120

4. G.D. Smith, H.W. Sizek. "Introduction of an advanced superheater alloy for coal-fired boilers." Proceedings to Corrosion 2000, Paper 00256 ©2000 NACE Int.

5. "Inconel ® alloy 740." SMC-090 © Special Metals Corporation, 2003 (Feb 03)

6. "Nimonic ® alloy 263." SMC-054 © Special Metals Corporation, 2004 (Sept 04)

7. K. Kimura. "Creep Strength Assessment and Review of Allowable Tensile Stress of Creep Strength Enhanced Ferritic Steels in Japan." Proceedings of PVP2006/ICPVT-11 ©2006 ASME. PVP2006-ICPVT11-93294

8. N.D. Evans et. al. "Microstructure and phase stability in Inconel 740 during creep." Scripta Materialia 51 (2004) 503-507.

9. S. Zhao et al. "Microstructure stability and mechanical properties of a new nickel-based superalloy." Materials Science and Engineering A355 (2003) 96-105.

10. V. Vasudevan et al. unpublished research

11. X. Xie, C. Chi, H. Yu, Q. Yu, J. Dong, M. Chen, S. Zhao. "Structural Stability Study on Fossil Power Plant Advanced Heat-Resistant Steels and Alloys in China." *Proceedings to the 6th International Conference on Advances in Materials Technology for Fossil Power Plants*, Santa Fe, New Mexico, August 30-September 4, 2010. EPRI, March 2011: 1022300. Distributed by ASM International. 30-52.

12. X. Xie et al. "Modification of Ni-Cr-Co-Mo-Nb-Ti-Al Superalloy for USC Power Plant Application at Temperature above 750C." Materials Science Forun Vols. 561-565 (2007) pp 471-476

13. J.M. Sanders, J.E. Ramirez, B.A. Baker. "Weldability Invesigation of Inconel ® Alloy 740 for Ultrasupercitical Boiler Applications." Proceedings of the 5th International Conference on Materials…

14. T.B. Gibbons, B.E. Hopkins. "Creep behavior and microstructure of Ni-Cr base alloys." Metal Science Vol. 18 May 1984. 273-280

15. A. Manonukul, F.P.E. Dunne, D. Knowles. "Physically-based model for creep in nickel-base superalloy C263 both above and below the gamma solvus." Acta Materialia 50 (2002) 2917-2931

16. J.C. Zhao, V. Ravikumar, A.M. Beltran. "Phase Precipitation and Phase Stability in Nimonic 263." Metallurgical and Materials Transactions A. Vol 32A, June 2001. 1271-1282.

17. X.Z. Qin, J.T. Guo, C. Yuan, C.L. Chen, H.Q. Ye. "Effects of Long-Term Thermal Exposure on the Microstructure and Properties of a Cast Ni-Base Superalloy." Metallurgical and Materials Transactions A. Vol 38A, December 2007. 3014-3022.

18. R.A. Stevens, P.E.J. Flewitt. "The Effects of g' Precipitate Coarsening During Isothermal Aging and Creep of the Nickel-Base Superalloy IN-738." Materials Science and Engineering, 37 (1979) 237-247.

19. T.B. Gibbons, B.E. Hopkins. "The Influence of Grain Size and Certain Precipitate Parameters on the Creep Properties of Ni-Cr-Base Alloys." Metal Science Journal. Vol. 5, 1971. 233-240

20. M.J. Donachie, S.J. Donachie. Superalloys A Technical Guide. ASM International © 2002

21. W.R. Sun, S.R. Guo, D.Z. Lu, Z.Q. Hu. "Effect of Phosphorus on the Microstructure and Stress Rupture Properties in an Fe-Ni-Cr Superalloy." Metallurgical and Materials Transactions A. Volume 28A, March 1997. 649-654

22. L. Remy, J. Laniesse, H. Aubert. "Precipitation Behaviour and Creep Rupture of 706 Type Alloys." Materials Science and Engineering, 38, 1979. 227-239.

23. S. Muller, J. Rosler. "Optimisation of Inconel 706 for Creep Crack Growth Resistance." Proceedings of the 5th International Charles Parsons Turbine Conference.

24. Y.F. Gu, H. Harada, C. Cui, D. Ping, T. Fukuda, J. Fujioka. "The Development of Ni-Co-Base Superalloys for the Next Generation Turbine Discs." Proceedings of the 7th International Charles Parsons Turbine Conference, 2007.

25. Y.H. Zhang, D.M. Knowles. "Prestraining effect on creep behaviour of nickel base C263 superalloy." Materials Science and Technology, August 2002, Vol. 18. 917-923.

26. B.S. Rho, S.W. Nam, X. Xie. "The effect of test temperature on the intergranular cracking of Nb-A286 alloy in low cycle fatigue." Journal of Materials Science 37 (2002) 203-209.

27. B.F. Dyson, M.J. Rogers. "Prestrain, Cavitation, and Creep Ductility." Metal Science, 1974, Vol. 8. 261-266.

28. M.S. Loveday, B.F. Dyson. "Prestrain-Induced Particle Microcracking and Creep Cavitation in IN597." Acta Metallurgica, 1983, Vol. 31. 397-405

29. J.P. Shingledecker. "Creep-Rupture Behavior and Recrystallization in HR6W and Haynes Alloy 230 Cold-Bent Boiler Tubing for Ultrasupercritical (USC) Steam Boiler Applications." *Submitted to Energy Materials, 2007.*

30. B.W. Roberts. "Influence of Multiaxial Stressing on Creep and Creep Rupture." <u>ASM Handbook. Vol. 8 Mechanical Testing</u>. ASM International, 1995, 343-345.
31. J.M. Church, J.M. Brear, D.R. Humphrey. "Rationalisation of the Multiaxial Stress Rupture Behaviour of Components." *Key Engineering Materials.* Vols. 171-174 (2000) pp. 61-68 © Trans Tech Publications, Switzerland.
32. R.J. Browne, D. Lonsdale, P.E.J. Flewitt. "Multiaxial Stress Rupture Testing and Compendium of Data for Creep Resisting Steels." *Journal of Engineering Materials and Technology*, Oct. 1982, Vol. 104, 291-296.

2. THE ROLE OF ETA PHASE FORMATION ON THE CREEP STRENGTH AND DUCTILITY OF INCONEL ALLOY 740 AT 1023 K (750°C)

A version of this chapter was originally published by J.P. Shingledecker and G.M. Pharr:

J.P. Shingledecker, G.M. Pharr. "The Role of Eta Phase Formation on the Creep Strength and Ductility of INCONEL Alloy 740 at 1023 K (750 °C)." *Metallurgical and Materials Transactions A.,* 2012, 10.1007/s11661-011-1013-4

This chapter was the original work of the author and has been reformatted from the journal article which is published to conform to the thesis requirements. No changes, other than editorial corrections and placement of tables and figures to aid the reader, have been made.

Abstract

INCONEL® alloy 740 is an age-hardenable nickel-based superalloy proposed for advanced ultrasupercritical steam boiler applications operating at high-stress and long-times above 973K (700°C), where creep will be the dominate deformation mode. During high-temperature exposure, the alloy can form eta phase platelets that many have suggested may be detrimental to creep strength and ductility. In this study, creep-rupture tests were conducted on smooth and notched bars of INCONEL® alloy 740 at 1023K (750°C) for times up to 20,000 hours. Examination of the creep-rupture life, creep ductility, failure modes, and microstructure by quantitative electron microscopy show that a small amount of eta phase does not diminish the creep performance. Applied stress appears to have a minor effect on the precipitation of the eta phase but not its growth rate. Based on the observation that the microstructure after 20,000 hours of creep exposure has reached equilibrium in comparison to thermodynamic calculations, it is concluded that 20,000 hour creep tests are adequate for prediction of the long-term creep performance.

Introduction

Increased efficiency and decreased emissions of pulverized coal-fired boilers can be simultaneously realized by increasing steam temperatures and pressures [1]. Studies have shown that compared to a standard U.S. subcritical steam boiler, an advanced ultrasupercritical (A-USC) steam boiler operating with steam parameters of 1033K (760°C) and 35 MPa will increase the thermal efficiency to 46% HHV (Higher Heating Value), thereby reducing levels of all effluents, including CO_2, by 20 to 25% [2]. The main limitation to realizing such a boiler is a lack of materials from which components can be manufactured (tubing and piping), and operate for long-times (>100,000 hours) in such an aggressive environment [3]. The age hardenable nickel-based alloy INCONEL® alloy 740 (referred to as alloy 740) was developed specifically for this application [4,5].

16

However, several studies of aging and creep of this alloy at temperatures from 866 to 1122K (593 to 849°C) have shown the formation of Ni_3Ti eta phase platelets, and authors have suggested this may decrease the microstructural stability and thus creep strength of the material [6,7,8].

In this work, long-term creep-rupture tests, up to ~20,000 hours, were conducted on smooth bar and notched specimens of alloy 740. The creep behavior and rupture ductility of notched and un-notched specimens were evaluated. Microstructural analyses, including optical microscopy (OM) and scanning electron microscopy (SEM), were conducted on failed specimens to examine the creep failure mode and microstructural development, with particular attention to eta phase formation. Thermodynamic calculations of the phase fractions were compared to quantitative microstructural observations. The results suggest that the eta phase formation in alloy 740 at 1023K (750°C), which is approximately 3 volume percent, is not detrimental to long-term creep strength and ductility.

Experimental Procedure

The material used for this study was a ~75 mm thick plate furnished in the solution annealed condition {1393K (1120°C) followed by a water quench} with alloy chemistry shown in Table 2-1. The grain size of the as-received material measured on polished metallurgical mounts using the mean lineal intercept procedure was found to be 187.6 μm (equivalent volumetric grain size of 281.4 μm or ASTM grain size 1.5).

Table 2-1 Chemical composition of INCONEL® Alloy 740 used in this study

Heat #	Elemental analysis in Wt % except where noted									
	C	Si	Mn	P	S	Ag (ppm)	Al	B	Bi	Co
BLT2819	0.029	0.53	0.26	<0.005	<0.001	<0.1	0.98	0.004	<0.1	19.90
							Pb			Zn
	Cr	Cu	Fe	Mo	Nb	Ni	(ppm)	Ti	V	(ppm)
	24.4	0.02	0.45	0.50	1.99	bal	0.8	1.78	<0.01	1.1

Smooth bar creep-rupture specimens having a 6.4 mm diameter (dia.) with a 31.8 mm gauge length (GL) and one large smooth bar sample having a 25.4 mm dia. and 114.3 mm GL were machined for testing. Two different notched bar specimens were utilized as shown in Figure 2-1. The ASTM V-notch specimens were manufactured with a notch root dia. of 6.4 mm, a gauge dia. of 9.5 mm, a notch opening of 60°, and a root radius of 0.1 9 mm. The modified Bridgeman notched bar was manufactured with a 25.4 mm notch root radius, a 44.5 mm

gauge dia., a 6.4 mm notch opening, and a 3.2 mm notch radius. The specimens were extracted from the plate so that the gauge section was parallel to the rolling direction. In addition, the specimens were cut a minimum of 12.5 mm from the plate edge where the grain size was slightly finer. Prior to testing, all specimens were given a standard aging heat-treatment of 1073K (800°C) for 16 hours. For the large smooth bar and modified Bridgeman notch tests, 4 strain gauges were mounted around the specimen to measure bending. The specimens were step loaded at room temperature to the target stress level, with measurements verifying that bending strains were less than +/-8%. Creep-rupture tests were conducted in accordance with ASTM E139. All but one specimen was tested to rupture.
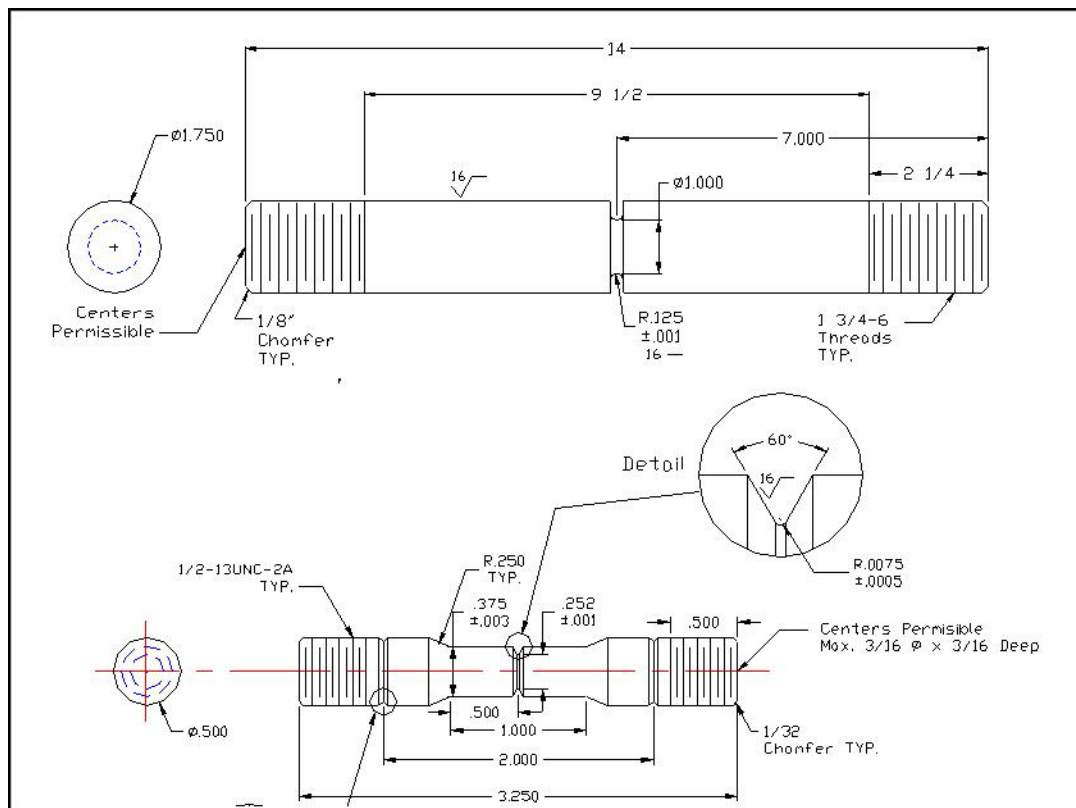
Figure 2-1 Notched bar specimens (note dimensions in inches, 1 inch = 25.4 mm)

After testing, specimens were sectioned, mounted in epoxy, and polished using standard metallographic techniques. Specimens used for optical microscopy (OM) and grain size determination were etched using a solution of 40 ml H_2O, 40 ml HNO_3, and 20 ml HF. Scanning electron microscopy (SEM) was performed on polished (unetched) samples in both secondary (SE) and back-scatter (BSE) electron imaging modes. To quantitatively assess microstructural features,

18

length measurements were made on digitally captured images, and area fraction measurements were obtained by placing a digital grid on each image for point counting. A minimum of 390 intersections and two images were utilized for area fraction measurements, with lower area fractions utilizing three images. Thermodynamic calculations of the equilibrium microstructural phases were carried out utilizing JMatPro™ version 4.0 with the Ni database [9].

Results

Creep-rupture tests

Creep-rupture tests were performed at stresses between 180 and 370 MPa at 1023K (750°C). The test results are summarized in Table 2-2. The stress reported in Table 2-2 for the notched bars is the net section stress (σ_{net}), which is calculated using the area of the notch root and is not corrected for multiaxial creep effects. Figure 2-2 shows the time to rupture as a function of stress for these samples. For the smooth bar, the data are well described by a power-law fit with no deviation after ~20,000 hours. Results for the large diameter specimen were indistinguishable when compared to the standard specimen at the same test conditions (320MPa); the two samples failed at 664.2 and 658.5 hours, respectively.   The figure clearly shows that the notched bar tests had rupture lives six to nine times longer than the smooth-bar samples at equivalent stresses.

Figure 2-3 shows the engineering ductility observed in the tests. For the smooth bars, the rupture elongation and reduction of area do not change with increasing test time. Only the shortest rupture time sample (311.9 hours) had a smaller reduction of area. All fractures were in the sample gauge sections. The reductions of area measured in the notched specimens were significantly lower than the equivalent smooth bar tests. Figure 2-4 presents a plot of the minimum creep rate versus stress. A power-law exponent of 6.7 was obtained by fitting the data, with no evidence of a change in mechanism at low stress levels.

Table 2-2   Creep-rupture test results

Specimen	Stress (MPa)	Temp. K(ºC)	Rupture Life (hrs)	Elongation (%)	Reduction of Area (%)	Min. Creep Rate (%/hr)
Standard - smooth	370	1023(750)	311.9	15	7.1	2.7E-03
Standard - smooth	320	1023(750)	658.5	12.7	15.4	8.6E-04
Large Dia. - smooth	320	1023(750)	664.2	11.6	20.3	8.4E-04
Standard - smooth	300	1023(750)	1020.2	13.4	15.1	4.1E-04
Standard - smooth	265	1023(750)	2185.4	10.9	15.5	1.8E-04
Standard - smooth	220	1023(750)	7355.2	11.4	15.8	5.6E-05
Standard - smooth	200	1023(750)	*13,000	-	-	7.6E-05
Standard - smooth	180	1023(750)	20789.4	10.9	15.1	1.3E-05
ASTM V-notch	370	1023(750)	2017.3	-	1.6	-
ASTM V-notch	320	1023(750)	6212.7	-	2.8	-
Modified Bridgeman	320	1023(750)	7217.7	-	2.6	-

*Test stopped
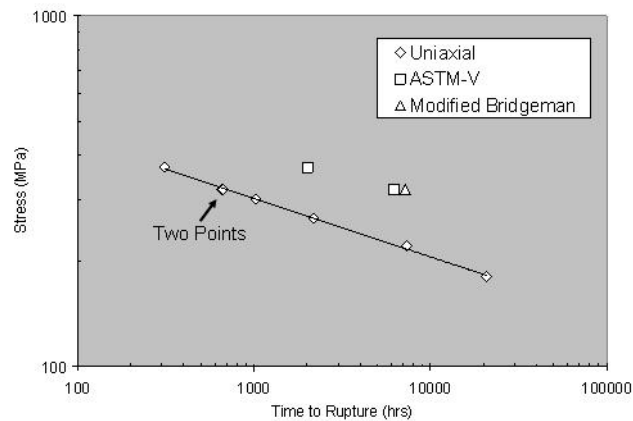
Figure 2-2 Stress versus time to rupture observed in creep tests at 1023K (750°C).
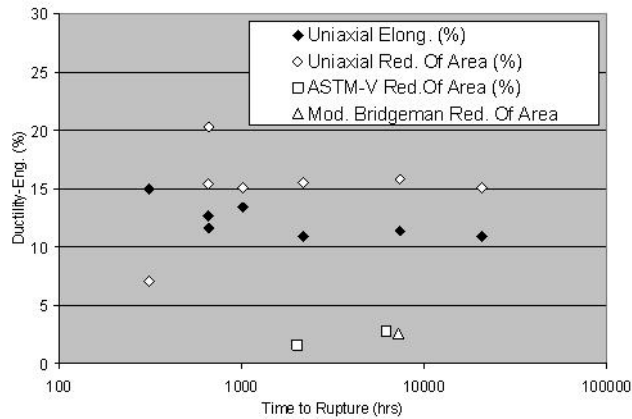
Figure 2-3 Engineering rupture ductility (elongation=Elong., reduction of area=Red. Of Area) as a function of rupture time.
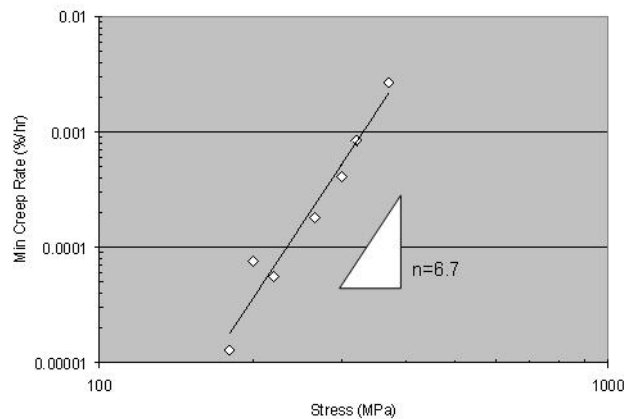
Figure 2-4 Minimum creep-rate versus applied stress for smooth bar samples.

Microstructure

Figure 2-5 shows the microstructure in the vicinity of a grain boundary for five smooth bar specimens crept under different conditions. The images were obtained by SEM using BSE imaging. The microstructure after 658.5 hours (figure 5a) is relatively clean with the grain boundary showing two distinct phases, a darker phase identified by previous researchers as $M_{23}C_6$ and a lighter phase identified as the G-phase [6,7]. G-phase is a fcc silicide with a nominal compositions of $M_6Ni_{16}Si_7$ (where M=metal ion). The intragranular gamma prime precipitates are difficult to resolve due to their small size. After 1020.2 hours (Figure 2-5b), a new phase - the eta phase - has begun to form along the grain boundary. This was observed in the gauge section of the specimen, but not in the shoulder where the stresses were considerably smaller. The $M_{23}C_6$ and G-
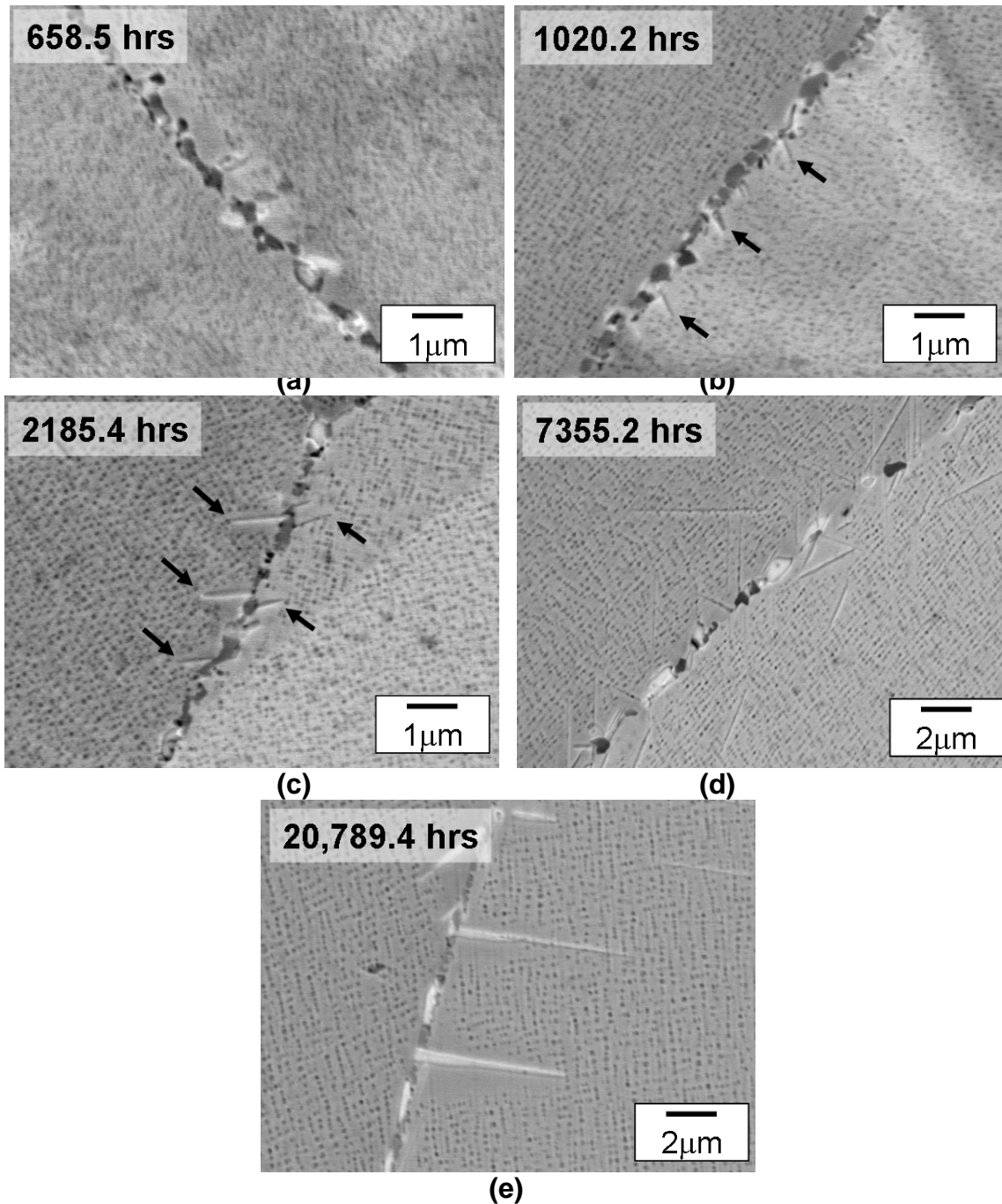
Figure 2-5 Backscatter electron (BSE) images in regions near grain boundaries of smooth bar alloy 740 specimens after creep rupture at 1023K (750°C) for (a) 658.5 hours (320MPa), (b) 1020.2 hours (300MPa), (c) 2185.4 hours (265MPa), (d) 7355.2 hours (220MPa), and (e) 20,789.4 hours (180MPa). Arrows on (b) and (c) indicate eta phase. Note: scale bars are not all the same.

phase can still be identified, and gamma prime precipitates have coarsened slightly and are now observable. At 2185.4 hours (Figure 2-5c), the eta phase appears in both the gauge section and the shoulder and has elongated significantly in the direction perpendicular to the boundary. The gamma prime is similar in size to the 1020.2 hours sample, and around some of the grain boundary precipitates there is a region that does not contain gamma prime (gamma prime denuded zone). The 7355.2 hour sample (Figure 2-5d) shows the same trends, with increasing size of the eta and gamma prime phases. Special attention was paid to evaluating the grain boundary orientation relative to the applied stress in the creep-rupture test, but no clear trends in behavior were observed in any of the specimens. Lastly, the 20,789.4 hour sample (Figure 2-5e) shows, in addition to the grain boundary phases, clearly longer and larger eta phase platelets that are surrounded by gamma prime denuded zones. The gamma prime has also coarsened and is tending toward a cuboidal shape.

Figures 2-6 and 2-7 show images of grain boundary wedge cracking (WC) and cavitation observed in tested specimens. Wedge cracking predominated in the highest stressed smooth bar test (311.9 hour at 370 MPa). A mixture of wedge cracking and grain boundary cavitation was observed in the smooth bar tests at 320 MPa, which failed at ~660 hours. Longer-term and lower stress tests all exhibited grain boundary cavitation as the predominate failure mode (Figure 2-7). Careful examination of the grain boundary cavities indicated that they form preferentially in the gamma prime denuded region of the grain boundary. They often form close to the grain boundary phase and are not uniquely associated with the eta phase platelets or the gamma prime denuded region around the eta phase. In fact, figure 2-7 (a) shows two grain boundary cavities whose growth appears to be constrained by impingement on eta phase platelets.
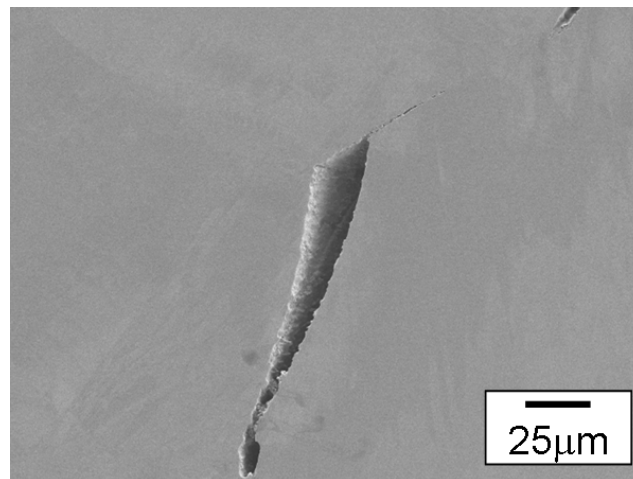
Figure 2-6 Secondary electron (SE) image of grain boundary wedge crack in a smooth bar creep-rupture test after 311.9 hours (370MPa)

<center>(a)   (b)</center>
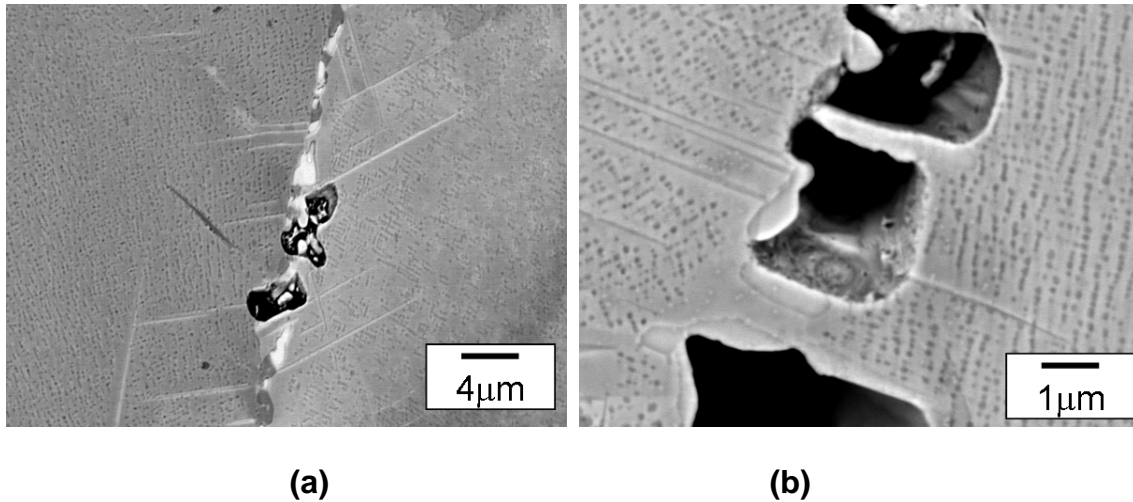
Figure 2-7 Example of grain boundary cavities from BSE images in: (a) smooth bar creep-rupture test after 20,789.4 hours rupture (180 MPa) and (b) modified Bridgeman notch test after 7217.7 (320 MPa).

Discussion

Creep-rupture

The smooth bar time to rupture and rupture ductility data show that alloy 740 has good creep ductility that is insensitive to test conditions at 1023K (750°C). The only 'lower ductility' failure which occurred at the highest stress level appears to correlate with a change in fracture mode from grain boundary cavitation to wedge cracking. The high stress and short-time of the test may have favored crack propagation over cavitation leading to a modest change in rupture ductility, as measured by reduction of area.   Over the range of test conditions, the power law exponent did not change, indicating no change in creep mechanism during testing.

Engineering structures and components are normally subjected to complex multiaxial loading states, and as such, the basic creep-rupture test (smooth bar in this study) may be inadequate since it does not account for multiaxial effects [10]. It is well known that multiaxial creep-rupture life "depends on the synergism of deformation and fracture, [11]." To assess the notched bar rupture life and ductility, the stress state in the notch during steady-state creep can be obtained from procedures in the European Code of Practice [12] which utilizes skeletal stress concepts not requiring detailed finite element analysis.   To implement this, the Von Mises or effective stress (σ_{VM}), the mean stress (σ_m), and the maximum principle stress (σ_1) were all estimated from the specimen geometries and the net section stress (σ_{net}) using the analytical procedures in the code. They are included in Table 2-3 for the two notched specimens in this study. The skeletal stress values calculated for the modified Bridgeman notch were found to

be comparable to average constraint factors developed by Marriott and Carter for creep of modified notched bars [13].

Table 2-3 Normalized stress ratio's obtained for notched bars in this study (from procedures in ref. [12].)

	σ_{VM}/σ_{net}	σ_m/σ_{net}	σ_1/σ_{net}	σ_m/σ_{VM}	σ_1/σ_{VM}
ASTM V	0.65	0.95	1.37	1.46	2.11
Mod. Bridgeman	0.70	0.70	1.10	1.03	1.65

A number of different multiaxial stress rupture criteria (MSRC) have been established to empirically relate uniaxial rupture data to multiaxial rupture data. The first is generally credited to Sdobyrev [11,14], who in 1958 proposed that cavity nucleation is governed by the effective von Mises stress (σ_{VM}) and that cavity growth is determined by the maximum tensile (principle) stress (σ_1). Under these conditions, a single material dependent term, α (originally λ) can be used to describe creep failure according to the condition:

$$\sigma_{MSCR} = \alpha\sigma_1 + (1-\alpha)\sigma_{VM}$$

(Equation 1)

Figure 2-8 compares the smooth bar rupture data to that for the notched bars for various stresses: σ_{net}, σ_1, σ_{VM}, and σ_{MSCR} with $\alpha=0.09$. Clearly, the maximum principle stress does not adequately describe the creep strength relationship for the uniaxial and multiaxial stress states. The von Mises effective stress is a relatively good match, but Equation 1 with an $\alpha=0.09$ is found to give the best convergence of the data. This suggests mixed-mode creep failure in alloy 740 with cavity initiation (not cavity growth) as the dominate mode.
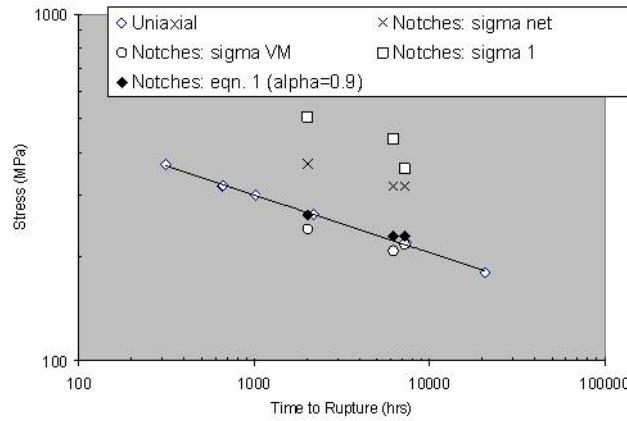
Figure 2-8 Analysis of notched bar rupture life showing how the multiaxial stress rupture criteria (MSCR) in equation 1 with a value of α (alpha) = 0.09 (solid diamonds) correlates with the smooth bar rupture data (Uniaxial) and compares with the net section stress (sigma net), Von Mises (sigma VM) effective stress, and the maximum principle stress (sigma 1) calculated for the notched bars.

The smooth bar creep ductility was insensitive to test conditions below 320MPa, but the reduction of area measurements in the notched bars were lower by a factor of ~5 compared to the smooth bars. To evaluate the effect of the stress-state on multiaxial ductility, the true strain at failure (as measured by reduction of area) of each test was normalized by dividing it by the average true strain at failure for the uniaxial tests. Figure 2-9 shows how these normalized strains vary with σ_m / σ_{VM}, the ratio of the mean normal stress $\sigma_m = (\sigma_1 + \sigma_2 + \sigma_3)/3$ stress to the von Mises effective stress. Manjoine has proposed that multiaxial effects are often well-described by a triaxiality factor (TF) defined by this ratio [15], that is:

$$TF = \frac{\sigma_1 + \sigma_2 + \sigma_3}{\sqrt{\dfrac{(\sigma_1 - \sigma_2)^2 + (\sigma_2 - \sigma_3)^2 + (\sigma_3 - \sigma_1)^2}{2}}} \qquad \text{Equation (2)}$$

where σ_1, σ_2, and σ_3, are the principle stresses. He also proposed that in the case of 'ductility exhaustion,' where the material has sufficient ductility to relax peak stresses, the strain limit for multiaxial failure would be the strain limit in simple tension divided by the TF, or:

$$\frac{\varepsilon_{true}^{Multiaxial}}{\varepsilon_{true}^{Uniaxial}} = \frac{1}{TF} = \frac{\sigma_{VM}}{3 \times \sigma_m} \qquad \text{Equation (3)}$$

26
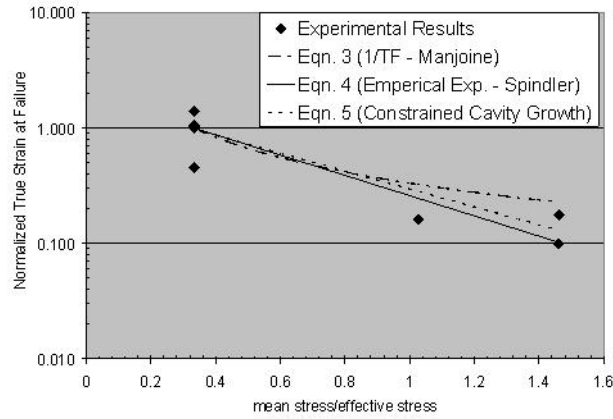
Figure 2-9 Effect of multiaxiality on rupture ductility for notched bar tests

Spindler proposed an empirical model for rupture ductility under multiaxial stress states for austenitic stainless steels which is given by:

$$\frac{\varepsilon_{true}^{Multiaxial}}{\varepsilon_{true}^{Uniaxial}} = \exp(p(1-\frac{\sigma_1}{\sigma_{VM}}) + q(\frac{1}{2} - \frac{3}{2}\frac{\sigma_m}{\sigma_{VM}}))$$ Equation (4)

where p and q are constants with values of approximately 0.15 and 1.25, respectively [16]. Spindler et al. considered theoretical descriptions of constrained cavity growth modified by a nucleation term and concluded that under these conditions [17]:

$$\frac{\varepsilon_{true}^{Multiaxial}}{\varepsilon_{true}^{Uniaxial}} = \frac{2\sigma_1}{3(\sigma_1 - \sigma_m)} \times \left(\frac{\sigma_{VM}}{\sigma_1}\right)^{(1+2.75)}$$ Equation (5)

Equations 3, 4, and 5 have been plotted for comparison to the experimental data in Figure 2-9. Good agreement is generally found between all the models and the experimental data, with increasing multiaxiality significantly reducing the rupture ductility. Based on the limited experimental data, Spindler's equation developed for stainless steel is the best description for alloy 740, and Manjoine's triaxiality factor approach is slightly non-conservative. The observation that there is a weak dependence of the rupture life on the maximum principle stress is consistent with this since Manjoine's theory is based on ductility exhaustion which assumes no void growth (no effect of principle stress). Overall, it can be concluded that the observed rupture ductilities of the notched bars are within the expectations of all the models. Furthermore, alloy 740 is 'notch tough', displaying significant notch strengthening on the rupture life.

Microstructure

Figure 2-10 shows the precipitate phases (the gamma matrix phase is not included) as a function of temperature as predicted from thermodynamic calculations (JMatPro™). At 1023K (750°C), the testing temperature, the volume percent of the MC carbide phase (where M=metal ion and C=carbon), eta phase, and gamma prime are 0.28%, 2.32%, and 16.98%, respectively. SEM observations of creep tested specimens identified eta phase and gamma prime (depending on test condition), but the MC was not evaluated. Additionally, $M_{23}C_6$ and the G-phase, which was not included in the thermodynamic database, were observed on grain boundaries. The figure shows that $M_{23}C_6$ is a predicted phase at slightly lower temperatures {~1000K (~730°C)}, and the sigma phase, the only other precipitate with high levels of chromium, is also predicted at lower temperatures, although it has not been observed [7, 8, 18].
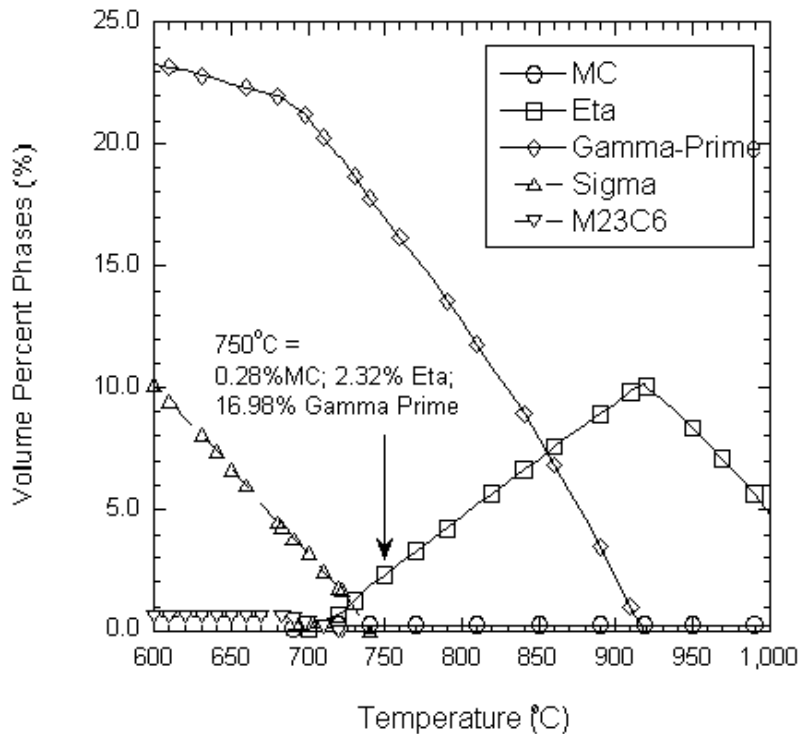
Figure 2-10 Phases as a function of temperature for alloy740 based on thermodynamic calculations using JMatPro™ version 4.0 with the Ni database [9].

A number of important observations can be made by examination of figure 2-5 in relation to the thermodynamic calculations. First, a precipitate free zone or gamma prime denuded zone forms around the grain boundaries after ~680 hours and persists throughout testing. Grain boundaries decorated with $M_{23}C_6$ and the

G-phase will deplete the adjacent matrix of elements including: Cr, C, Nb, Si, and Ti. Nb and Ti are elements that are incorporated in the gamma prime phase in alloy 740 [6], and their reduction may reduce the local stability of the gamma prime. A gamma prime denuded region consisting of only a gamma matrix will be much weaker than the grain interior which is strengthened by the well-known creep strengthening effect of gamma prime [19]. Analysis of the notched-bar creep data shows that the rupture behavior is controlled by the effective stress, which requires grain boundary sliding (cavity initiation). This suggests that the precipitate free zones adjacent to the grain boundaries lead to creep deformation consistent with observed notched bar creep behavior.

The second observation is the formation of the eta phase platelets. Figure 2-5 clearly shows that the eta phase precipitates form on grain boundaries after an incubation period and then grow into the grain interior as a function of time. To better understand the role the eta phase may play in determining the creep strength and ductility of alloy 740, quantitative analysis was conducted to determine its extent. Figure 2-11 is a plot of the area fraction of the eta phase as a function of rupture time for the gauge section (high stress) and shoulder (low stress) of the creep-rupture specimens. The eta phase was observed after ~680 hours in the specimen gauge but not until ~1000 hours in the specimen shoulder, suggesting a weak effect of applied stress on its formation. The stress may reduce the kinetic driving force necessary for precipitation or may enhance matrix diffusion as the eta phase precipitates at the expense of the gamma prime. The former appears to be more likely because, as shown in figure 2-12, the growth of the eta phase platelets, plotted as average eta phase length as a function of time to rupture, did not vary significantly between the shoulder and the gauge. Inspection of figure 2-11 shows that the area fraction of eta phase after ~20,000 hours is 1.6% to 3.3%, depending on location, with the thermodynamic prediction of 2.32 vol% in the middle of this range. Thus, after ~20,000 hours of creep at 1023K (750°C), alloy 740 approaches the predicted equilibrium microstructure, suggesting that longer-term data extrapolation may be possible.
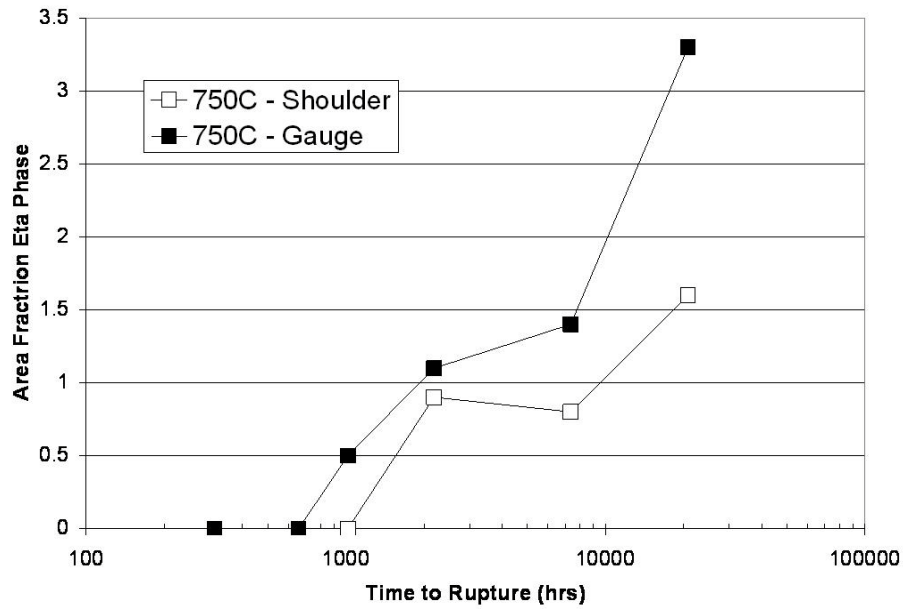
Figure 2-11 The area fraction of eta phase measured from the shoulder and gauge section of creep tested specimens (after rupture).
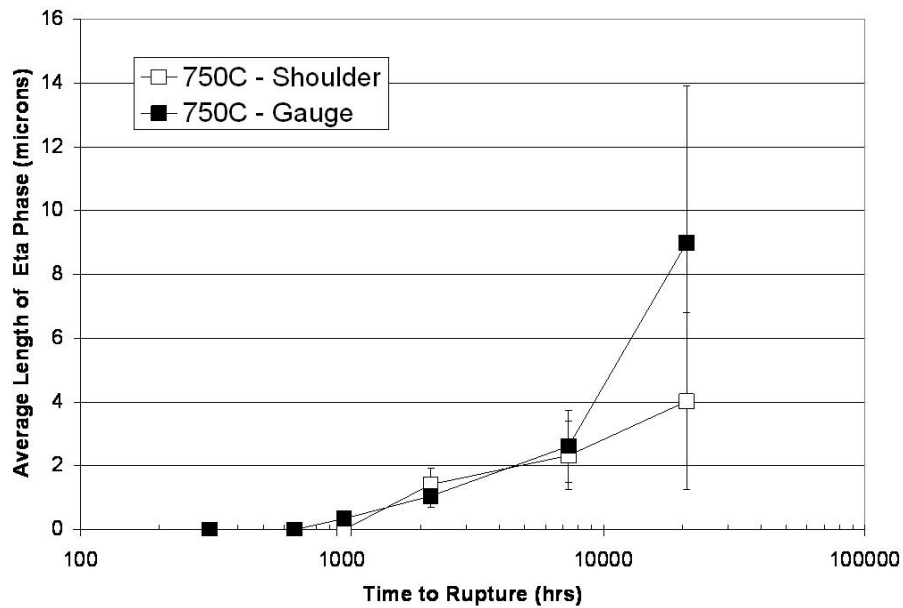
Figure 2-12 Average length of the eta phase after creep-rupture testing as a function of rupture time for both the shoulder (low-stress) and gauge (high-stress) regions of the sample. The scale bars are one standard deviation.

Role of eta phase and creep-rupture

The microstructural results clearly show that small but appreciable amounts of eta phase form in alloy 740 after only a few thousand hours and reach equilibrium concentrations after ~20,000 hours. However, during this time, no change was observed in the creep mechanism or rupture ductility. Furthermore, no divergence in rupture life was observed at longer-times. This is in contrast to other studies of alloy 740 [6,7,8,18] which suggest that eta phase formation will effect the long-term creep strength by reducing the amount of gamma prime in the alloy. Investigations of iron and nickel-based superalloys report that the eta phase is 'sometimes' a primary strengthening precipitate [20]. Studies which showed possible creep strengthening effects due to eta phase include those of Remy et al. on Fe-Ni superalloy 706 [21] and Gu et al. on modified alloys based on Udimet 720Li [22]. On the other hand, the eta phase observed in creep studies of Nimonic 263 [23] and superalloy castings [24] seemed to have no effect on the creep behavior. Sun et al. suggested that phosphorus additions to GH761 (a wrought nickel-based superalloy) 'lowered the stability of gamma prime, and eta preferentially formed reducing stress-rupture life,' but few data were presented to support this conclusion, and little change was observed in post-test elongation [25]. No quantitative data were furnished on eta phase formation, growth, or volume fraction in any of these studies.

In addition to the quantitative microscopy, the notched bar rupture and ductility analysis indicates that the gamma prime denuded regions probably play an important role in the creep deformation and failure of alloy 740. Muller and Rosler studied creep crack growth in alloy 706 and found that the creep-crack growth resistance increased (growth rate decreased) with heat-treatments that caused precipitation of eta phase platelets extending into the grains, but when 'film-like' eta phase formed on the grain boundary and grew in a direction parallel along the grain boundary, the resistance decreased [26]. In this work, the formation of the eta phase, which elongates away from the grain boundary and into the grains, does not adversely affect the creep ductility. If creep strain is greatest in the grain boundary gamma prime denuded regions, then the formation of eta phase platelets across these regions may in fact be beneficial to creep strength and ductility by providing an obstacle to grain boundary sliding and preventing cavity growth. Isolated microstructural evidence of such an effect is observed in Figure 2-7.

Summary and Conclusions

A study was conducted on INCONEL® alloy 740 to examine its creep strength and ductility at 1023K (750°C). This is the first study, based on the authors' knowledge, for any iron or nickel-based alloy which quantitatively shows that precipitation of the eta phase does not reduce the creep-rupture strength or ductility. Specific findings include:

1. There is no change in creep mechanism up to ~20,000 hours of testing time.
2. Creep fracture is controlled predominately by grain boundary cavitation, resulting in rupture ductilities that are independent of test time.
3. The rupture ductility in notched bar specimens that have different multiaxial stress states was found to be in good agreement with theoretical and empirical models.
4. After ~20,000 hours, the measured eta phase area fractions were consistent with thermodynamic equilibrium calculations, suggesting that the data generated in this study may be used for long-term rupture strength prediction.
5. Applied stress had a minor effect on eta phase precipitation and no effect on eta phase growth rate.
6. The formation of a small amount of eta phase, 2 to 3%, did not affect creep strength or ductility

Considering all these findings, it appears the precipitate free gamma prime denuded region adjacent to grain boundaries plays in important role in the creep deformation of the alloy, and that eta phase precipitates, which extend from grain boundaries across the gamma prime denuded regions, may be beneficial to creep strength and ductility.

Chapter 2 References

1. R. Viswanathan, R. Purgert, U. Rao: Materials for Advanced Power Engineering 2002, Proceedings Part II, Forschungszentrum Julich GmbH, 2002. pp. 1109-1129

2. R. Viswananthan, J.F. Henry, J. Tanzosh, G. Stanko, J. Shingledecker, B. Vitalis, R. Purgert: J. .Mater. Eng. Perform., 2005, 3., Vol. 14., pp. 281-292

3. J.P. Shingledecker, I.G. Wright: Proceedings to the 8th Liege Conference on Materials for Advanced Power Engineering 2006, Forschungszentrum Jülich GmbH, 2006, pp. 107-120.

4. G.D. Smith, H.W. Sizek: Proceedings to Corrosion 2000, Paper 00256 ©2000 NACE Int.

5. "Inconel ® alloy 740." SMC-090 © Special Metals Corporation, 2003 (Feb 03)

6. N.D. Evans, P.J. Maziasz, R.W. Swindeman, G.D. Smith: Scr. Mater., 2004, Vol. 51. pp. 503-507.

7. S. Zhao, X. Xie, G.D. Smith, S.J. Patel: Mater. Sci. and Eng., 2003, Vol. A355, pp. 96-105.

8. X. Xie, S. Zhao, J. Dong, G.D. Smith, B.A. Baker, S.J. Patel: Mater. Sci. Forum, 2007, Vols. 561-565, pp. 471-476.

9. N. Saunders, A.P. Miodownik, J.-Ph. Schille : J. Mater. Sci. 2004, Vol. 29, pp. 7237-43.

10. B.W. Roberts: ASM Handbook. Vol. 8 Mechanical Testing. ASM International, 1995, pp. 343-345.

11. J.M. Church, J.M. Brear, D.R. Humphrey: Key Eng. Mat., 2000, Vols. 171-174, pp. 61-68.

12. G.A. Webster, S.R. Holdsworth, M.S. Loveday, K. Nikbin, I.J. Perrin, H. Purper, R.P. Skelton, M.W. Spindler : Fatigue Fract. Eng. Mater. Struct., 2004, Vol. 27, pp. 319-342.

13. D.L. Marriott, P. Carter.: Proceedings of PVP2005, 2005, PVP2005-71419.

14. R.J. Browne, D. Lonsdale, P.E.J. Flewitt.: J. Eng. Mat. Tech., 1982, Vol. 104, pp. 291-296.

15. M.J. Manjoine: Trans. ASME, April 1975, pp. 156-161.

16. M.W. Spindler: Fatigue Fract. Eng. Mater. Struct., 2003 Vol. 27, pp. 273-281.

17. M.W. Spindler, R. Hales, R.P. Skelton, Proceedings of the 9th International Conference on Creep and Fracture of Engineering Materials and Structures, ed. J.D. Parker, IOM London, UK, 2001.

18. X. Xie, S. Zhao, J. Dong, G.D. Smith, B.A. Baker, S.L. Patel: Proceedings of the 5th International Conference on Advances in Materials Technology for Fossil Power Plants. (Marco Island, FL, Oct. 3-5, 2007) © 2008 Electric Power Research Institute, 220-230.

19. F.R.N. Nabarro, H.L. de Villiers. : The Physics of Creep. © Taylor & Francis Ltd 1995, pp. 187-190.

20. M.J. Donachie, S.J. Donachie: Superalloys A Technical Guide. ASM International, Materials Park, OH, 2002, pp. 25-27.

21. L. Remy, J. Laniesse, H. Aubert: Mater. Sci. Eng., 1979, Vol. 38, pp. 227-239.
22. Y.F. Gu, H. Harada, C. Cui, D. Ping, T. Fukuda, J. Fujioka: Proceedings of the 7th International Charles Parsons Turbine Conference, 2007.
23. Y.H. Zhang, D.M. Knowles: Mater. Sci. Technol., August 2002, Vol. 18. pp. 917-923
24. X.Z. Qin, J.T. Guo, C. Yuan, C.L. Chen, H.Q. Ye.: Metall. Mater. Trans. A., December 2007, Vol 38A, pp. 3014-3022.
25. W.R. Sun, S.R. Guo, D.Z. Lu, Z.Q. Hu: Metall. Mater. Trans. A. March 1997, Vol. 28A,. pp. 649-654
26. S. Muller, J. Rosler.: Proceedings of the 5th International Charles Parsons Turbine Conference; Cambridge, UK 3-7 July 2000. pp. 444-458.

3. TESTING AND ANALYSIS OF FULL-SCALE CREEP-RUPTURE EXPERIMENTS ON INCONEL ALLOY 740 COLD-FORMED TUBING

This chapter is the original work of the author and has been formatted to conform to the thesis requirements. No changes, other than editorial corrections and placement of tables and figures to aid the reader, have been made.

Abstract

Full-scale pressurized creep-rupture tests were conducted on Inconel ® alloy 740 cold-formed tube bends to evaluate the effect of cold-work on the performance of tube bends for high-temperature creep applications. A new method of analysis is developed that can be used to simplify the complexities of structural (geometric) effects and material degradation due to cold-work. Results show that Inconel ® alloy 740 behaves similarly to other age-hardenable nickel-based alloys subjected to cold-work prior to creep testing with large reductions in rupture life and ductility and a corresponding moderate increase in minimum creep rate. The results also demonstrate that the full-size test method can be a beneficial to understanding the performance of large components in service.

Introduction

Power steam boiler superheater and reheater components operate at temperatures and pressures where creep is the dominant deformation mode, and the fabrication of these components often involves extensive cold-bending of tubing. Because material creep behavior can be negatively affected by cold work, the ASME Boiler and Pressure Vessel Code imposes strain limits for forming without a post-bending heat-treatment that depend on the material, operation temperature, and strain level [1]. The limits are based primarily on field experience. In order to use new materials in boiler design, one method to evaluate the long-term performance of cold-formed tube bends is to conduct full-size pressurized creep-rupture experiments on fabricated bends [2]. The advantages of conducting full-scale tests are that strain gradients produced by forming are accounted for in the test, the complexity of creep stress redistribution and damage development is realistically reproduced, and the results can be applied directly to real components. The disadvantage is that it is difficult to separate out the effects of multiaxial creep loading and changes in material creep

behavior due to cold work. Thus, the primary objective of this study is to develop a simplified analysis method to accomplish this.

The material we have chosen to investigate is the age-hardenable nickel-based alloy Inconel ® 740, hereafter referred to as alloy 740. This material is a prime candidate for the highest temperature superheater and reheater components to be used in Advanced Ultrasupercritical (A-USC) steam cycles with operating steam temperatures up to 760°C. Such materials will help to increase efficiency and decrease emissions of all effluents (including CO_2) in coal-fired power plants by up to 25% over current technology [3,4]. However, very little is known about the effect of cold-work on creep in the alloy [5]. Therefore, full-scale pressurized creep-rupture tests were utilized to assess the practical forming limits of the alloy and develop an improved understanding of its creep behavior in the cold-worked condition.

Background – Cold-work and creep of nickel-based alloys

For nickel-based materials subjected to plastic deformation (pre-strain) prior to creep, creep-rupture life may increase or decrease depending on the alloy system [6]. Age-hardenable nickel-based alloys of composition similar to alloy 740, which are primarily strengthened by the precipitation of gamma prime, all display significant decreases in rupture life and rupture ductility and a small increase in minimum creep-rate when subjected to prior cold plastic deformation with pre-strain levels between 0.35-25% [7-13]. The reduction in creep ductility and rupture life is due to a marked increase in cavity density in the pre-strained material as compared to un-strained material [7,11]. Research shows that very fine (submicron size) cavities are formed on grain boundaries during cold deformation [8] and in some cases are associated with grain boundary particle microcracking [9] or particle matrix interface separation [13]. In general, the density of pre-strained cavities is greatest on grain boundaries parallel to the applied pre-strain stress, but creep cavitation occurs on grain boundaries normal to the axis of the applied creep stress. Torsional creep experiments designed by Dyson and co-workers showed that when the creep stress was applied on the axis orthogonal to the applied tensile stress, a larger reduction in creep life and ductility was observed compared to applying the pre-strain and creep stress in parallel direction [8]. This is important in consideration of tube bend performance because the stress due to the applied pressure (hoop stress) is normal to the applied bending (cold-strain) stress. The reduced creep resistance (increase in creep rate) has been found to be independent of cavitation and may be attributed in an increase in mobile dislocation density [7,10]. Only one limited study is reported on Inconel ® alloy 740 which showed the rupture life was reduced by half when pre-strain was 7.5% [11].

Experimental Procedure

Alloy 740 tubes and cold-formed tube bends with a nominal 50.8mm diameter (dia.) and 10.2mm wall thickness and a measured composition of (wt%): Ni-0.03C-0.28Mn-0.42Fe-0.54Si-24.43Cr-0.94Al-1.81Ti- 20.00Co-0.55Mo-1.98Nb-0.0030B-(S<0.001-P<0.005) were provided by Foster Wheeler Development Corp. Tensile creep specimens (un-strained) were machined from the tubes with a 6.35mm gauge dia. and 31.75mm gage length, aged at 1073K (800°C) for 16 hours, and uniaxial creep tests were conducted at 1073K (800°C) in accordance with ASTM E139. Tubes in the solution annealed condition were bent using conventional boiler tube bending equipment at room temperature to nominal radii of 171.5mm, 127mm, and 76.2mm.

Test specimens were fabricated by sectioning the tube bends into a "J-shaped" arrangement which included the entire 180° bend and a short,~100mm, straight tube section on one end. Solid end caps (alloy 230) were welded (manual GTAW, alloy 263 filler metal) to each end of the specimen, and the tube was partially filled with 304 stainless steel balls to reduce the volume of gas needed for testing. A pressure stem was welded to the end cap which protruded through the furnace and was attached to standard high-pressure stainless steel autoclave tubing. Figure 3-1 shows the J-bend specimen during fabrication. Prior to testing, the fabricated tube bend specimens were aged for 16 hours at 1073 (800°C). Paint was used to make marks at ~25mm intervals along the extrados of the bend and straight section. Prior to testing, after predetermined intervals, and after failure, the tube diameter was measured at each mark at 0, 45, 90, and 135° around the circumference.

All specimens were tested simultaneously in a large furnace with type K thermocouples attached directly to the specimens to monitor temperature. Ar-5%He gas pressure was applied and measured individually on each specimen by an in-line pressure transducer. Testing was conducted at 1073K (800°C) +/-2K (2°C) and 485.4bar +/- 1.8 bar. Tests were interrupted periodically for strain measurement, and conducted until a through-wall leak was detected. Destructive metallographic assessments were conducted after testing utilizing optical microscopy (OM) and scanning electron microscopy (SEM). Reference [2] provides photographs of similar test specimens and the facility utilized for testing.
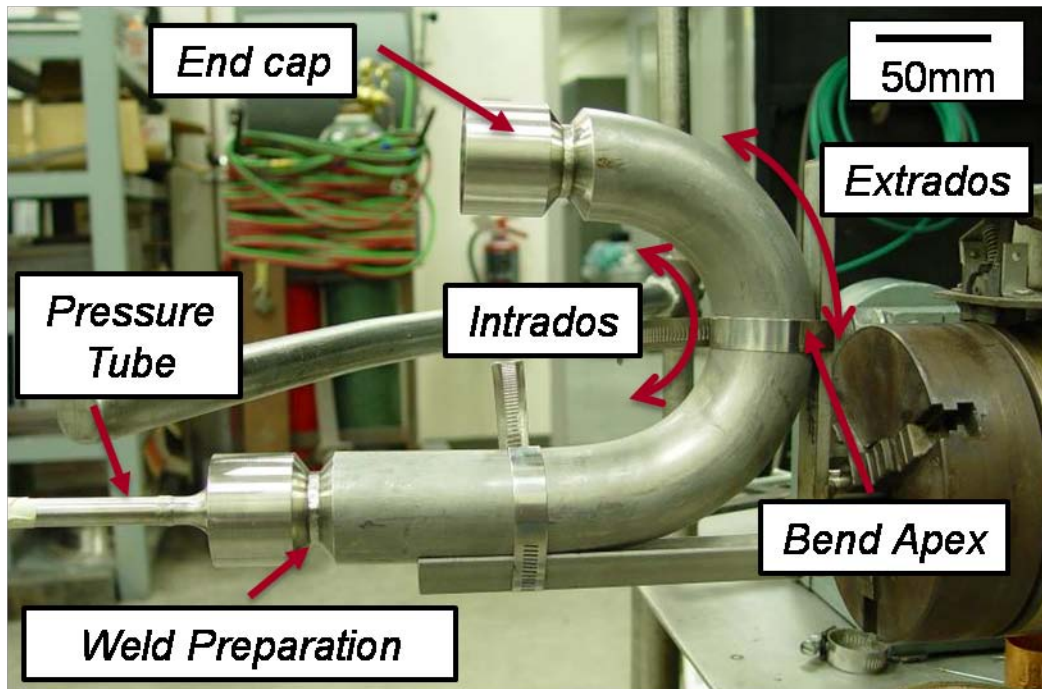
Figure 3-1 J-bend pressurized creep test specimen (35%OFS sample) during fabrication after partial welding of end caps.

Results

Tube Bends

The ASME outer fiber strain (OFS) for the bends was calculated from:

$$OFS\ (\%) = (100r/R) \qquad \text{(Equation 1)}$$

where r is the tube radius and R is the bend radius [1]. Table 3-1 provides the calculated cold-strain and time to rupture results for the tube bends. The tighter radius bends with higher cold-strain failed at shorter times compared to the bends with less cold-strain. Figure 3-2 is a macroscopic image of the extrados on the bend apex for the 35%OFS sample after rupture; extensive macroscopic cracking is clearly observed.

Table 3-1 Tube Bend Test Results

Nominal Sample Radius	Calculated OFS (Eqn 1.)	Time to Rupture (hrs)	Failure location	Macroscopic Notes
76.2mm	35%	2124.4	~60deg from extrados towards the neutral axis in bend	Extensive cracking on the extrados of the outside surface of the bend apex
127mm	25%	3711.2	Extrados, near bend apex	Extensive cracking on the extrados of the outside surface of the bend apex
172mm	15%	4991.2	Extrados, near bend apex	Extensive cracking on the extrados of the outside surface of the bend apex

Figure 3-2 Macroscopic cracking on the extrados of the 35% OFS sample near the bend apex after rupture (2124.4 hours). Sample markings are ~25mm apart; the scale is in inches (1inch=25.4mm)

Uniaxial Creep Data

Results of uniaxial creep tests on un-strained specimens conducted at 250, 180, and 130MPa are plotted with additional data from other heats of alloy 740 [14, 15] in figures 3-3, 3-4, and 3-5. A time-temperature parameter analysis of an alloy 740 uniaxial time-to-rupture, t_r (hours), database has been fit with good accuracy to [14]:

$$\text{Log}(t_r) = -C + A_1/T + A_2\text{Log}(\sigma)/T + A_3\sigma/T \qquad \text{(Equation 2)}$$

where C is the Larson-Miller constant = 19.70, A_1= 3.3095E04, A_2=-3.4551E04, A_3=-4.5335, σ is stress (MPa), and T is temperature (K). The data from this study and other heats compare well with Equation 2. The minimum creep rate data, $\dot{\varepsilon}_{min}$ (%/hr), in Figure 4 was fit to usual form [16] with a power-law (Norton) exponent of 5.3 giving:

$$\dot{\varepsilon}_{min} = 3.45\times10^{-16}\sigma^{5.31} \qquad \text{(Equation 3)}$$
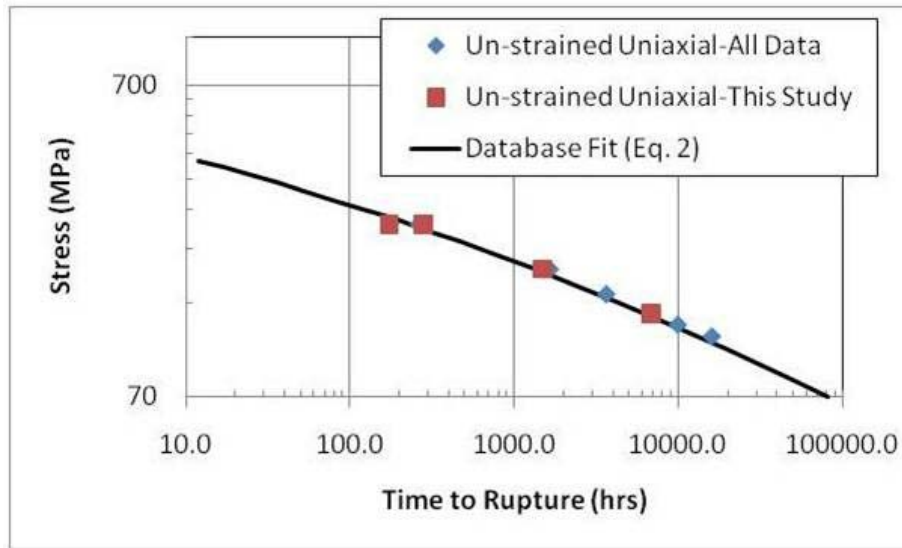
Figure 3-3 Time to rupture data at 1073K (800°C) from this study on alloy 740 tubes plotted with expected behavior from equation 2
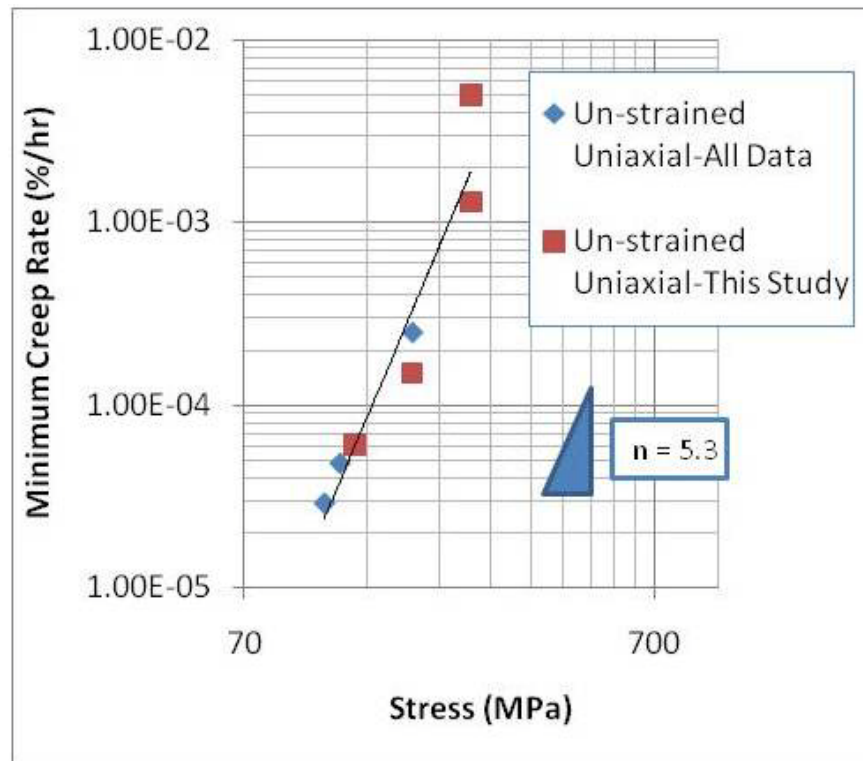
Figure 3-4 Plot of minimum creep rate as a function of stress at 1073K (800°C) for alloy 740
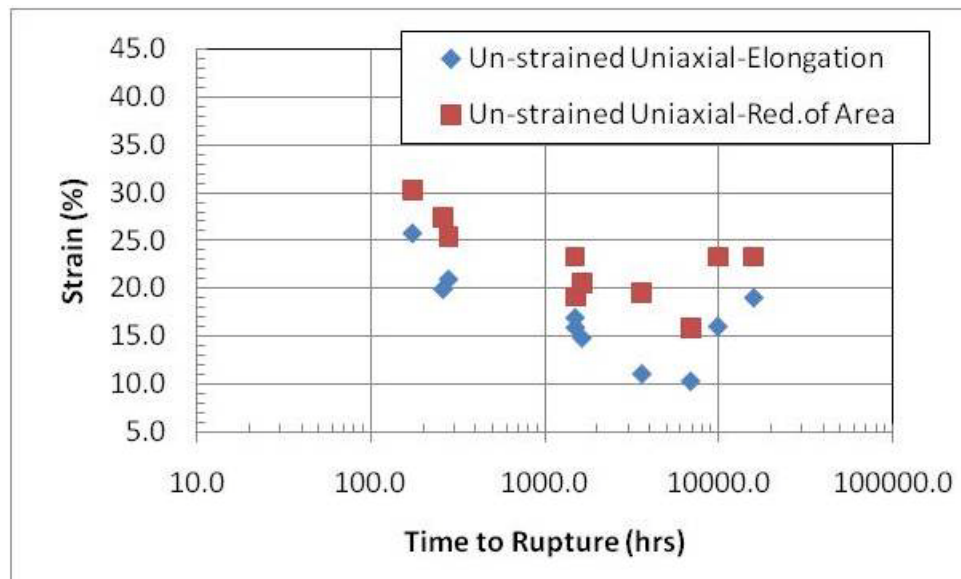
Figure 3-5 Plot of engineering strain at failure as a function of rupture time for alloy 740 at 1073K (800°C)

The elongation at failure data, Figure 3-5, was converted to true strain at failure (ε_r) and fit to the following equation for rupture times up to 7,000 hours:

$$\varepsilon_r = -0.045 \times \ln(t_r) + 0.499 \qquad \text{(Equation 4)}$$

Microstructure

Figure 3-6 is a SEM secondary electron image of the gauge section of an un-strained uniaxial specimen after creep testing to failure for 1633.6 hours. Wedge cracks and cavities are dispersed thoughout the specimen on grain boundaries perpendicular (normal) to the applied stress. Figure 3-7 is an OM image taken after failure of the 15%OFS tube bend test. The location is the bend apex at the outer diameter (OD) of the extrados. Extensive cavitation and microcracking is observed at a much higher density compared to Figure 6. The creep damage is aligned normal to the direction of the applied pressure (hoop) stress. Figure 3-8 shows this same location at a higher magnification. Cavities are primarily located on grain boundaries and in some cases twin boundaries normal to the applied hoop stress. The 25 and 35%OFS samples showed similar creep damage after testing in the same location.
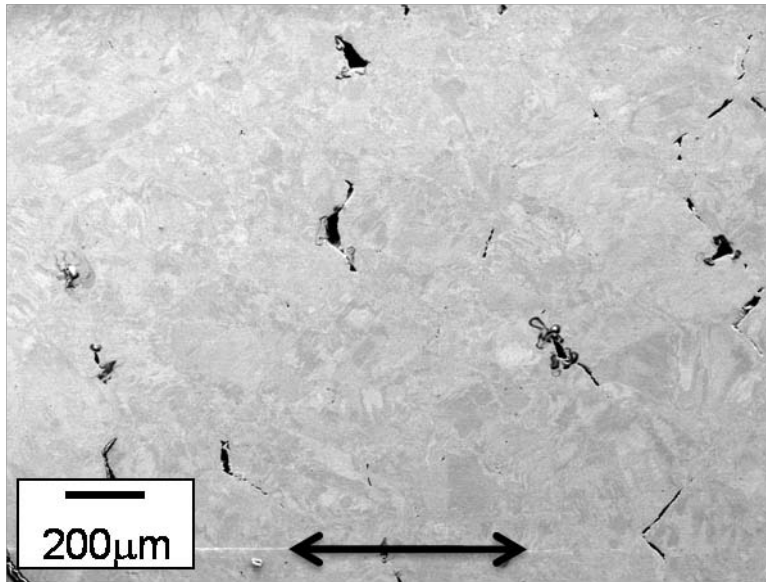
Figure 3-6 SEM secondary electron image of un-strained alloy 740 near the rupture locations after creep testing at 1073K (800°C) and 180MPa. Rupture time = 1633.6hrs; applied stress direction indicated by arrows
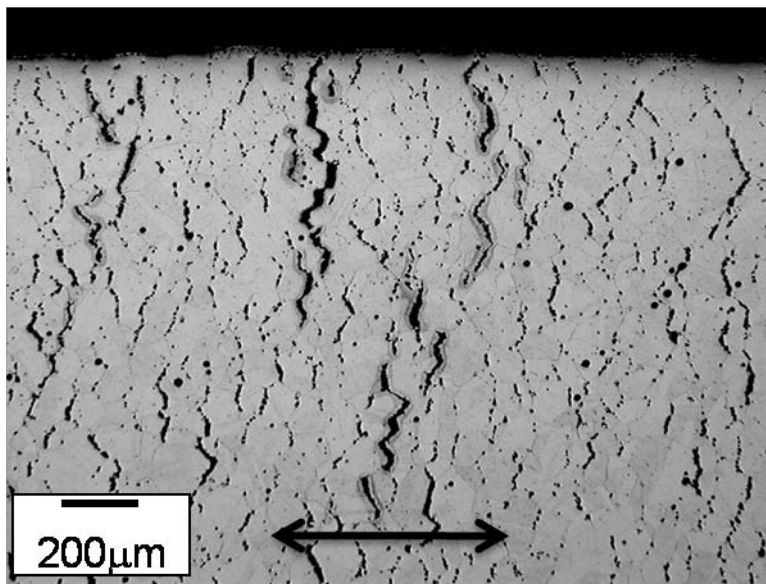
Figure 3-7 OM image of 15%OFS tube bend test near rupture the OD surface of the bend extrados at the bend apex. Rupture time = 4991.2 hrs; arrows indicate hoop stress direction
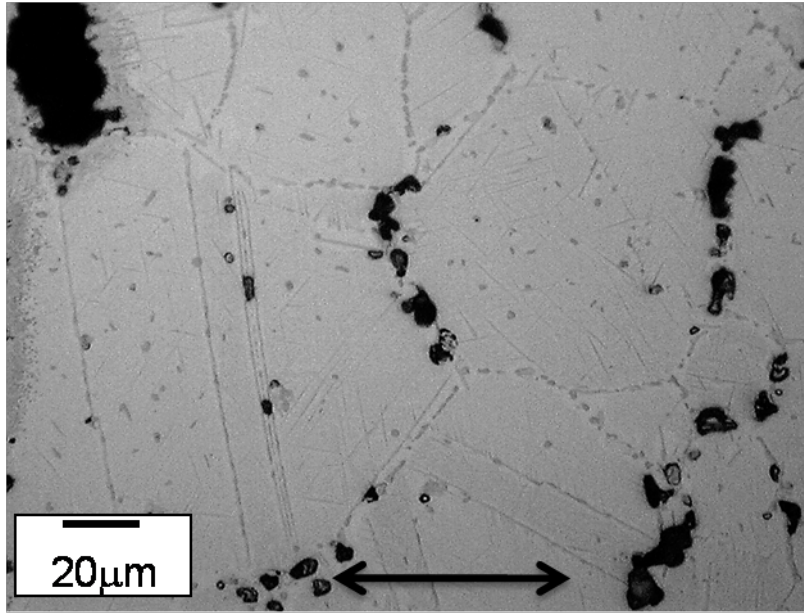
Figure 3-8 OM image showing creep cavities in the 15%OFS tube bend test near rupture the OD surface of the bend extrados at the bend apex. Rupture time = 4991.2 hrs; arrows indicate applied hoop stress direction

Figure 3-9 is a number of optical images taken around the circumference of the 15% OFS tube bend for both the OD and the inner diameter (ID). The images include the apex starting at the extrados, moving 60° radially from the extrados towards the neutral axis (90°), and at the intrados (180° from the extrados) The highest degree of cavitation and microcracking is observed at the OD of the extrados. Cavitation is found in all locations, and the 120° location (not shown) was similar to the 60° findings. In these locations most cavities are isolated, but the ID of the 60° location and the OD of the intrados showed some cavity alignment, indicating a slightly more advanced degree of creep damage. Similar evaluations conducted on the 35% and 25%OFS samples revealed that the microstructures displayed similar trends. For the 15% and 25% OFS samples, intergranular creep failure initiated on the OD and progressed via linked microcracks. Similarly, the 35%OFS sample had extensive creep damage on the extrados OD (see Figure 2), but in contrast to the other tube tests, failed at the 60° location with damage initiating on the ID.
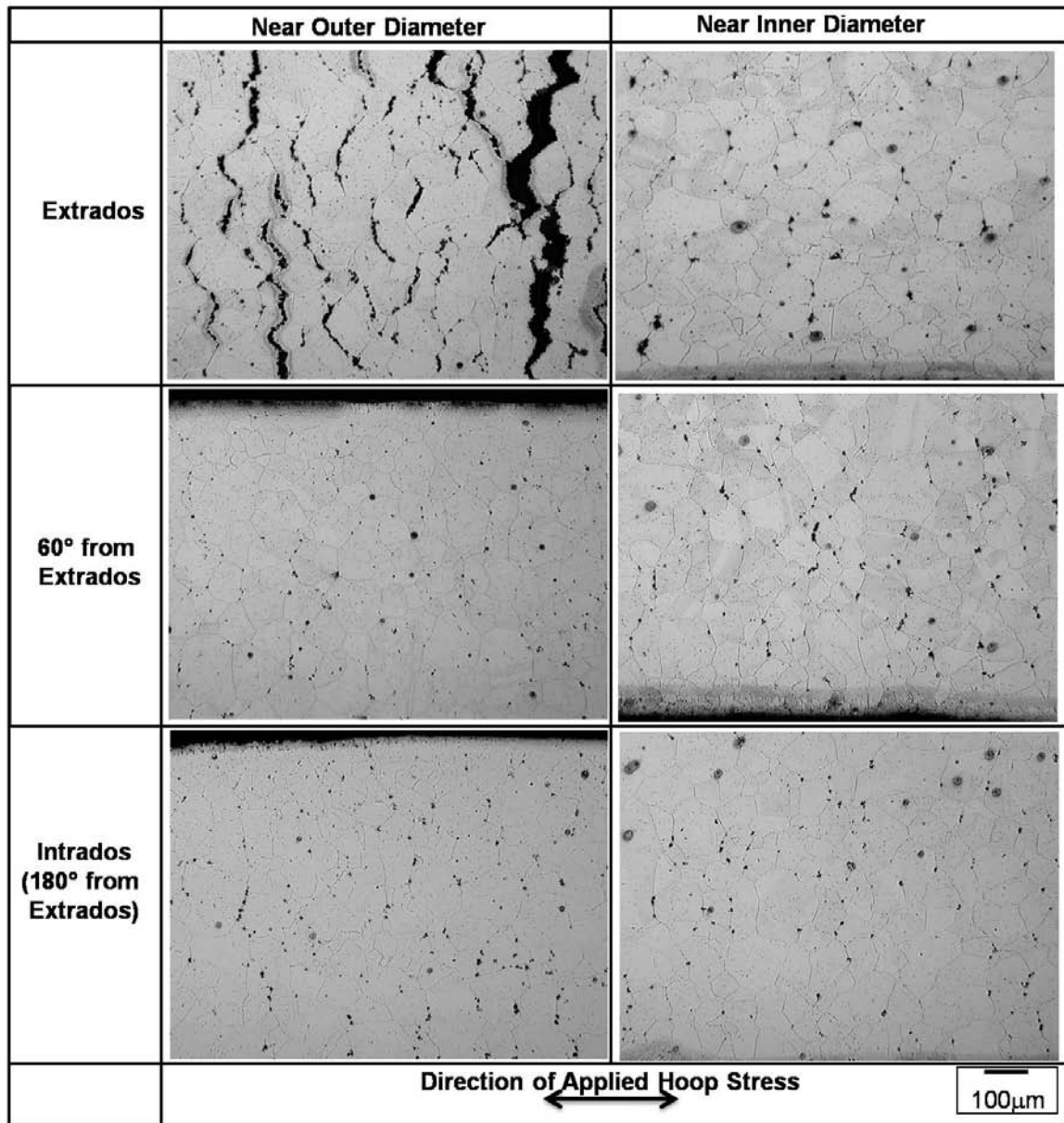
Figure 3-9 OM of locations around the circumerfenenc near the OD and ID surfaces of the 15%OFS tube bend sample at the bend apex after testing at 1073K (800°C) for 4991.2 hours.

Discussion

Analysis of Tube Bend Data

To evaluate the tube bend test results in terms of rupture life, rupture ductility, and creep deformation, several assumptions were made. For rupture life, a reference stress, which can be thought of as the 'average' stress in a component that controls creep deformation, was considered to relate the stress in the uniaxial creep test to the more complex geometry of the thick-wall tube bend. Recent work comparing large databases of pressurized straight tube creep-rupture tests have shown the one particular definition of the reference stress ($\sigma_{REF}^{StraightTube}$) for a tube under internal pressure gives good agreement over a range of tube sizes, conditions, and materials [17, 18, 19]. This definition, which has recently been adopted as an alternative for design of components in ASME boiler and pressure vessel code Section I [1], is given by:

$$\sigma_{REF}^{StraightTube} = \frac{P}{\ln(r_o / r_i)} \qquad \text{(Equation 5)}$$

where P is the internal pressure, r_o is the external radius, and r_i is the internal radius [17]. Similar methods have provided a reference stress ($\sigma_{REF}^{TubeBend}$) for a tube bend based on the tube thickness (t), the radius of the bend (a), and the mean diameter of the tube (b) given by:

$$\sigma_{REF}^{TubeBend} = \frac{Pb}{t} \frac{(1-b/2a)}{(1-b/a)} \qquad , \qquad \text{(Equation 6)}$$

although there is limited experimental data to verify its accuracy [20, 21]. The stresses calculated for the tube bends and the straight tube section are provided in Table 3-2, which shows that the stress in the bends approach the straight tube stress as bend radius increases. Figure 3-10 compares the tube bend time to rupture results with the uniaxial un-strained data, the expected behavior for alloy 740 (Eq. 2), and the minimum expected rupture life (-20% on stress). The figure shows that, even accounting for the increase in stress due to the tube geometry, the data for the tube bend failures all fall well below the uniaxial behavior and even below the minimum life. Therefore, creep life is significantly reduced in alloy 740 due to cold-straining to levels of 15% or greater.

Evaluation of creep ductility must take into account any ovality in the tube bend. Ovality was calculated based on the maximum (d_{max}) and minimum (d_{min}) diameter measurements on the OD as follows:

$$\text{Ovality (\%)} = 100 \times 2 \times (d_{max} - d_{min})/(d_{max} + d_{min}) \qquad \text{(Equation 7)}$$

Table 3-2 Tube bend test and analysis results

Sample	Stress (MPa) – Eq. 5 & 6	Time to Rupture (hrs)	Average Un-strained Uniaxial Life (hrs) -Eq. 2	OD Strain at Failure (%)	True Strain at Failure	Calculated Strain at Failure - Eq.4 x Eq. 9	OD Minimum Creep Rate (%/hr)	Calculated Uniaxial Min Creep Rate (%/hr) – Eq. 3
76.2mm–35%OFS	114.7	2124.4	10637.8	1.43	0.014	0.108	3.3e-4	3.0e-5
127mm–25% OFS	106.3	3711.2	14747.0	1.75	0.018	0.091	1.5e-4	2.0e-5
172mm–15% OFS	103.6	4991.2	16447.1	1.75	0.018	0.081	1.2e-4	1.8e-5
Average of Straight Tube Section	95.0		23638.3				1.9e-5	1.1e-5
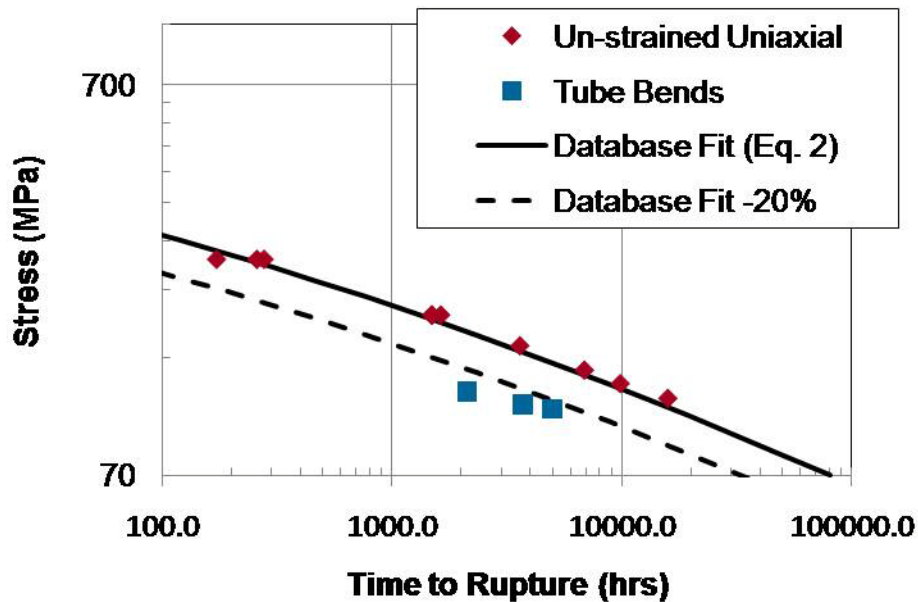
Figure 3-10 Time to rupture for tested tube bends (stress calculated from equation 6) compared to un-strained uniaxial data and minimum (-20%) data.

Since the degree of ovality may change during creep, the circumference of the oval tube, which in earlier work was only considered as a circle [2], was approximated to obtain an average strain using:

$$Circumference = \pi\sqrt{\frac{(d_{max})^2 + (d_{min})^2}{2}}$$

(Equation 8)

Figure 3-11 shows the calculated ovality and strain measurements based on Eqs. 7 and 8 for the 15%OFS sample including the bend and straight section regions. At time zero, when the OD creep strain is 0, the sample has 2 to 3 % ovality. As creep strain accumulates, the ovality decreases. The creep strain in the bend region is relatively uniform despite differences in measured ovality, presumably because creep deformation is uniform and Eq. 8 accounts for the changing ovality. At failure, the ovality in the bend is nearly zero and the scatter is the same as the straight tube section. Data from power plant piping operating in the creep regime which failed with over 100,000 hours of service showed a similar finding, that is, that ovality was reduced during operation, but did not reach zero ovality until failure [22]. Thus, the tube bend tests, although less than 5,000 hours, appear re-produce realistic long-term in-service behavior.
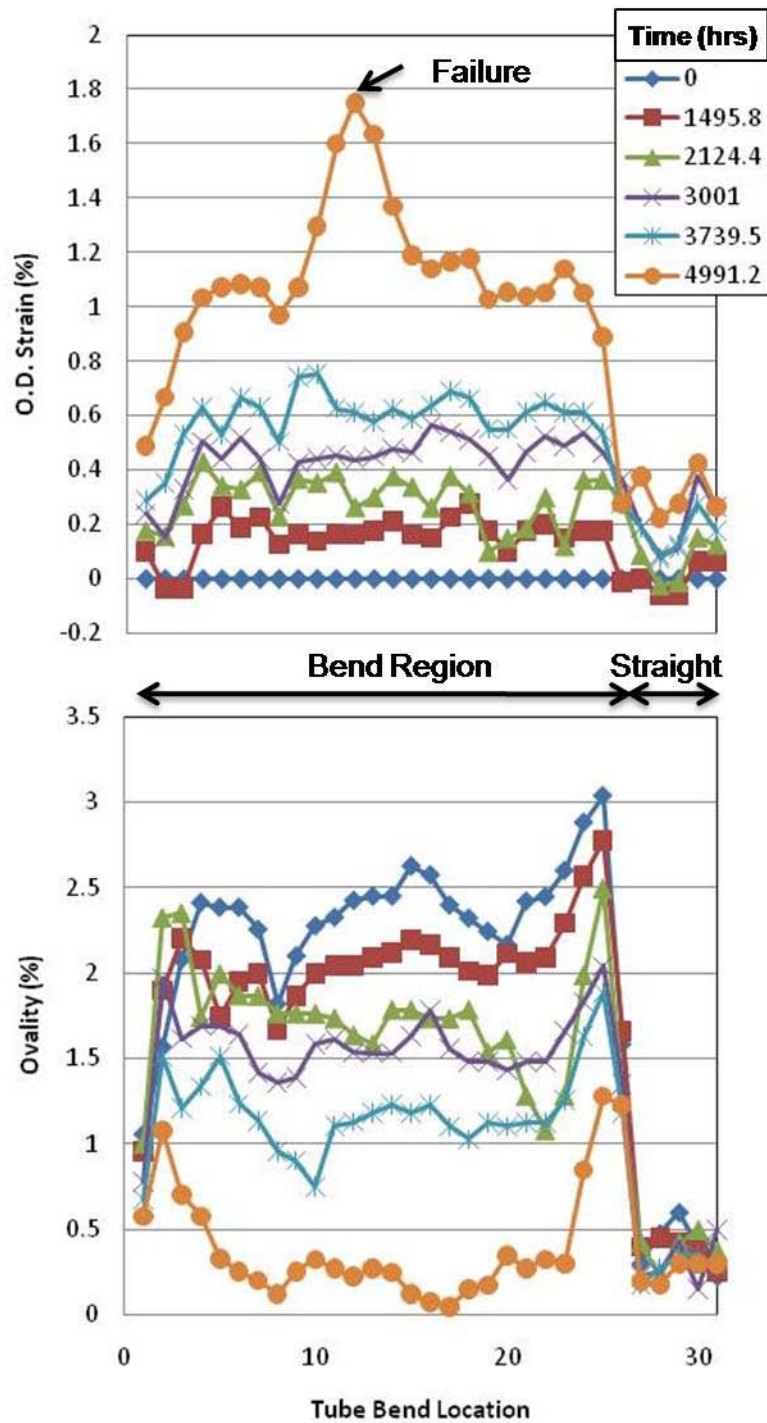
Figure 3-11 Change in ovality and measured outer diameter strain as a function of location along tube bend test specimen and with time for 15%OFS sample

To analyze the observed failures strains in Table 3-2, the effects of multiaxiality on creep were considered. Research on notched bars of alloy 740 tested at 750°C showed that ductility obeyed Spindler's equation [23, 24]:

$$\frac{\varepsilon_{true}^{Multiaxial}}{\varepsilon_{true}^{Uniaxial}} = \exp(p(1-\frac{\sigma_1}{\sigma_{VM}})+q(\frac{1}{2}-\frac{3}{2}\frac{\sigma_m}{\sigma_{VM}})) = 0.702(tube) \quad , \qquad \text{(Eq. 9)}$$

where p and q are constants (= 0.15 and 1.25, respectively), σ_1 is the maximum principle stress, σ_{VM} is the effective stress, and σ_m is the mean stress. This gives a ratio of multiaxial strain at failure to uniaxial strain at failure of ~0.70 for a tube under internal pressure. The tube geometry is considered for simplicity since the authors have no knowledge of an approximation for the principle stresses in the bend. Utilizing the relationship established for uniaxial ductility (Eq. 4) and the ratio obtained from equation 9, Table 3-2 compares the calculated strain at failure to the actual measured true strain at failure for the tube bends. These data show the tube bends failed at significantly lower ductility compared to the prediction, approximately 0.1 to 0.2 of the calculated strain at failure. Therefore, the dramatic reduction in rupture ductility of alloy 740 tube bends is primarily due to the effect of pre-strain (cold-work) and not multiaxility.

To evaluate the creep deformation, the OD strain measurements were averaged for the data collected on each bend and on each straight section. These data along with the rupture strain are plotted in Figure 3-12. The uniaxial creep tests on alloy 740 showed an increasing creep-rate (tertiary creep) with little to no primary or secondary creep typical of many nickel-based alloys. The tube 'creep-curves' in Figure 3-12 exhibit the same behavior. Since limited interrupted measurements were made on the tubes, the minimum creep rate was measured based on the first recorded datapoint, but could be slightly lower if shorter-term measurements were made. The data are reported in Table 3-2 and compared to the expected minimum creep-rate calculated from Eq. 3. The minimum creep rate for the straight section of the tube is in good agreement with the calculated uniaxial value indicating the reference stress is an appropriate approximation for the creep behavior of the structure, and the minimum creep rate based on the first OD measurement is reasonably accurate. With decreasing bend radius, the creep rate progressively increases which is consistent with increasing stress in the bend itself. However, when compared to the uniaxial expectations, the creep rates are ~6-10 times greater in the bends than the uniaxial data. Therefore, it appears cold-work does have a measurable weakening effect on creep deformation behavior of alloy 740.
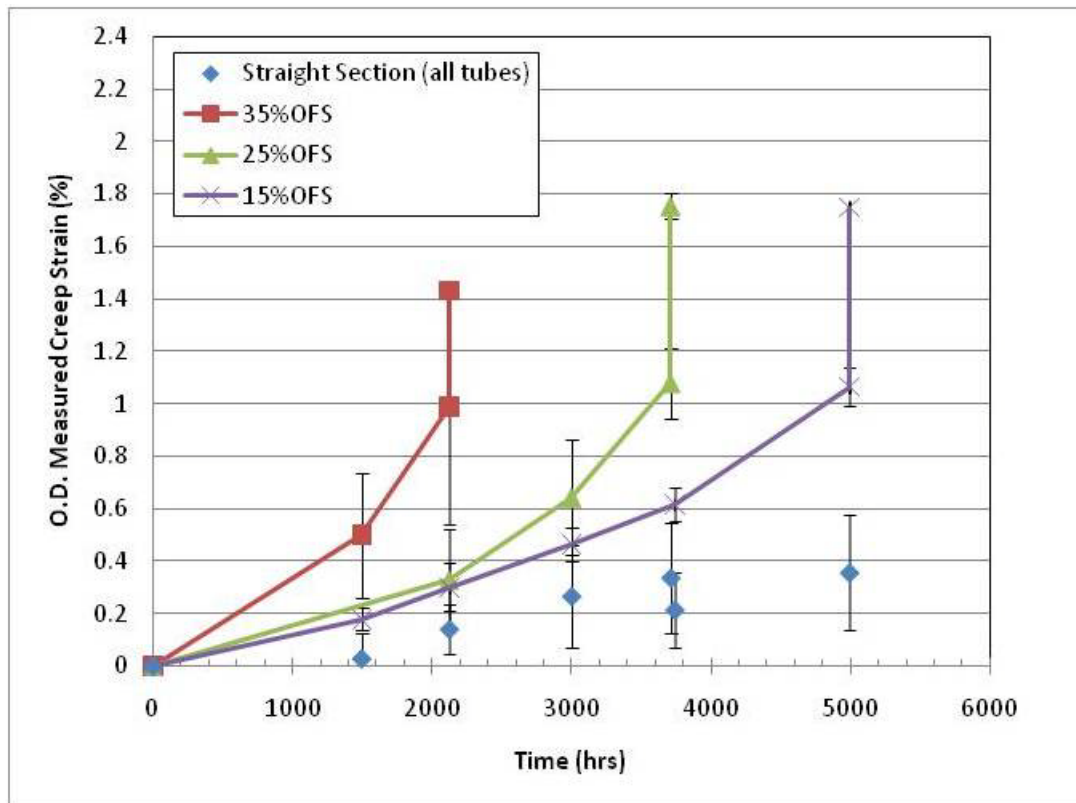
Figure 3-12 OD Creep strain as a function of time for the tube bend tests and average measurements made on the un-strained straight sections of the specimens.

Microstructure and Evaluation of Data

Extensive cavitation was noted in the region of highest strain (OD of the extrados) after creep testing in all the samples (Figure 3-6). The cavity density is much higher compared to the un-strained uniaxial tests (Figure 3-5), and cavitation is primarily on grain boundaries normal to the applied stress, which in this case is the pressure (hoop) stress. The damage is consistent with other nickel-based alloys with similar levels of gamma prime such as Nimonic 80A [7] and alloy 263 [10] which were pre-strained prior to creep. In this work, alloy 740 was cold-strained in the solution annealed condition whereas all the other reported tests induced cold-strain after the aging heat-treatment (which was used to precipitate gamma prime). The current work shows, that regardless of processing path, cold-work is detrimental to creep by greatly increasing the cavitation density.

A second important observation is the role of compressive cold-strain. Figure 3-9 shows that the region of highest compressive cold strain (OD of the intrados), which should be equal in magnitude to the OD of the extrados if bending is uniform, had significantly less creep damage that the region of highest tensile

52

cold strain. Since grain interior slip is considered to be the main source of submicron cavitation [8], and because the applied creep stress (hoop stress) was normal to the cold-strain stress, little difference should be expected. However due to conservation of volume and the type of bending utilized, the extrados of the tube bend was thicker than the intrados. Since the analysis methodology did not account for this change in thickness, the reduction in cavitation may be simply explained by a thicker wall leading to a lower stress.

The final failure location of the 25% and 15%OFS samples was in the region of highest tensile cold-strain, indicating that cold-work is a significant factor in controlling the creep life of the tube bend. Advanced damage was observed on the 35% sample in the same location, but failure initiated on the ID. There are two factors which could lead to higher stresses in this area. First, when a thick-walled tube is elastically loaded, the highest stress is on the tube ID, but during creep this stress relaxes and the highest creep stress redistributes to the tube OD [25]. Because the 35% test was the shortest in duration, the high stresses may not have fully relaxed, leading to ID damage. A second factor is the change in ovality. As the data clearly show, the creep process reduces the ovality in the tube and the strain measurements are based on an averaged circumference. However, in reality, the strain must be non-uniform, and careful inspection of the raw OD measurement data revealed that most of the creep strain accumulation was not at the intrados or extrados of the bend but rather between the two. Thus, while creep damage is unequivocally linked to the extrados where the tensile cold-strain was highest, measured creep deformation was more pronounced towards the neutral axis. The ID of the 60° location had both higher tensile cold strain and the stress redistribution due to ovality, and hence even in the longer-term test, the level of creep damage in that location is higher than other regions around the tube, expect for the area of highest cold-strain (Figure 3-8).

The analysis methodology presented in the previous section showed that the rupture life reduction, reduction in creep ductility, and increase in minimum creep rate could not be explained by geometric effects alone, but rather that prior cold-work had a significant impact on component lifetimes and creep behavior. To examine if the reductions were within expectations based on similar alloy performance, the data from references [7-13] were normalized relative to uniaxial experiments on un-strained material in the same studies. In this work, a parallel uniaxial study was not conducted, so the comparison is made between the measured property from the tube bend test and the expected or calculated property of interest from the analysis methods applied to uniaxial un-strained specimens in this work, all of which is found in Table 3-2. The OFS calculation was used as the amount of cold-work for this comparison since the results showed the creep damage was concentrated and ultimately rupture life was controlled by the location in the tube with this nominal level of strain.

Figure 3-13 is a comparison of the normalized rupture life data as a function of cold-strain. An exponential line was fit through the data from Ref.[7,8,10,11,12]. Data from IN597 [9] and Astroloy [13] were not fit because these alloys have much higher amounts of gamma prime compared to alloy 740 and the other alloys. Additionally, the research shows particle/interface cracking as a possible mechanisms leading to enhanced cavitation which is not expected since alloy 740 was formed in the annealed condition. The tube bends were not included in the extrapolation, but inspection of the figure shows the tube bend data is generally consistent with the other data. At 15% and greater cold work, the rupture life is 0.25 or less than the non-strained material and decreases with increasing cold-work. Few data are available beyond 15%, so the extrapolation is slightly conservative, but overall the tube bend analysis appears adequate for considering the effect of rupture life reduction due to cold-work in alloy 740.

Figure 3-14 shows a similar result for normalized creep-rupture ductility. Again, the tube bend analysis is generally consistent with the exponential extrapolation of similar literature data. The comparison from the tube bend analysis captures the same trend as the data and shows the reduction is approximately 0.2 to 0.1. The analysis takes into account the reduction in ductility due to multiaxial creep as well as the material behavior observed in un-strained specimens where ductility was a function of test time.

Figure 3-15 is a plot of increase in minimum creep rate as a function of material and cold-work. A linear extrapolation of the available literature data on age-hardenable nickel-based alloys shows very good agreement both in relative increase and absolute values. This suggests that alloy 740 behaves similarly to the other alloys and that the methodology presented in this work for approximating stress in the tube bends is accurate for creep prediction.
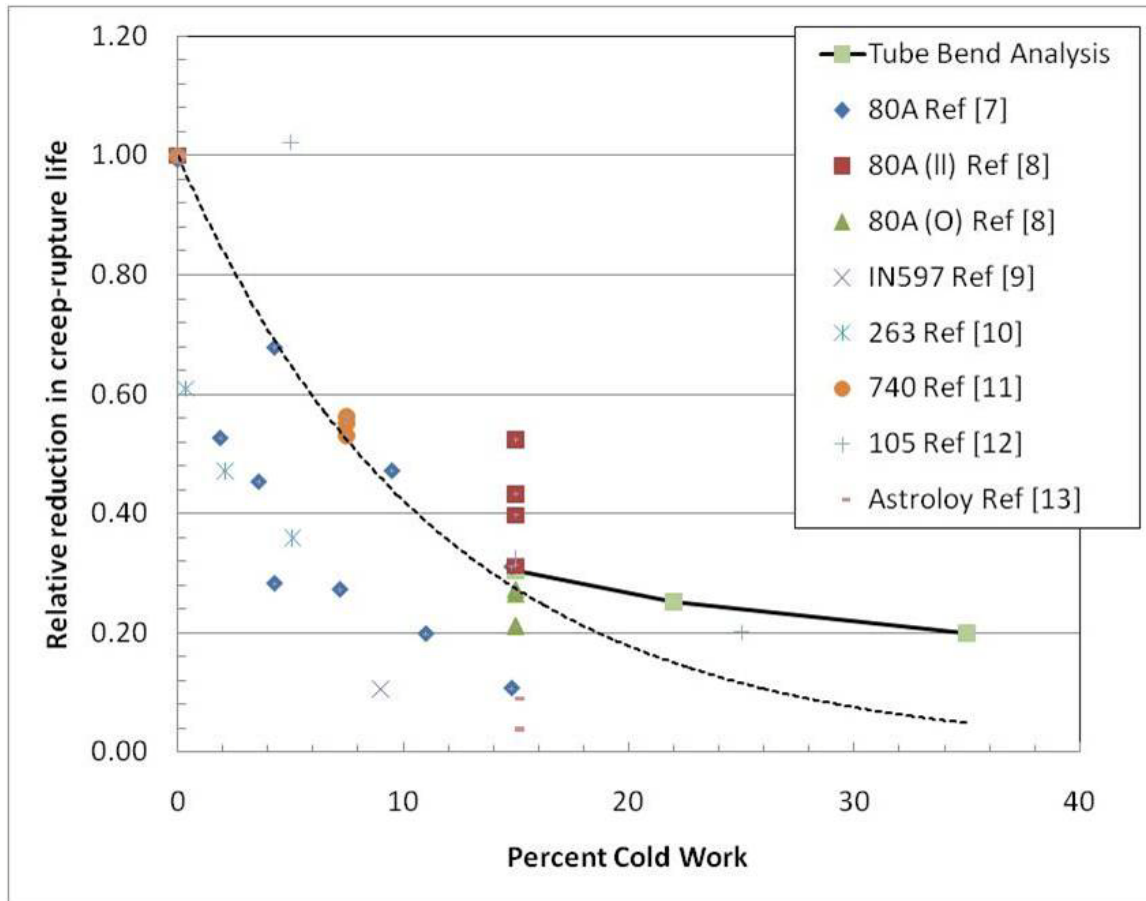
Figure 3-13 Relative reduction in rupture life for age-hardenable nickel-based alloys. The dashed line is a fit and extrapolation of references [7,8,10,11.12]. The tube bend analysis suggests similar behavior for alloy 740.
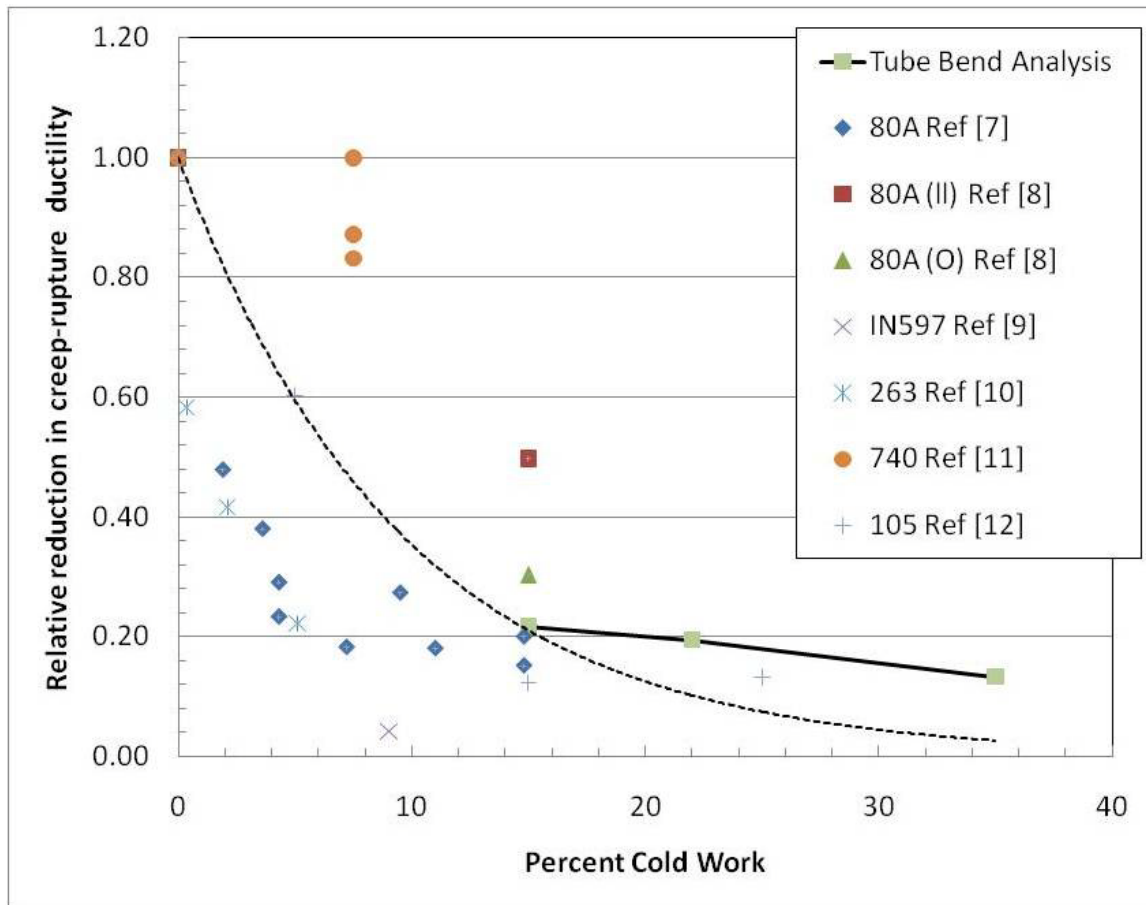
Figure 3-14 The relative reduction in creep-rupture ductility for age-hardenable nickel-based alloys. The dashed line is a fit and extrapolation of references [7,8,10,11.12]. The tube bend analysis suggests similar behavior for alloy 740.
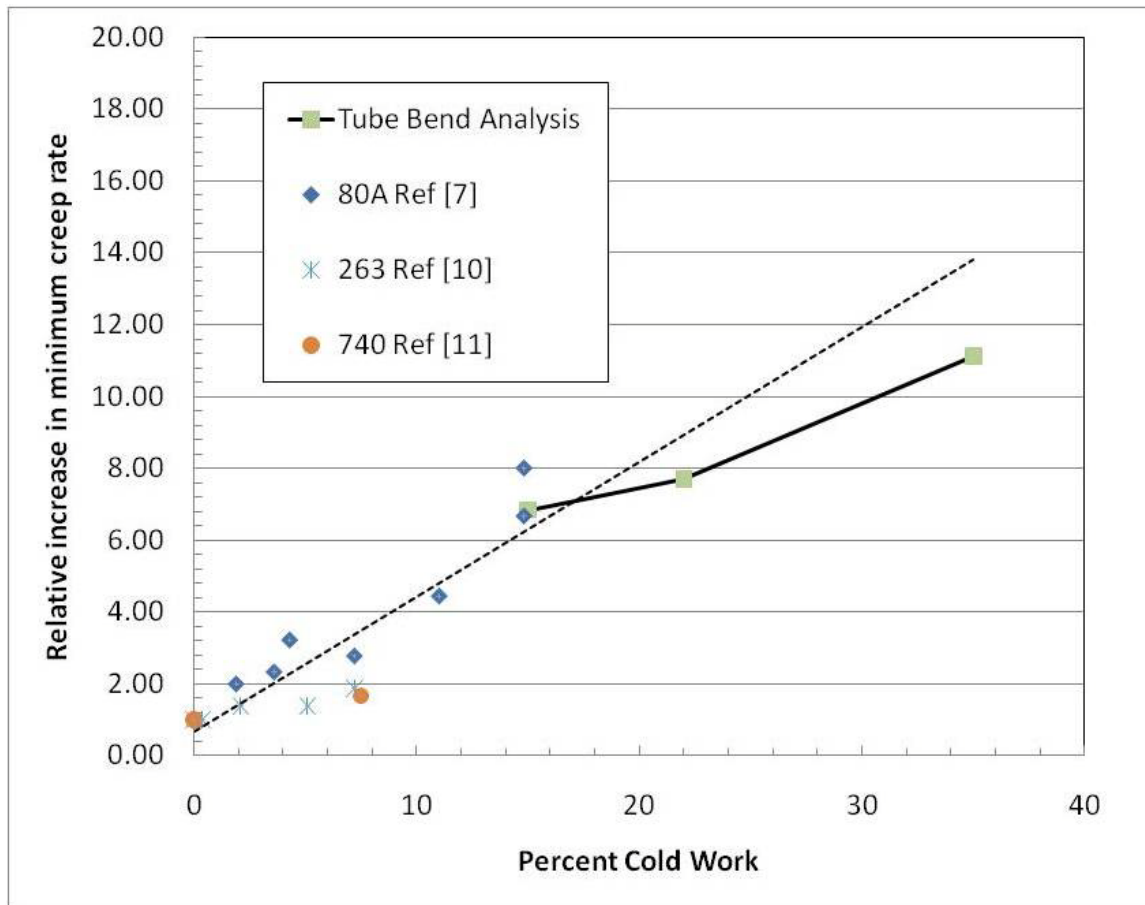
Figure 3-15 Increase in minimum creep rate as a function of cold-work for age-hardenable nickel-based alloys. The dashed line is a linear fit to available data from references [7, 10, and 11]. The tube bend analysis shows similar behavior for alloy 740.

Conclusions

Full-scale pressurized creep-rupture tests were conducted on alloy 740 cold-formed tube bends to evaluate the effect of cold-work on the performance of tube bends for high-temperature applications. Results show that the full-size test method can be used to understand the performance of these components in service. Specifically, the methodology provides a way to simplify the complexities of structural (geometric) effects and material degradation due to cold-work during creep. Observed changes in ovality were similar to in-plant observations, comparisons with expectations from uniaxial creep-rate data, and comparisons with literature data on similar alloys, thus verifying the validity of the analysis methods.

Specific finding for alloy 740 were:

- Cold-work is detrimental to the creep behavior of alloy 740 even when aging is conducted after cold-working
- The rupture life reduction, significant reduction in creep ductility, and moderate increase in minimum creep rate are similar to other nickel-based alloys
- The number of creep cavities is greatly increased in the tube bend tests normal to the pressure (hoop) stress with the areas of highest tensile cold strain having micro and macro cracking, consistent with literature data on similar alloys
- At 15%OFS (cold-work), the reduction in creep life for alloy 740 is greater than the minimum scatterband for creep data; thus, creep based designs with alloy 740 should consider lower cold-forming limits

Additional research is required to clarify the differences observed in creep damage for tensile and compressive cold-strain and identification of a minimum acceptable cold-work limit for the alloy.

Chapter 3 References

1. "2010 ASME Boiler and Pressure Vessel Code, Section I – Rules for Construction of Power Boilers." © 2010 The American Society of Mechanical Engineers

2. J.P. Shingledecker, Creep rupture behaviour and recrystallisation in HR6W and Haynes alloy 230 cold bent boiler tubing for ultrasupercritical steam boiler applications, Energy Mater., 2(4), 2008, p 235-240

3. R. Viswanathan, R. Purgert, and U. Rao, Materials for Ultra-Supercritical Coal-Fired Power Plant Boilers, Materials for Advanced Power Engineering 2002 - Proceedings Part II (Liege, Belgium), Forschungszentrum Julich GmbH, 2002, p 1109-1129

4. R. Viswananthan, J.F. Henry, J. Tanzosh, G. Stanko, J. Shingledecker, B. Vitalis, and R. Purgert, U. S. Program on Materials Technology for Ultra-Supercritical Coal Power Plants, J. Mater. Eng. Perform. 14(3), 2005, p 281-292

5. J.P. Shingledecker and I.G. Wright, Proceedings to the 8th Liege Conference on Materials for Advanced Power Engineering 2006 (Liege, Belgium), Forschungszentrum Jülich GmbH, 2006, p 107-120

6. M. McLean and B.F. Dyson, Modeling the Effects of Damage and Microstructural Evolution on the Creep Behavior of Engineering Alloys, J. Eng. Mater. Tech., 122, 2000, p 273-278

7. B.F. Dyson and M.J. Rodgers, Prestrain, Cavitation, and Creep Ductility, Met. Sci., 8, 1974, p. 261-266

8. B.F. Dyson, M.S. Loveday, and M.J. Rodgers,Grain boundary cavitation under various states of applied stress, Proc. R. Soc. Lond. A, 394, 1976, p 245-259

9. M.S. Loveday and B.F. Dyson, Prestrain-Induced Particle Microcracking and Creep Cavitation in IN597, Acta Metall., 31, 1983, 397-405

10. Y.H. Zhang and D.M. Knowles, Prestraining effect on creep behavior of nickel base C263 superalloy, Mater. Sci. Tech., 18, 2002, 917-923

11. K. Kubushiro, K. Nomura, S. Takahashi, M. Takahashi, and H. Nakagawa, Effect of Pre-Strain on Creep Properties of Alloy 740, Advances in Materials Technology for Fossil Power Plants, Proceedings from the Sixth International Conference, Aug. 31-Sept. 3, 2010 (Santa Fe, NM, USA), EPRI, ASM International, 2010, p 164-170

12. H. Burt, I.C. Elliott, and B. Wilshire, Effects of room-temperature prestrain on creep-fracture behaviour of Nimonic 105, Met. Sci., 15, 1981, p 421-424

13. T. Saegusa, M. Uemura, and J.R. Weertman, Grain Boundary Void Nucleation in Astroloy Produced by Room Temperature Deformation and Anneal, Metal. Trans. A, 11A, 1980, p 1453-1458

14. R. Viswanathan, J. Shingledecker, J. Hawk, and S. Goodstine, Effect of Creep in Advanced Materials for Use in Ultrasupercritical Power Plants, Proceedings Creep & Fracture in High Temperature Components, 2nd ECCC

Creep Conference, April 21-23, 2009 (Zurich, Switzerland), DEStech Publications, Inc., 2009, p 31-43

15. J. Shingledecker and M. Santella, Oak Ridge National Laboratory, Oak Ridge, TN, 2010, unpublished research

16. T.H. Courtney, Mechanical Behavior of Materials, 2nd e., McGraw-Hill, 2000, Chap. 7

17. J.D. Fishburn, Single technically consistent design formula for the thickness of cylindrical sections under internal pressure, Proceedings of the ASME Pressure Vessels and Piping Conference 2005 – Codes and Standards PVP2005 (V1), American Society of Mechanical Engineers, 2005, p 291-295

18. I.J. Perrin and J.D. Fishburn, A perspective on the design of high-temperature boiler components, Int. J. Pressure Vessels Piping, 85, 2008, p 14-21

19. John P. Shingledecker, Tensile and Creep-Rupture Evaluation of a New Heat of Haynes Alloy 25, ORNL/TM-2006/609, Oak Ridge, TN, February 2007

20. A.G. Miller, Review of limit loads of structures containing defects, Int. J. Pressure Vessels Piping 32, 1988, p 197-327

21. Boiler Materials for Ultrasupercritical Coal Power Plants – Task 8, An Overew of Reference Stress Apporach, USC T-6, NETL/DOE/OCDO, EPRI Palo Alto, CA, 2003

22. L. Yu-De and L. Zi-Li, Creep strain, elliptical release and additional stress of the elbows in main steam piping, Int. J. Pressure Vessels Piping, 57, 1994, p. 135-139

23. J.P. Shingledecker, G.M. Pharr, The role of eta phase formation on the creep strength and ductility of INCONEL® alloy 740 at 1023K (750°C), Met. Trans. A, in press

24. M.W. Spindler, The multiaxial creep ductility of austenitic stainless steels, Fatigue Fract. Eng. Mater. Struct., 27, 2003, p. 273-281

25. I. Finnie and W.R. Heller, Creep of Engineering Materials, McGraw-Hill, 1959, Chap. 7

4. INFLUENCES OF COMPOSITION AND GRAIN SIZE ON CREEP-RUPTURE BEHAVIOR OF INCONEL ® ALLOY 740

A version of this chapter has been submitted by J.P. Shingledecker, N.D. Evans, and G.M. Pharr:

J.P. Shingledecker, N.D. Evans, G.M. Pharr. "Influences of Composition and Grain Size on Creep-Rupture Behavior of Inconel® Alloy 740." *Submitted to Materials Science and Engineering A*, March 2012 – In review

This chapter is the original work of the author and has been formatted to conform to the thesis requirements. The inclusion of N.D. Evans as a co-author is due to his research which is specific to the image and EDS data in Figure 4-7 and the EDS (measured) data in Table 5 which was integrated into the overall work of the author and helps support the conclusions.

Abstract

Creep-rupture experiments were conducted on multiple heats of the nickel-based superalloy INCONEL® 740 at temperatures between 923 and 1123K (650 and 850°C). The interactions between chemistry, microstructure, and creep performance were evaluated by analysis of creep data, optical microscopy, electron microscopy, and computational thermodynamics. The data show that grain size has a modest effect on the creep-rupture strength. Computational thermodynamics verified experimental observations of the formation of eta phase as a function of temperature and alloy chemistry, but the kinetics for the precipitation of eta phase did not agree with the experimental findings. Despite the formation of eta phase and the concomitant reduction in volume fraction of gamma prime, the creep resistance of the alloy is insensitive, within the range of chemistries tested, to the volume fraction of gamma prime. The creep ductility was found to increase with test temperature. Precipitation of a large volume fraction of eta phase (greater than 7%) appears to reduce the creep-rupture ductility, but smaller amounts do not produce adverse effects.

Introduction

INCONEL® alloy 740, hereafter referred to as alloy 740, is an age-hardenable nickel-based superalloy proposed for advanced ultrasupercritical (A-USC) for steam boiler applications at high-stress and temperatures of 973K (700°C) and above where creep will be the dominant deformation mode [1]. A-USC steam boilers with operating temperatures up to 1033K (760°C) will help to increase efficiency and decrease emissions of all effluents, including CO_2, in coal-fired power plants by up to 25% in comparison to current technology [2,3]. The typical microstructure of alloy 740 is a gamma matrix containing gamma prime precipitates and very little precipitation at the grain boundaries. After high-temperature aging, the gamma prime coarsens, and grain boundary $M_{23}C_6$ carbides, G-phase (a complex silicide), and the plate-like eta phase forms [4,5]. Studies on alloy 740 have shown that this microstructure, and in particular the

formation of eta phase, is sensitive to alloy chemistry [6].   Earlier research on alloy 740 by the authors showed that the formation of a small amount of eta phase, which grows by consuming gamma prime precipitates, is not detrimental to the creep strength or ductility at 1023K (750°C) [7]. However, a comprehensive investigation covering a broader range of temperatures, chemical compositional variations, and microstructural changes has not been conducted to determine the critical microstructural elements that affect creep-rupture performance. These issues are addressed in this report.

Experimental Procedure

Creep-rupture tests were conducted on six different heats of alloy 740. The chemistries of the heats, which are given in Table 4-1, meet the requirements of ASME Boiler and Pressure Vessel Code Case 2702 [8]. All heats were produced via commercial processes and represent a range of product forms including tube, bar, and plate. The materials were furnished in the solution-annealed condition with the exception of heat E, which was hot-rolled at 1463K (1190°C). To produce larger grain sizes, heats A and E were given additional solution annealing heat-treatments at 1463K (1190°C) and 1393K (1120°C), respectively. Prior to creep testing, the materials were all given a standard aging heat-treatment in the range 1033 to 1073K (760 to 800°C) for 4 to 16 hours.

Table 4-1 Measured composition of heats (wt%)

ID	C	Mn	Fe	S	Si	Ni	Cr	Al	Ti	Co	Mo	Nb	P	B
A	0.03	0.28	0.42	0.0010	0.54	bal	24.43	0.94	1.81	20.00	0.55	1.98	0.005	0.0030
B	0.03	0.26	0.46	0.0010	0.53	bal	24.38	0.98	1.77	19.90	0.50	1.97	0.005	0.0043
C	0.03	0.26	0.46	0.0010	0.54	bal	24.34	0.97	1.78	19.80	0.50	1.99	0.005	0.0037
D	0.03	0.27	1.02	0.0002	0.45	bal	24.31	0.75	1.58	19.63	0.52	1.83	0.003	0.0006
E	0.06	0.30	0.69	0.0060	0.48	bal	24.86	1.20	1.41	19.90	0.53	2.05	0.004	0.0010
F	0.04	0.31	1.05	0.0100	0.30	bal	24.28	1.30	1.50	19.88	0.53	1.57	0.002	0.0007

bal = Balance

Creep-rupture tests were conducted on smooth bar samples in accordance with ASTM E139 at temperatures between 923 and 1123K (650 and 850°C), with the resultant rupture lives ranging from 150 to 24,000 hours. After testing, selected specimens were sectioned, mounted in epoxy, and polished using standard metallographic techniques. Specimens used for optical microscopy (OM) and grain size determination were etched using a solution of 40 ml H_2O, 40 ml HNO_3,

and 20 ml HF. Scanning electron microscopy (SEM) was performed on polished, unetched samples in both secondary (SE) and back-scatter (BSE) electron imaging modes. Energy dispersive spectroscopy (EDS) was conducted for a semi-quantitative chemical analysis of the precipitates. Thermodynamic calculations of the equilibrium microstructural phases and precipitation kinetics were performed using JMatPro™ version 5.0 with the Ni database [9].

Results

Chemistry and grain size

Inconel 740 is hardened by gamma prime precipitates. The key elements controlling the amount of gamma prime and its stability are Ti, Al, and Nb [10,11], as highlighted in Table 4-2. Inspection of Tables 4-1 and 4-2 shows that heats A, B, and C have nominally the same chemical composition with a Ti/Al ratio of ~1.8 and a total amount of Ti and Al (Ti+Al) of ~2.8 wt%. Heat D has a similar Ti/Al ratio but a reduced amount of the hardening elements. Heat E has the same amount of total hardening elements as heats A, B, and C but a Ti/Al ratio close to 1. Heat F is similar to E but with reduced Nb. Although very few tests were conducted on Heat F, it was included in the study because it is the more weldable '740H' composition, with research showing that the reduced Nb enhances thick section weldability [12, 13].

Table 4-2 Summary of important chemical composition differences.

ID	Ti/Al ratio	Ti+Al (wt %)	Ti+Al+Nb (wt%)
A	1.93	2.75	4.73
B	1.81	2.75	4.72
C	1.84	2.75	4.74
D	2.11	2.33	4.16
E	1.17	2.61	4.66
F	1.15	2.80	4.37

The grain size varied among the various heats, but this cannot be directly related to solution annealing temperature since multiple product forms (thicknesses) were evaluated. Table 4-3 summarizes the grain sizes of the various heats. Figure 4-1 shows typical microstructures for the solution annealed and aged condition, which is characterized by relatively equiaxed grains with numerous annealing twins. Solution annealed heat E had a bimodal grain size distribution (see differences in Figures 1a and 1b); an average of the two measured grain sizes is given in the table.

64

Table 4-3 Summary of grain size measurements.

ID	Solution Annealing Temperature K (°C)	Grain Size (μm)
A	1393 (1120)	82.4
A	1463 (1190)	165
B	1393 (1120)	188
C	1393 (1120)	127
D	1473 (1200)	169
E	*1463 (1190)	89.6
E	1393 (1120)	**113

*Material furnished in hot-rolled condition
** Bimodal grain size distribution, average grain size reported
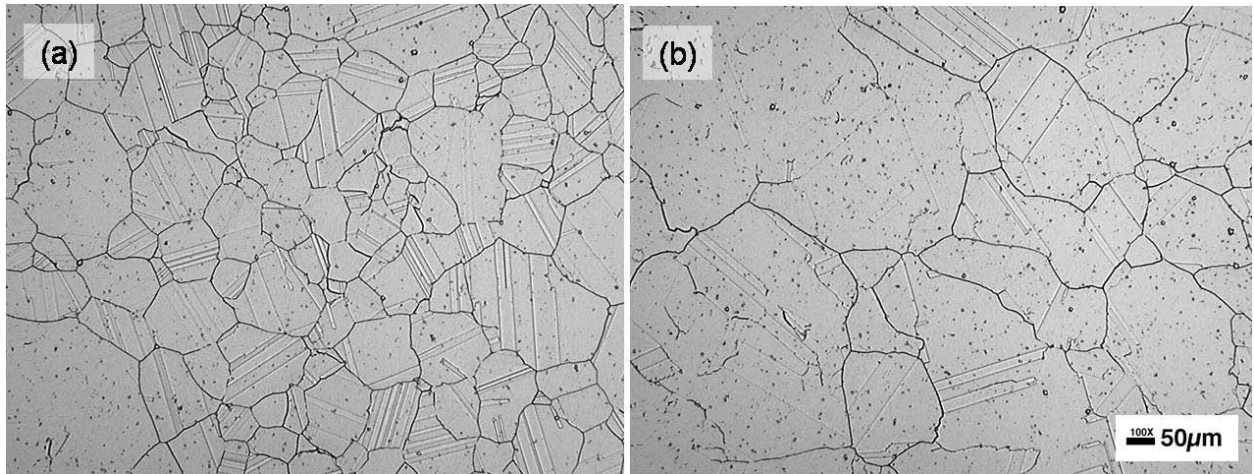

Figure 4-1 Typical optical micrographs for alloy 740 after solution annealing and aging. The images were taken from the fine grain (a) and coarser grain (b) regions in heat E, which was the only heat to show any large variation in grain size.

Creep-Rupture Testing

A total of 90 creep rupture tests were conducted to produce more than 450,000 hours of creep-rupture data. Since the data covered a range of times, temperatures, and stresses, the data were analyzed utilizing a polynomial fit. A regression analysis was conducted to minimize the error in time to rupture (t_r) using a fitting equation of the form:

$$\log(t_r) = -C + \frac{A_1}{T} + \frac{A_2 \log(\sigma)}{T} + \frac{A_3 \log(\sigma)^2}{T} + \frac{A_4 \log(\sigma)^3}{T} \quad \text{Equation 1}$$

where C is the Larson Miller Parameter (LMP) constant, T is the temperature in Kelvin, σ is the creep stress in MPa, and the A_x are the regression coefficients. The Larson Miller Parameter is a time-temperature parameter defined as:

$$LMP = T(K) \cdot (\log(t_r) + C) \qquad\qquad . \qquad\qquad \text{Equation 2}$$

Table 4-4 is a summary of the constants developed for this dataset. Based on this fit, the optimized LMP constant (C) was 19.4 which is similar to other reported values for the alloy based on shorter-term data [14].

Figure 4-2 shows that the time to rupture data and the predictions of equation 1 are in reasonable agreement. Figure 4-3 is a plot of the optimized LMP fit for all the data compared for specific heats and grain sizes. The plots in Figures 3a and 3b indicate that for a given heat of material (Heats A and E), larger grain sizes produce a moderate increase in creep-rupture strength (a,b). However, when comparing similar grain size heats, variations in the Ti/Al ratio for similar Ti+Al contents or visa-versa show no discernable effects on the creep-rupture life.

Figure 4-4 is a plot of rupture ductility (elongation at failure) as a function of the time to rupture. Taken as a whole, the data indicate no clear trend in the rupture ductility with rupture time but a possible trend with testing temperature. Only rupture elongation has been plotted because a comparison of rupture elongation and reduction of area showed that the values are consistent for a given specimen, that is, there was no geometric instability during testing so the elongation was approximately equal to the reduction of area.

Table 4-4 Regression coefficients for Equation 1

Constants	Value
C	19.392
A1	2.336 x10^4
A2	5.532 x 10^3
A3	-2.065x10^3
A4	-1.027 x10^2
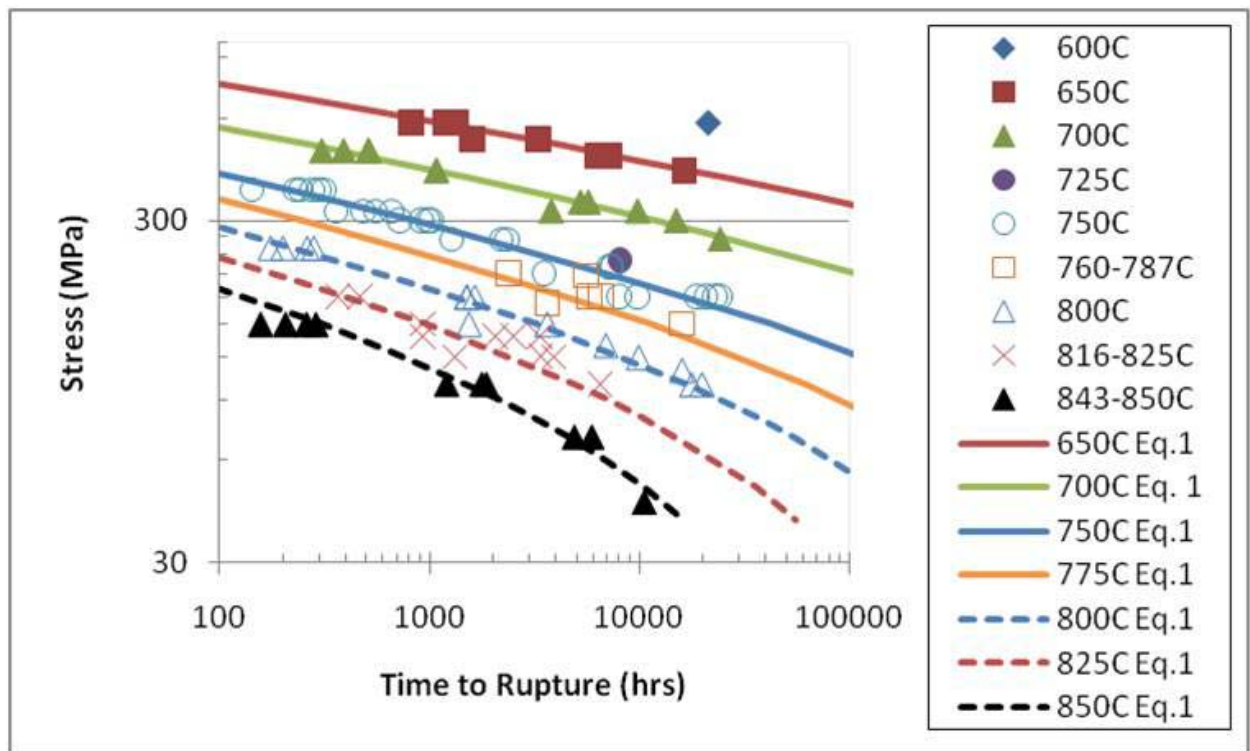
Figure 4-2 Time-to-rupture data for alloy 740 compared to equation 1
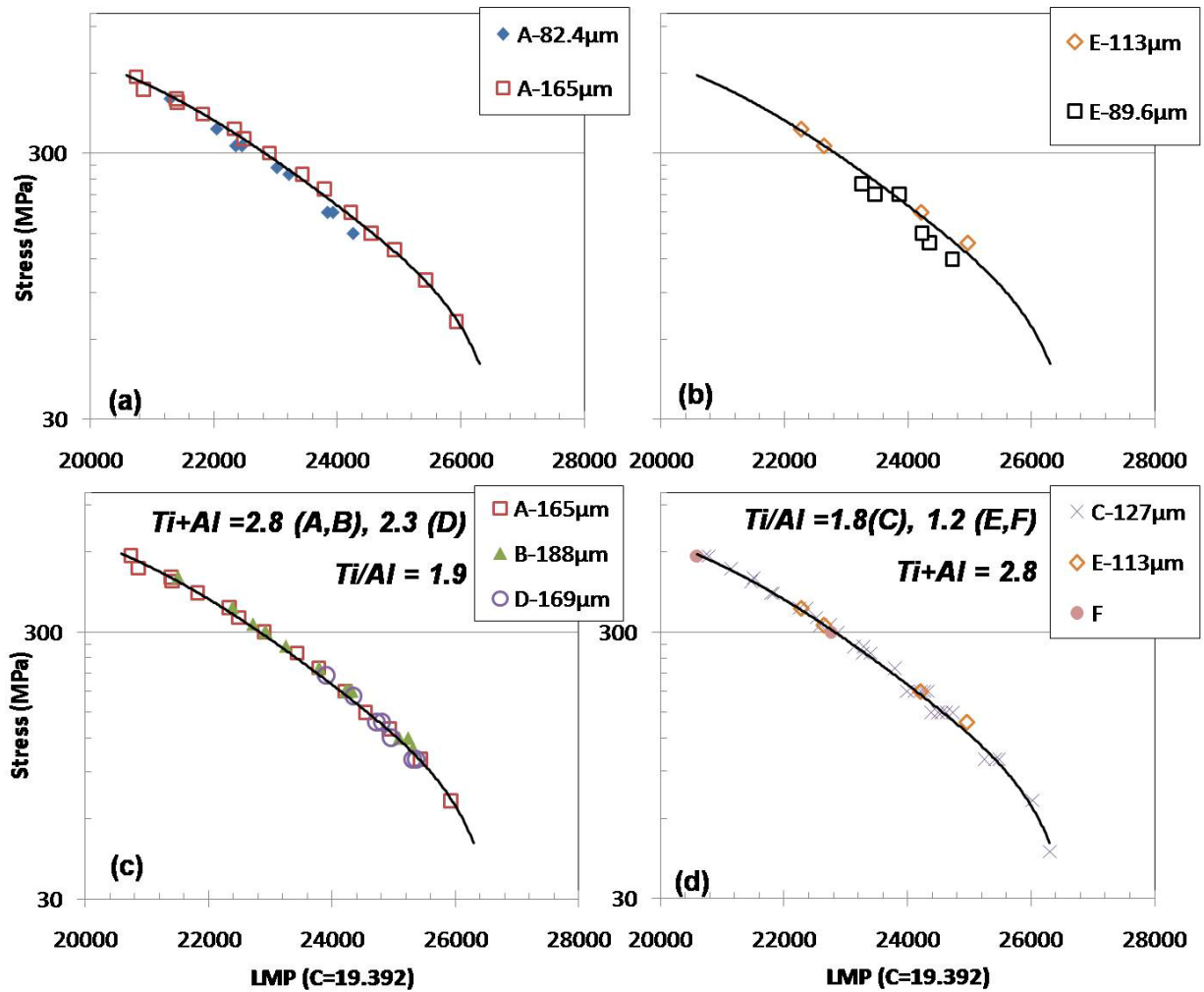
Figure 4-3 Stress versus Larson Miller Parameter (LMP) for various sets of data which show a moderate grain size effect (a,b) but no effect of Ti+Al content or the Ti/Al ratio (c,d).

68
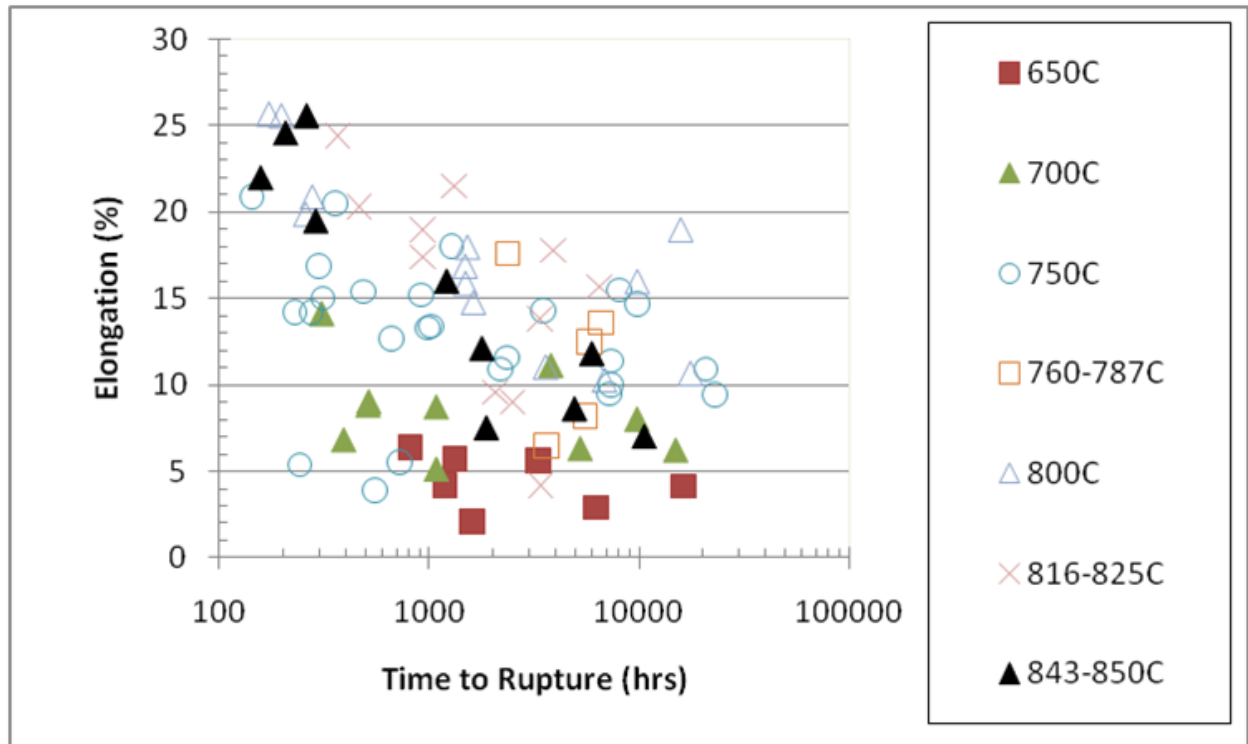
Figure 4-4 Rupture ductility (elongation) plotted as a function of time for various test temperature ranges.

Computational Thermodynamics

Equilibrium thermodynamic calculations for phase stability and phase transformations were conducted using the commercial code JMatPro™ V5. Since heats A, B, and C had equivalent chemistries, they were treated as a single composition. Phase stability calculations verified all the major phases identified in previous microstructural studies [4-7, 15] with the exception of the sigma phase which was predicted to be stable at temperatures only less than ~1023K (750°C).   Therefore, the formation of sigma phase was suspended for the equilibrium calculations reported in this work. Additionally, to calculate the maximum amount of gamma prime possible, all phases except the matrix (gamma) and gamma prime were suspended for some evaluations. Since gamma prime precipitation is very rapid compared to other precipitates (such as eta phase), suspending the formation of other phases allows the total amount of 'metastable' gamma prime to be estimated. Since alloy 740 was tested in the aged condition, this calculation is more representative of the starting condition of the material prior to testing. As will be shown, the creep tested specimens approach the equilibrium calculated structure.

Figure 4-5 shows the calculated equilibrium and metastable contents of gamma prime for each chemistry. The maximum amount of metastable gamma prime is directly related to the amount of Ti and Al in the alloy, with Heat D having the lowest volume fraction and all other heats having similar amounts. In contrast, the equilibrium gamma prime volume fraction depends strongly on temperature and chemistry. The alloys with the higher Ti/Al ratios (Heats A, B, C, and D) showed significant reductions in gamma prime compared to the metastable predictions due to precipitation of other phases (mainly eta phase). Figure 4-6 is a plot of the predicted eta phase stability. The temperature range and amount of eta phase varies substantially with alloy chemistry.
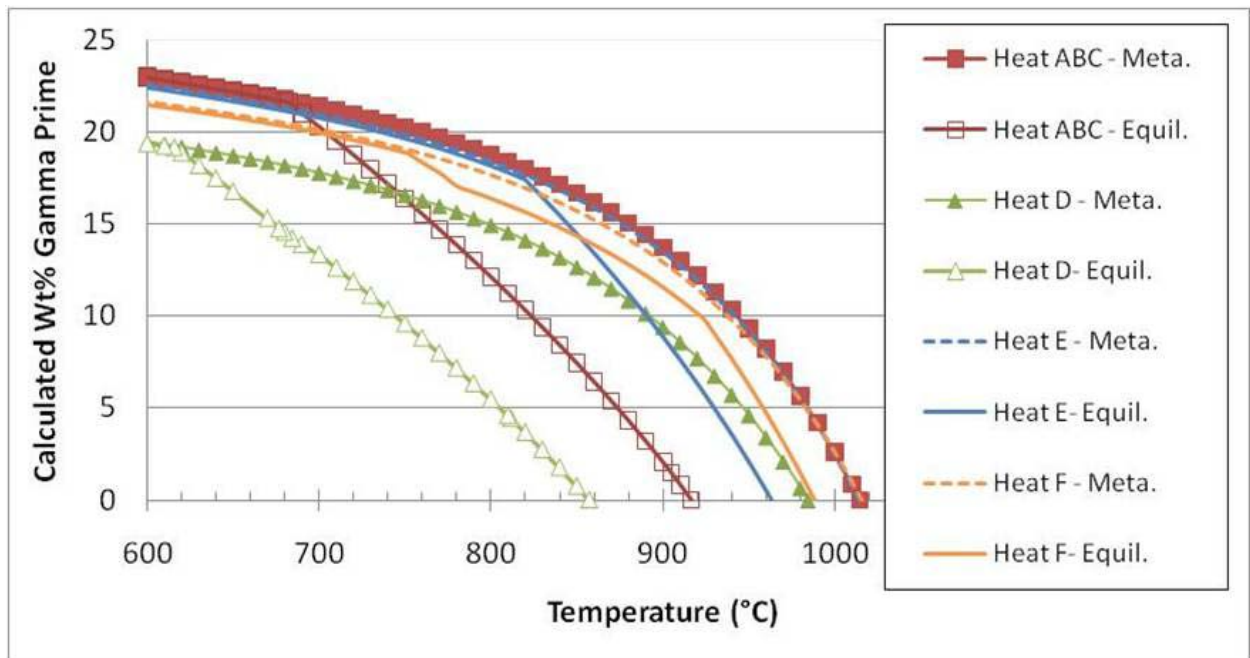
Figure 4-5 Amounts of equilibrium and metastable gamma prime predicted as a function of temperature and alloy chemistry.
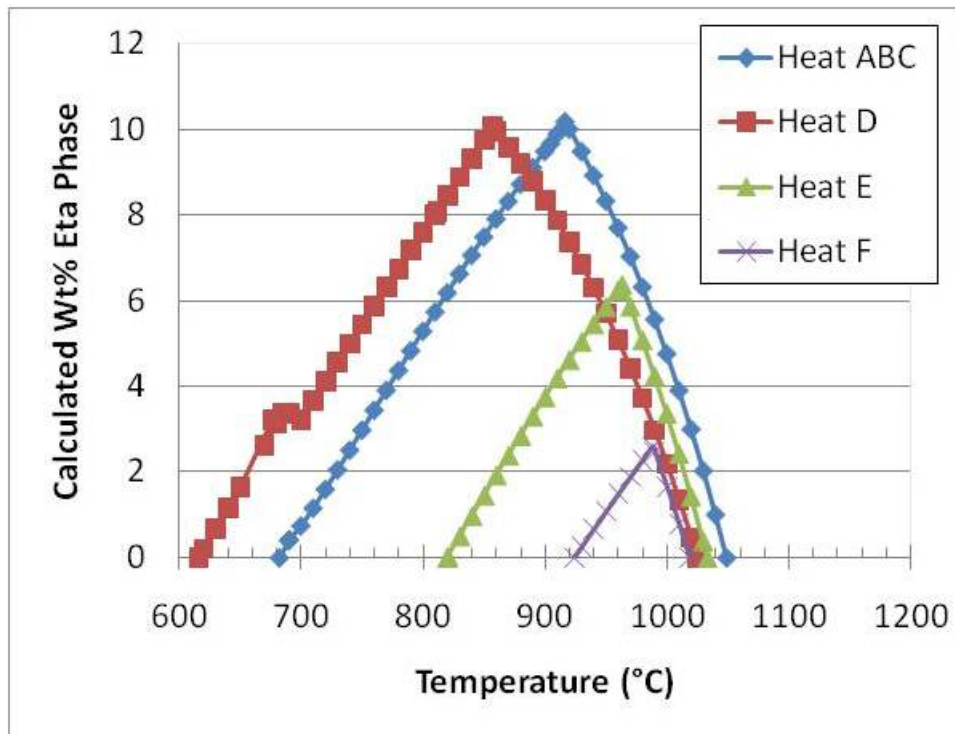
Figure 4-6 Predicted eta phase stability as a function of temperature.

Microstructure

A scanning electron microscopy investigation was conducted on select samples of heats B and E with particular emphasis on eta phase formation. Figure 4-7 shows a back-scattered electron image (BSE) of heat E after creep-rupture testing for 927 hours at 1089K (816°C). A single isolated eta phase precipitate was identified. The semi-quantitative EDS analysis of the precipitate showed good agreement with the predicted eta phase composition (Table 4-5). Some differences in Cr, Co, and Nb are most likely due to contributions from the EDS spectra from the gamma matrix, since the excitation volume at 15 kV is most likely greater than the extent of the entire eta phase. Figure 4-8 is a series of microstructures after creep testing showing the gamma prime matrix with fine gamma prime precipitates and grain boundary phases. Grain boundary carbides and G-phase are observed for the 973K (700°C) Heat B sample and 1023K (750°C) Heat E sample. With increasing temperature, Heat B readily forms copious amounts of eta phase whereas Heat E does not. A single isolated eta phase is shown in Heat E after testing for 1321 hrs at 1098K (825°C), as indicated by the arrow on the figure. In the samples with plate-like eta phase, gamma prime denuded regions (precipitate free zones) are also observed. A summary of the eta phase observation for all the samples in Heats B and E is

provided in Table 4-6. The Table includes data from reference [7], which were obtained using the same heat of material (Heat B). The observations in Table 6 are separated into those from the highly stressed gauge section and the less highly stressed shoulder.

Failure modes were examined for a number of samples. As described in reference [7], some wedge cracking was observed in short-life samples, but most creep damage was associated with grain boundary cavitation. Figure 4-9 shows SEM images of typical grain boundary cavities which usually form in the gamma prime denuded regions of the sample.
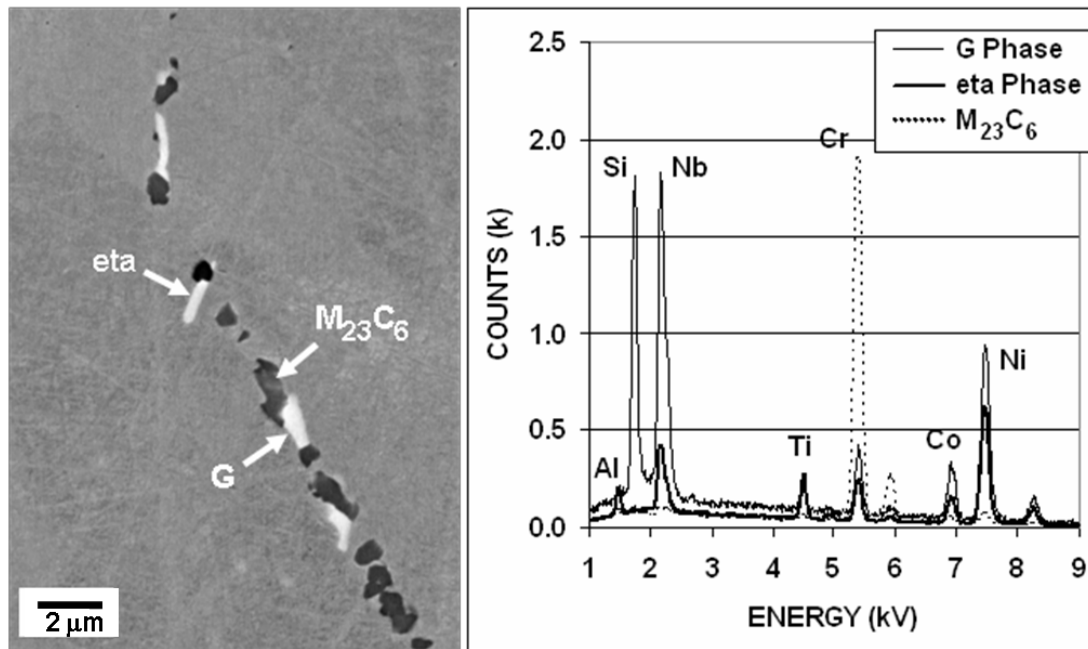
Figure 4-7 Back scattered SEM Image (left) and corresponding EDS spectrum (right) of Heat E after creep testing at 1089K (816°C) for 927 hours showing a single isolated eta phase precipitate along with grain boundary carbides and G-phase silicide.

Table 4-5 Measured composition (EDS) of the eta phase after creep testing at 1089K (816°C) compared to the calculated composition at 1093K (820°C).

Wt%	Ni	Cr	Co	Ti	Fe	Nb	Al
Measured	71	1.3	8.9	10.4	0.1	6	2.3
Calculated (820°C)	61.1	0.15	14.3	9.9	0.1	12.1	2.35
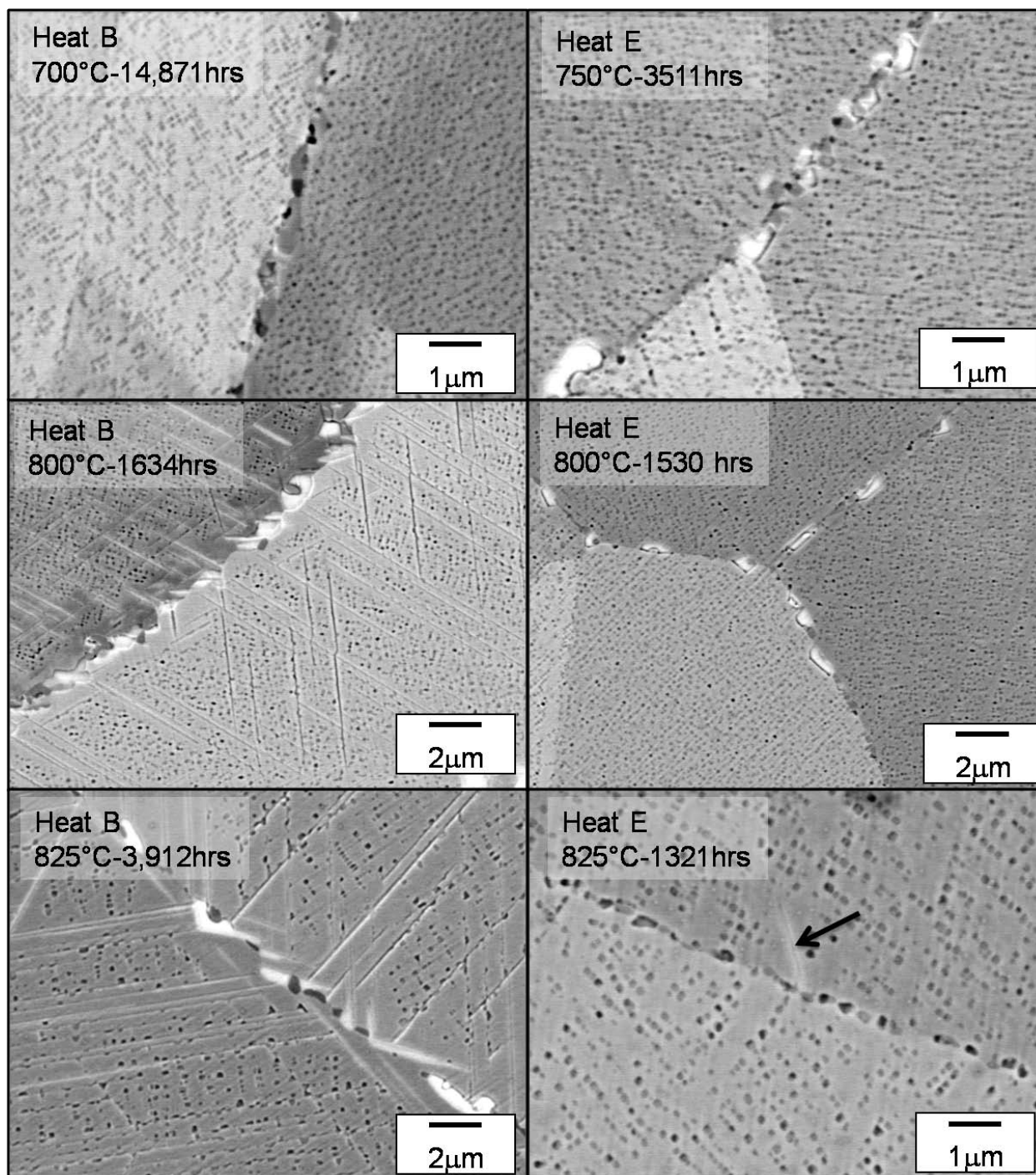
Figure 4-8 Back scattered SEM Images comparing Heat B and E after creep testing for various times and temperatures. Eta phase platelets were observed in heat B at 1073-1098K (800 and 825°C), and a single isolated eta phase was found in heat E at 1098K (825°C).

73
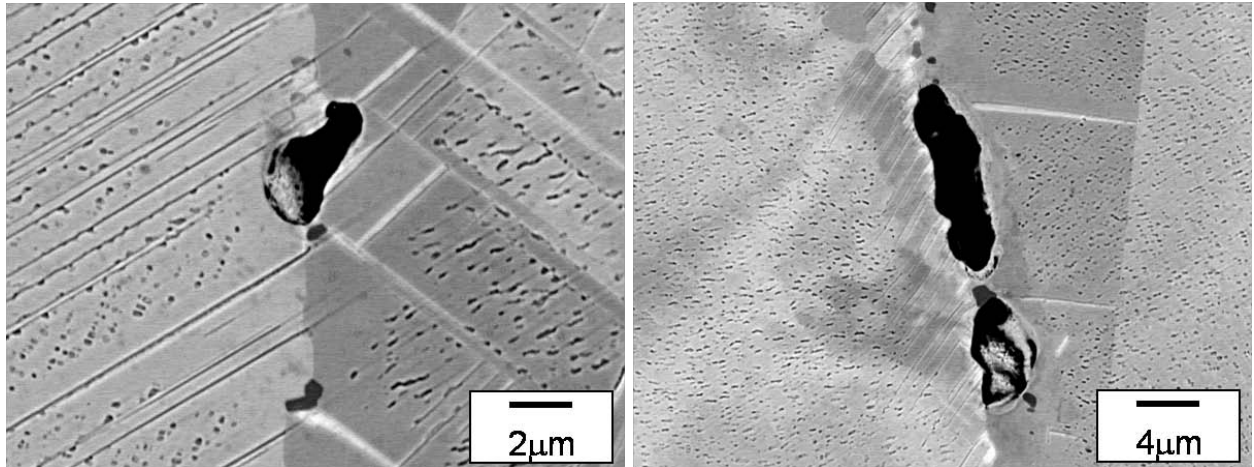
Figure 4-9 Grain boundary cavities in Heat B after creep-rupture testing at 120MPa and 1098K (825°C) for 3912 hours.

Table 4-6 SEM observations from failed creep-rupture specimens.

Heat	Rupture Time (hrs)	Temperature (°C)	Eta in gauge	Eta in shoulder
B	512.5	700	no	no
B	14871.3	700	no	no
B	311.9	750	no	no
B	658.5	750	no	no
B	1020.2	750	yes	no
B	2185.4	750	yes	yes
B	7355.2	750	yes	yes
B	20789.4	750	yes	yes
B	1633.6	800	yes	yes
B	9854.7	800	yes	yes
B	15863.6	800	yes	yes
B	3912	825	yes	yes
E	3511	750	no	no
E	2371	775	no	no
E	1530.1	800	no	no
E	927.1	816	Isolated	no
E	1320.7	825	Isolated	Isolated

Discussion

Utility of Computational Results for Predicting Microstructural Variations

In order to utilize the computational results, it is first prudent to evaluate the predictive capabilities of the computational software, especially for the formation of eta phase. Table 4-5 shows that the basic calculations for the composition of the eta phase composition are in good agreement with the experimental results. However, as shown in Figure 4-10, there is a large discrepancy between the times needed for the eta phase to form (in Heat B) as simulated using the precipitation module of JMatPro V5 and the experimental observations; specifically, the simulations suggest that the precipitation kinetics are much faster than they actually are. On the other hand, the amount of eta phase, approximately 3.5 at% once precipitation is complete, is in very good agreement with the experimental measurements.
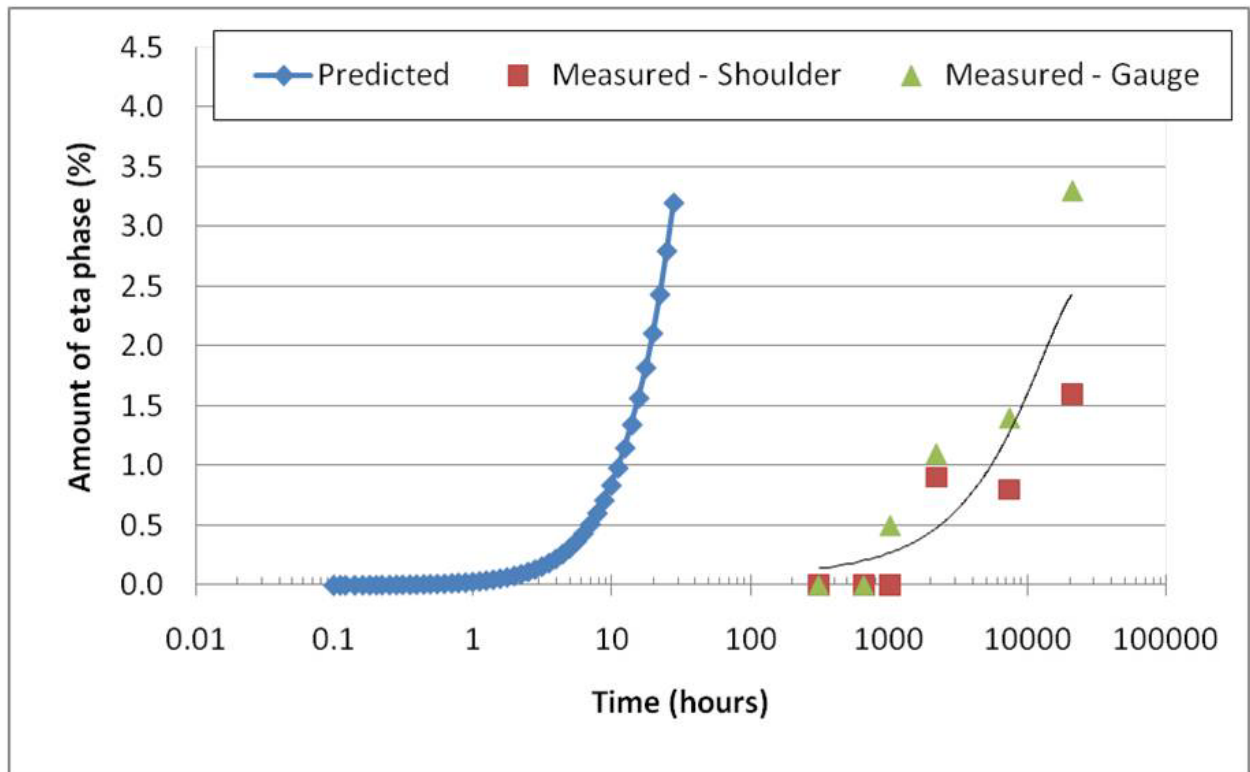
Figure 4-10 Predicted and measured [7] eta phase area fractions at 1023K (750C) for heat B.

To further investigate the phase stability calculations, the data in Table 4-6 and calculated weight fractions reported in Figure 4-6 for eta phase stability are directly compared in Figure 4-11, where the experimental data are plotted on a time-temperature-transformation diagram for eta phase formation along with the equilibrium eta phase start temperatures (plotted at 100,000 hours). After long times, the temperature regimes of eta phase stability appear to be in very good agreement with the experimental data. These observations are also qualitatively consistent with other work on eta phase formation in a range of nickel-based alloys [15]. The estimated eta phase start curves are also included on the figure. The data show that a minor adjustment in the Ti/Al ratio from 1.8 to 1.2 greatly reduces the range of eta phase stability. The eta phase start curve from a detailed electron microscopy study on a similar alloy, Nimonic 263 [16], which has nominally the same amount of Ti+Al as alloy 740 and a Ti/Al ratio of ~2, is also included in Figure 4-11. There is reasonable agreement with the alloy 740 observations for a Ti/Al ratio of 1.8.
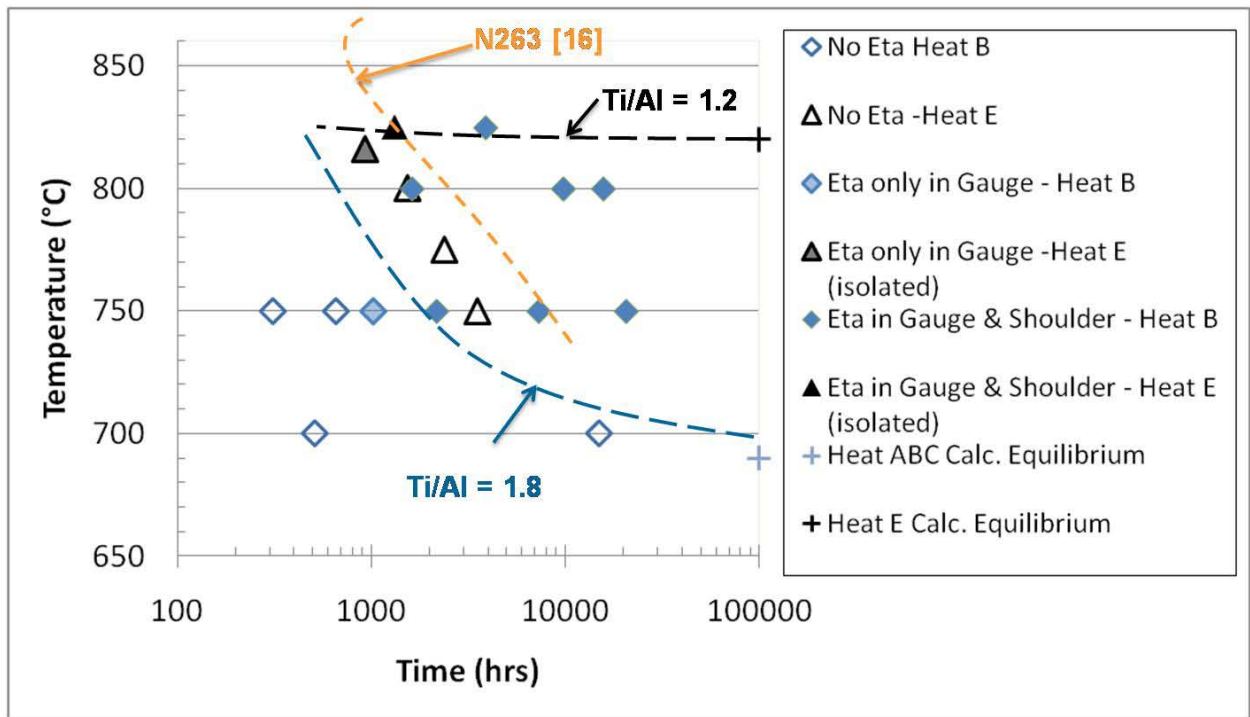
Figure 4-11 Time-temperature-transformation diagram for eta phase formation in Heats B and E. Also shown for comparison is the eta phase start curve for alloy Nimonic 263 [16].

The JMatPro V5 software utilizes a Johnson-Mehl –Avrami model with driving forces and compositions developed from the thermodynamic databases for

precipitation kinetics, but nucleation terms are not well described [17]. Based on the large discrepancy for the start of precipitation in Figure 4-10, it is likely some modification for eta phase nucleation in nickel-based alloys is warranted.

Grain size and creep-rupture strength

The time to rupture results in Figure 4-3 appear to indicate a moderate grain size dependence in alloy 740 but do not show a notable trend for creep strength as a function of alloy chemistry for similar grain sizes.   To clarify these apparent trends, the difference between the logarithm of the time to rupture calculated from equation 1 and the logarithm of the measured time to rupture is plotted as a function of grain size in Figure 4-12. All the data appear to fit a general increasing trend with the exception of the heat E with a grain size of 113µm. Curiously, this was the only heat with a bimodal grain size distribution. A review of the microscopy on heat E showed the larger grain size regions were approximately 140 µm, which may explain the observed discrepancy.
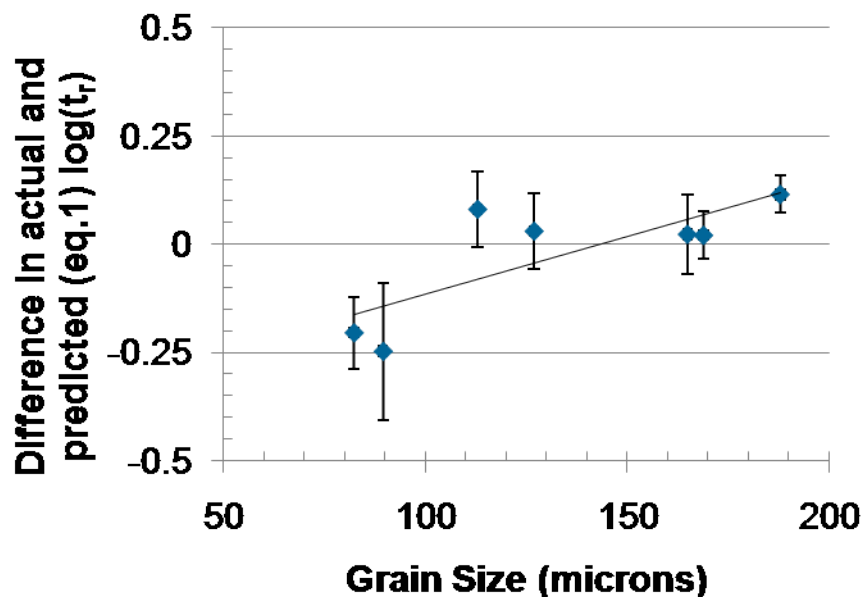
Figure 4-12 Difference in the logarithim of the measured time to rupture and predicted time to rupture (eq.1) as a function of grain size. Error bars are +/- one standard deviation.

A similar comparison was made to evaluate the grain size dependence of the minimum creep-rate data using the Monkmann-Grant approach. This led to the following relationship that was developed by fitting the available data (with t_r in hours and $\dot{\varepsilon}_{min}$ in %/hour) to the Monkman-Grant equation:

$$t_r = 2.719\dot{\varepsilon}_{min}^{-0.810} \qquad\qquad \text{Equation 3}$$

The differences between the measured (actual) and calculated (from equation 1 and 3) minimum creep rate are plotted in Figure 4-13. The trend is similar where creep strength increases (rate decreases) with increasing grain size, but there is more uncertainty in the data by evidence of the larger error bars. Heat E with a grain size of 113μm shows slightly anomalous behavior, but is within the scatter of the data. The linear fits in Figures 4-12 and 4-13 suggest that 140μm as the 'zero' or average behavior of the dataset, with coarser grain sizes having greater creep strength and longer lives.
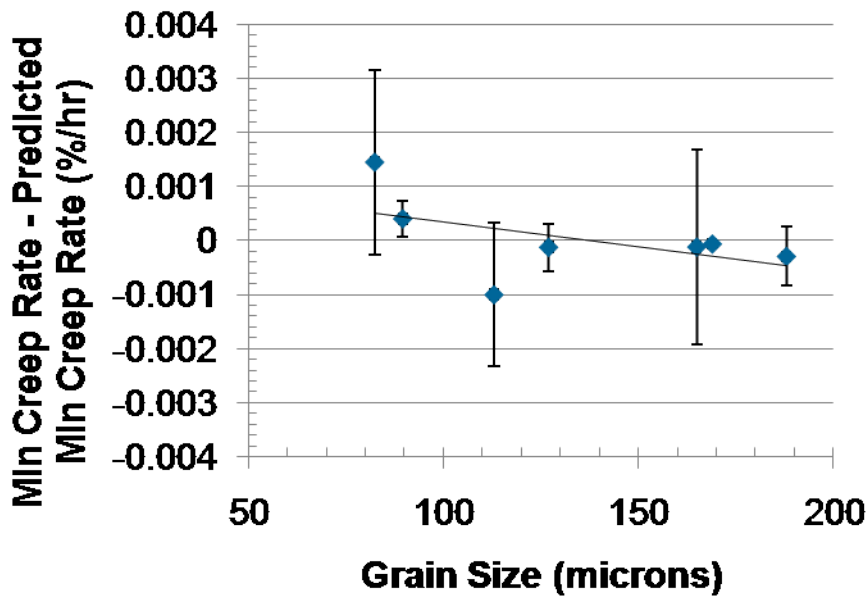
Figure 4-13 Difference in measured and predicted (Eqns. 1 and 3) minimum creep rate as a function of grain size for alloy 740.

The finding that grain size affects creep strength in alloy 740 is consistent with other research on high chromium nickel-based alloys with similar levels of Ti, Al, and Nb. Model Ni-Cr-Al-Ti-Nb alloys studied by Gibbons and Hopkins with varying levels of gamma prime showed that alloys with 0 to 5 % gamma prime did not exhibit a grain size effect on creep strength but that alloys with large volume fractions (up to 31%) showed a significant dependence [18]. Further work by the same authors on commercial nickel-based alloys with~20vol% gamma prime (similar to alloy 740), creep tested at 1073K (800°C) and having a composition of Ni-24wt%Cr-20wt%Co-C-Ti-Al-Nb-Mo, showed that the minimum

creep rate decreased by over one order of magnitude when grain sizes was changed from 80μm to 300μm [19]. In the present study, the grain size varied from 82.4 to 188μm. Based on the linear fit to the data used for Figure 4-12, the expected variation in rupture life due to grain size is +/- 0.20 log(t_r) for the grain sizes evaluated. For a 1000 hour rupture test, the corresponding difference in minimum creep rate (from equation 3) is ~1.3E-03 and 3.8E-04 %/hr for the finest and coarsest grain sizes, respectively (about one order of magnitude). Thus, the data in this work substantiates earlier observations that a decrease in creep rate with increasing grain size is representative of this class of alloys.

Eta phase and gamma prime effect on creep-rupture behavior

The time to rupture results in Figure 4-3 indicate there is no significant effect of alloy chemistry on creep strength, yet the computational equilibrium calculations, verified through microscopy in this study and other studies on aged alloy 740 [6,21,22] , clearly indicate significant changes in the volume fraction of gamma prime and the eta phase stability. To examine these factors in more detail, the calculated equilibrium microstructures for the heats were compared on the basis of the total amount of eta phase and gamma prime. These are plotted against the Larson Miller parameter in Figure 4-14, where no significant trends are apparent. Heats having large amounts of thermodynamically stable eta phase have strengths equivalent to heats with little or no eta phase, and heats with only 1-5wt% of thermodynamically stable gamma prime have strengths equal to heats with larger amounts of gamma prime.
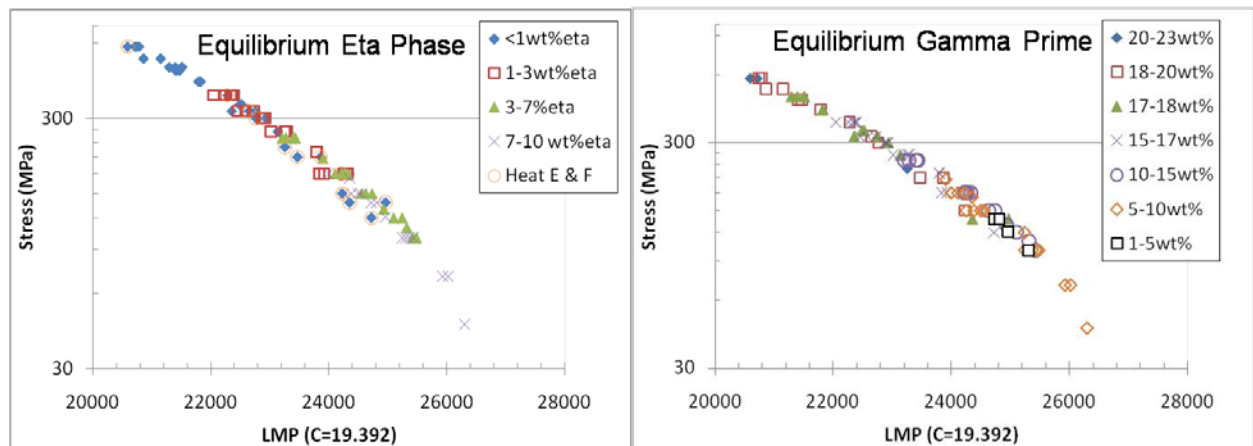

Figure 4-14 Thermodynamic equilibrium amounts of eta phase (left) and gamma prime (right) showing no significant effects on creep strength.

Given that it is well known that nickel-based alloy strength increases with increasing volume fraction of gamma prime [18-20], there are three potential reasons for the contrary trends observed here. First, the amount of metastable

79

gamma prime is similar in most of the alloys (Figure 4-5), and thus, since the formation of the eta phase is sluggish (Figure 4-10 and 4-11), the creep strength could be controlled mostly by the metastable gamma prime. This could be argued for the shorter-term tests, but for testing beyond 1,000 hours in the temperature range of interest, the microstructure clearly approaches the equilibrium predictions. In addition, heat D, which has a lower amount of metastable and equilibrium gamma prime has equivalent strength to heats A and B with similar grain size (Figure 4-3). Therefore, similar amounts of metastable gamma prime alone cannot explain the creep strength findings.

Second, the eta phase could contribute to the strength of the alloy system. Some studies suggest that the formation of eta phase in superalloys may have a beneficial effect on creep strength [23,24], but other studies could not verify this [7,25]. Based on the results in this study, it appears that creep strength is not affected by the amount of eta phase (Figure 4-14).   A separate study on model alloys designed to form only eta phase would be required to clearly delineate the potential for eta phase strengthening compared to gamma prime strengthening, which, to the authors knowledge, has not been performed.

Third, it is entirely possible that changes in the gamma prime and eta phase volume fractions are not the key controlling microstructural parameters for creep strength. This suggestion appears the most likely and is supported by observations in [18,19], where grain size had a larger effect on creep strength in Ni-Cr-Al-Ti-Nb alloys than the volume fraction of gamma prime for alloys with at least 5 vol.% gamma prime. Figure 8 shows that there is formation of gamma prime denuded regions (precipitate free zones) along grain boundaries and near eta phase precipitates which form at the expense of gamma prime, and Figure 4-9 shows that there is creep cavitation in these denuded regions. In addition, nearly continuous grain boundary carbide formation is observed in alloy 740 as shown in Figures 4-7 and 4-8. Grain boundary carbides are necessary to control grain boundary sliding in nickel-based alloys, but in 'low volume fraction gamma prime alloys' they can also cause the formation of gamma prime precipitate free zones [10]. It has been suggested that recovery in the precipitate free zones leads to grain boundary effects on creep strength [18,19] and reduced high-temperature ductility [26].

Figure 4-4 shows that there is an important effect of temperature on creep-rupture ductility irrespective of alloy chemistry. The temperature dependence of the average rupture elongation is plotted in Figure 4-15, where a linear relationship from 923 to1098K (650 to 825°C) is obtained, confirming that the rupture ductility in alloy 740 increases with increasing test temperature. The amount of scatter in the data are similar except for the tests at 1123K (850°C) where higher variability is encountered. Since eta phase formation is in part related to the formation of the precipitate free zones, the rupture elongation is

80

plotted against the Larson Miller parameter in Figure 4-16 in a way that identifies the effects of the equilibrium predicted eta phase content. The plot shows that the ductility is low at low LMP values, consistent with lower temperature testing. As the test temperature increases and hence the LMP increases, the ductility increases irrespective of eta phase volume fraction. At high LMP values (highest temperature and long time), some reduction in ductility (below 10% elongation) is observed in the heats containing 7-10 wt% eta phase. Since heat E is not predicted to form more than 3wt% eta phase (Figure 4-5) at the temperatures tested in this study, the data points from heat E have been identified in Figure 4-16 by circles. As indicated, there is only one heat E data point for a LMP of 25000 or greater, but its elongation is greater than 10%. To definitively establish the role of eta phase on ductility in alloy 740, longer-term higher temperature tests on heat E or F are required to validate the finding that greater than 7% eta phase may cause a reduction in creep ductility and explain the variations from the observed trend with temperature.
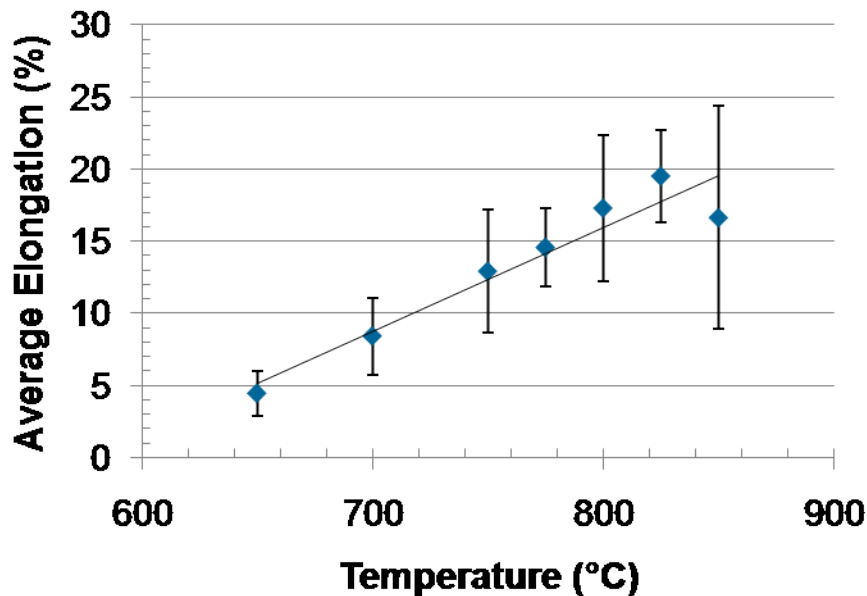
Figure 4-15 Average rupture elongation as a function of temperature for alloy 740
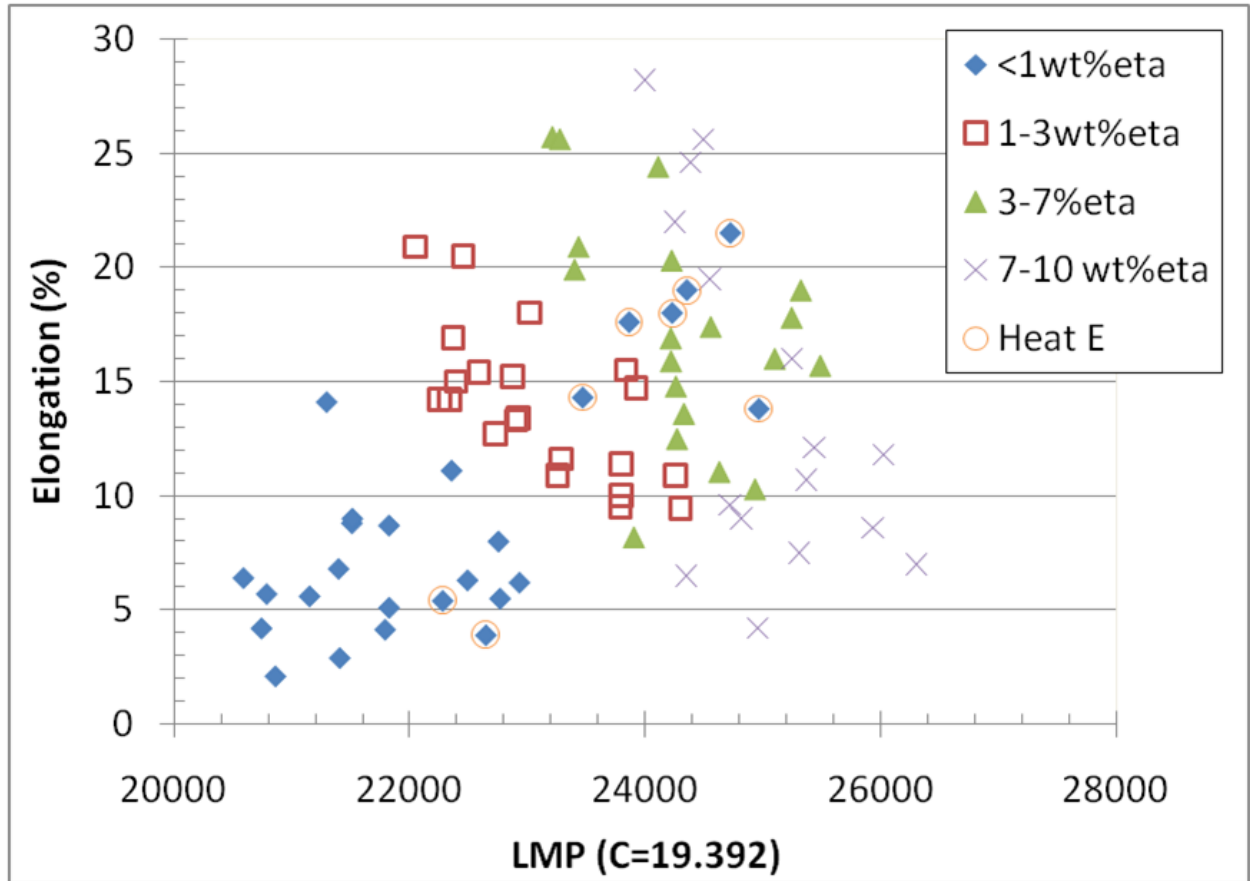
Figure 4-16 Creep-rupture ductility and equilibrium eta phase plotted as a function of the Larson Miller parameter (LMP).

In summary, no notable trends that relate the creep strength to alloy chemistry were identified for the range of alloy 740 compositions examined in this study. While the eta phase stability and gamma prime volume fraction showed clear chemistry dependent trends, the creep-rupture strength was unaffected by these parameters. The creep ductility increased with increasing test temperature, but when the eta phase content was greater than 7wt%, some reduction in ductility was observed at higher temperatures. Further testing is needed to validate this finding. These results, combined with findings on grain size and the supporting microstructural evidence, suggest that the formation of gamma prime denuded regions (precipitate free zones) along the grain boundaries may be the most critical microstructural factor effecting creep strength and creep ductility in the alloy.

Conclusions

An extensive study was conducted on how composition and grain size affect the long-term creep-rupture behavior of alloy 740. The study combined computational thermodynamic simulation, microstructural evaluation, and analysis of long-term creep data. The following conclusions were drawn from the observations:

- The computational thermodynamics showed very good agreement with eta phase stability, composition, and volume fraction.
- Small changes in the Ti/Al ratio in the alloy can have a profound effect on the amount of eta phase and the range of temperature over which it is stable.
- The computational thermodynamics software did not accurately predict the precipitation kinetics of the eta phase in alloy 740, presumably due to inaccurate nucleation kinetics.
- There is a moderate dependence of grain size on creep-rupture strength with larger grain sizes giving improved creep resistance and longer rupture lives.
- Within the range of compositions tested, the amount of gamma prime and formation of eta phase has no notable effect on the creep-strength.
- Creep ductility was found to increase with increasing temperature, but it may be reduced if the eta phase volume fraction exceeds ~7wt%. However, more research is needed to validate this finding.

Chapter 4 References

1. J.P. Shingledecker, I.G. Wright: Proceedings to the 8th Liege Conference on Materials for Advanced Power Engineering 2006, Forschungszentrum Jülich GmbH, 2006, pp. 107-120.
2. R. Viswanathan, R. Purgert, U. Rao: Materials for Advanced Power Engineering 2002, Proceedings Part II, Forschungszentrum Julich GmbH, 2002. pp. 1109-1129
3. R. Viswananthan, J.F. Henry, J. Tanzosh, G. Stanko, J. Shingledecker, B. Vitalis, R. Purgert: J. .Mater. Eng. Perform., 2005, 3., Vol. 14., pp. 281-292
4. N.D. Evans, P.J. Maziasz, R.W. Swindeman, G.D. Smith: Scr. Mater., 2004, Vol. 51. pp. 503-507.
5. S. Zhao, X. Xie, G.D. Smith, S.J. Patel: Mater. Sci. and Eng., 2003, Vol. A355, pp. 96-105.
6. X. Xie, S. Zhao, J. Dong, G.D. Smith, B.A. Baker, S.J. Patel: Mater. Sci. Forum, 2007, Vols. 561-565, pp. 471-476.
7. J.P. Shingledecker, G.M. Pharr. "The Role of Eta Phase Formation on the Creep Strength and Ductility of INCONEL Alloy 740 at 1023 K (750 °C)." *Metallurgical and Materials Transactions A.,* 2012, 10.1007/s11661-011-1013-4
8. "Case 2702 Seamless Ni-25Cr-20Co Material Section I". *Cases of the ASME Boiler and Pressure Vessel Code.* BPV-Supp.7. © 2011 American Society of Mechanical Engineers
9. N. Saunders, A.P. Miodownik, J.-Ph. Schille : J. Mater. Sci. 2004, Vol. 29, pp. 7237-43.
10. M.J. Donachie, S.J. Donachie: Superalloys A Technical Guide. ASM International, Materials Park, OH, 2002, pp. 25-27.
11. "Inconel ® alloy 740." SMC-090 © Special Metals Corporation, 2003 (Feb 03)
12. J.A. Siefert, J.M. Tanzosh, J.E. Ramirez. "Weldability of Inconel® Alloy 740." *Proceedings to the 6th International Conference on Advances in Materials Technology for Fossil Power Plants*, Santa Fe, New Mexico, August 30-September 4, 2010. EPRI, March 2011: 1022300. Distributed by ASM International. 1045-1066.
13. B.A. Baker, R.D. Gollihue. "Optimization of INCONEL® Alloy 740 for Advanced Ultra Supercritical Boilers. *Proceedings to the 6th International Conference on Advances in Materials Technology for Fossil Power Plants*, Santa Fe, New Mexico, August 30-September 4, 2010. EPRI, March 2011: 1022300. Distributed by ASM International. 96-109.
14. R. Viswanathan, J. Shingledecker, J. Hawk, and S. Goodstine, Effect of Creep in Advanced Materials for Use in Ultrasupercritical Power Plants, Proceedings Creep & Fracture in High Temperature Components, 2nd ECCC Creep Conference, April 21-23, 2009 (Zurich, Switzerland), DEStech Publications, Inc., 2009, p 31-43

15. N. Saunders, M. Fahrmann, C.J. Small. "The Application of Calphad Calculations to Ni-Based Superalloys." Superalloys 2000. Ed. K.A. Green, T.M. Pollock, R.D. Kissinger, TMS, Warrendale, 2000. 803

16. J.-C. Zhao, V. Ravikumar, A.M. Beltran. "Phase Precipitation and Phase Stability in Nimonic 263." Met. Mat. Trans. A, Vol. 32A, June 2001. 1271-1282.

17. N. Saunders, Z. Guo., X. Li, A.P. Miodownik, J-Ph. Schille. "Modeling the Material Properties and Behavior of Ni-Based Superalloys. Superalloys 2004. TMS, 2004.

18. T.B. Gibbons, B.E. Hopkins. "The Influence of Grain Size and Certain Precipitate Parameters on the Creep Properties of Ni-Cr-Base Alloys." Metal Science Journal. Vol. 5, 1971. 233-240.

19. T.B. Gibbons, B.E. Hopkins. "Creep behavior and microstructure of Ni-Cr base alloys." Metal Science, Vol. 18, May 1984. 273-280.

20. F.R.N. Nabarro, H.L. de Villiers. : The Physics of Creep. © Taylor & Francis Ltd 1995, pp. 187-190.

21. X. Xie, S. Zhao, J. Dong, G.D. Smith, B.A. Baker, S.L. Patel: Proceedings of the 5th International Conference on Advances in Materials Technology for Fossil Power Plants. (Marco Island, FL, Oct. 3-5, 2007) © 2008 Electric Power Research Institute, 220-230.

22. X. Xie, C. Chi, H. Yu, Q. Yu, J. Dong, M. Chen, S. Zhao. "Structural Stability Study on Fossil Power Plant Advanced Heat-Resistant Steels and Alloys in China." *Proceedings to the 6th International Conference on Advances in Materials Technology for Fossil Power Plants*, Santa Fe, New Mexico, August 30-September 4, 2010. EPRI, March 2011: 1022300. Distributed by ASM International. 30-52.

23. L. Remy, J. Laniesse, H. Aubert: Mater. Sci. Eng., 1979, Vol. 38, pp. 227-239.

24. Y.F. Gu, H. Harada, C. Cui, D. Ping, T. Fukuda, J. Fujioka: Proceedings of the 7th International Charles Parsons Turbine Conference, 2007.

25. Y.H. Zhang, D.M. Knowles: Mater. Sci. Technol., August 2002, Vol. 18. pp. 917-923

26. T.B. Gibbons, B.E. Hopkins. "High-Temperature Ductility of Ni-20% Cr-Base Alloys." Metals Science. Vol. 8., 1974. 203-208.

5. CONCLUSIONS

Inconel ® Alloy 740 is a new age-hardenable nickel-based alloy being evaluated for use in Advanced Ultrasupercritical (A-USC) Steam boiler applications. To improve the understanding of the alloy's creep-rupture behavior with a specific emphasis on the applicability for long-term service at temperatures as high as 760°C, a series of creep-rupture studies were conducted.

The first study (Chapter 2) examined the alloy's creep strength and ductility at 1023K (750°C). This is the first study, based on the authors' knowledge, for any iron or nickel-based alloy which quantitatively shows that precipitation of a small amount of eta phase does not reduce the creep-rupture strength or ductility. Specific findings include:

- There is no change in creep mechanism up to ~20,000 hours of testing time.
- Creep fracture is controlled predominately by grain boundary cavitation, resulting in rupture ductilities that are independent of test time.
- The rupture ductility in notched bar specimens that have different multiaxial stress states was found to be in good agreement with theoretical and empirical models.
- After ~20,000 hours, the measured eta phase area fractions were consistent with thermodynamic equilibrium calculations, suggesting that the data generated in this study may be used for long-term rupture strength prediction.
- Applied stress had a minor effect on eta phase precipitation and no effect on eta phase growth rate.
- The formation of a small amount of eta phase, 2 to 3%, did not affect creep strength or ductility

In the second study (Chapter 3), full-scale pressurized creep-rupture tests were conducted on cold-formed tube bends to evaluate the effect of cold-work on the performance of tube bends for high-temperature applications. Results show that the full-size test method can be used to understand the performance of these components in service. Specifically, the methodology provides a way to simplify the complexities of structural (geometric) effects and material degradation due to cold-work during creep. Observed changes in tube ovality were similar to in-plant observations, comparisons with expectations from uniaxial creep-rate data, and comparisons with literature data on similar alloys, thus verifying the validity of the analysis methods. Specific finding for Inconel ® Alloy 740 were:

- Cold-work is detrimental to the creep-rupture behavior of alloy 740 even when aging is conducted after cold-working

- The rupture life reduction, significant reduction in creep ductility, and moderate increase in minimum creep rate are similar to other nickel-based alloys
- The number of creep cavities is greatly increased in the tube bend tests normal to the pressure (hoop) stress with the areas of highest tensile cold strain having micro and macro cracking, consistent with literature data on similar alloys
- At 15%OFS (cold-work), the reduction in creep life for alloy 740 is greater than the minimum scatterband for creep data; thus, creep based designs with alloy 740 should consider lower cold-forming limits

The final study (Chapter 4) study was conducted to determine how composition and grain size affect the long-term creep-rupture behavior of alloy 740. The study combined computational thermodynamic simulation, microstructural evaluation, and analysis of long-term creep data. The following conclusions were drawn from the observations:

- The computational thermodynamics showed very good agreement with eta phase stability, composition, and volume fraction.
- Small changes in the Ti/Al ratio in the alloy can have a profound effect on the amount of eta phase and the range of temperature over which it is stable.
- The computational thermodynamics software did not accurately predict the precipitation kinetics of the eta phase in alloy 740, presumably due to inaccurate nucleation kinetics.
- There is a moderate dependence of grain size on creep-rupture strength with larger grain sizes giving improved creep resistance and longer rupture lives.
- Within the range of compositions tested, the amount of gamma prime and formation of eta phase has no notable effect on the creep-strength.
- Creep ductility was found to increase with increasing temperature, but it may be reduced if the eta phase volume fraction exceeds ~7wt%.

In summary, this research shows that provided cold-work and grain size are appropriately controlled, Inconel ® Alloy 740 has predictable creep strength and ductility despite the potential for variations in microstructure. Eta phase is not detrimental to creep strength in the alloy and grain size appears to have the largest influence on creep-rupture strength. This is most likely due to an important contribution from gamma prime denuded or precipitate free zones along grain boundaries where creep damage is concentrated.

Additional research is required to:

- Clarify the differences observed in creep damage for tensile and compressive cold-strain.
- Identify a minimum acceptable cold-work limit for the alloy.
- Confirm that greater than 7% eta phase is detrimental to creep ductility.
- Quantify the strengthening contribution (if any) from the formation of eta phase.

VITA

John P. Shingledecker, son of Ross and Mary Shingledecker, was born in 1978 in Midland, MI and spent most of his childhood in Fort Wayne, IN. He attended Michigan Technological University from 1997 to 2003 earning a Bachelor of Science and Master of Science in Materials Science and Engineering. He began work at Oak Ridge National Laboratory as a post-master Research Associate in 2003 and was hired as a full-time staff member in 2005. During this time he began his studies at the University of Tennessee. In 2008, he took a job at the Electric Power Research Institute (EPRI) to lead the institute's Fossil Materials & Repair Program which provides the electric power industry materials use and selection guidelines, welding and repair solutions, corrosion mitigation methodologies, and remaining life tools to increase power plant availability, reduce failures, and improve efficiency. In 2012 John completed his studies for a Ph.D. in Materials Science and Engineering from the University of Tennessee in Knoxville, TN.

John resides in Concord, NC with his beautiful wife of 9 years, Jennifer, and six amazing children: Olivia, Oscar, Vianne, Gabrielle, Levin, and Edmund.